LIPID NANOPARTICLES FOR DELIVERY OF NUCLEIC ACID THERAPEUTICS

by

Sam Chen

B.Sc., The University of British Columbia, 2009

A THESIS SUBMITTED IN PARTIAL FULFILLMENT OF

THE REQUIREMENTS FOR THE DEGREE OF

DOCTOR OF PHILOSPHY

in

THE FACULTY OF GRADUATE AND POSTDOCTORAL STUDIES

(Biochemistry and Molecular Biology)

THE UNIVERSITY OF BRITISH COLUMBIA

(Vancouver)

July 2016

Abstract

Nucleic acid therapies have the potential to enable the treatment of disorders previously untreatable. However, significant barriers prevent the rapid development of nucleic acid therapeutics and necessitate the use of sophisticated delivery systems. The overall objective of this dissertation is to develop more effective and tolerable lipid nanoparticles (LNPs) for nucleic acid delivery. Specifically, LNP that vary in size, stability and composition were tested for activity after subcutaneous and intravenous injection in order to optimize LNP properties. Furthermore, the incorporation of novel lipophilic pro-drugs co-delivered with nucleic acids was explored as a means to improve tolerability.

The first part of this dissertation explores the use of subcutaneous administration for LNP-siRNA. There are compelling reasons to develop LNP-siRNA that can be administered subcutaneously. These include the potential for self-administration, a prolonged therapeutic window due to a depot effect and access to cell types that are in contact with the lymphatic system, in addition to tissues available through the circulation. We found that particle size and PEG steric barrier are both important for drainage from the injection site and subsequent accumulation in the liver.

Although small LNP exhibited improved drainage and access to the systemic circulation, activity was impaired. The second part of this dissertation addresses this issue. The decrease in LNP activity can be attributed to the pronounced size dependent instability of LNP. By altering the amino-lipid content and the PEG-lipid used, the activity and stability of these systems can be greatly improved.

The previous two parts of this dissertation identified limitations to existing LNP systems. First, administration of LNP containing nucleic acids could result in immune stimulation. Second,

efforts to improve LNP activity must go beyond existing components. The last part of this dissertation proposes a general pro-drug strategy for enabling direct incorporation of additional compounds into the LNP. As an example dexamethasone, a corticosteroid commonly used to minimize infusion-related reactions, was used. Direct incorporation greatly improved the ability of dexamethasone to ameliorate immune stimulation by LNP containing nucleic acids. This work shows that when appropriately designed, LNP systems can have improved activity and tolerability, potentially expanding its clinical utility.

Preface

The preparation and analysis of all LNP-siRNA formulations and all subsequent *in vitro* experiments were performed by myself. *In vivo* experiments involving mice were performed by myself with the assistance of Ms. Yan Liu, Dr. Ying K. Tam, Dr. Paulo J.C. Lin and Dr. Yuen Yi C. Tam. Cryogenic transmission electron microscopy of LNP-siRNA in Chapter 3 was performed by myself with the assistance of Dr. Alex K. K. Leung and members of the BioImaging Facility (Bradford Ross and Garnet Martens) at The University of British Columbia. Synthesis of lipophilic dexamethasone pro-drugs in Chapter 5 was carried out by Dr. Josh Zaifman in collaboration with the laboratory of Dr. Marco A. Ciufolini in the department of Chemistry at The University of British Columbia.

Experimental designs and data analyses were performed by myself with important contributions, input and feedback from Dr. Yuen Yi C. Tam, Dr. Ying K. Tam, Dr. Paulo J. C. Lin, Dr. Alex K. K. Leung and Mr. Jayesh Kulkarni. I was responsible for the writing and preparation of the entire dissertation with the exception of the chemical synthesis of dexamethasone pro-drugs used in Chapter 5, which was written by Dr. Josh Zaifman and can be found in Appendix A. Drs. Pieter R. Cullis, Yuen Yi C. Tam and Karen Lam were responsible for editing this dissertation.

A portion of the introduction in Chapter 1 regarding the development of lipid nanoparticles for siRNA delivery (section 1.2) has been published as a mini-review article: Tam, Y.Y., Chen, S., and Cullis, P.R. (2013). Advances in Lipid Nanoparticles for siRNA Delivery. Pharmaceutics 5(3):498-507.

Chapter 3 of this dissertation regarding the subcutaneous administration of LNP-siRNA has been published in the Journal of Controlled Release: Chen, S., Tam, Y.Y., Lin, P.J., Leung,

A.K., Tam, Y.K., and Cullis, P.R. (2014). Development of lipid nanoparticle formulations of siRNA for hepatocyte gene silencing following subcutaneous administration. J Control Release. 2014 Dec 28;196:106-12.

Chapter 4 of this dissertation regarding the impact of particle size and polyethylene glycol content on LNP-siRNA activity has also been published in the Journal of Controlled Release: Chen, S., Tam, Y.Y., Lin, P.J., Sung M.M.H., Tam, Y.K., and Cullis, P.R. (2016). Influence of particle size on the in vivo potency of lipid nanoparticle formulations of siRNA. J Control Release. 2016 Aug 10;235:236-44.

Some of the data presented in Chapter 5 has been included in an invention disclosure.

All work and procedures involving animals presented in this dissertation have been approved by the Animal Care Committee at The University of British Columbia and were performed in accordance with guidelines established by the Canadian Council on Animal Care.

Animal Care and Ethics Protocol: A08-0668, A11-0359, A13-0022, A15-0026

Animal Care and Ethics Training Certificate: 6682-14, RBH-932-10, RA-133-11, RSx-71-12

Table of Contents

List of Tables

List of Figures

List of Abbreviations

ApoA	apolipoprotein A
ApoB	apolipoprotein B
ApoC	apolipoprotein C
ApoE	apolipoprotein E
AUC	Area-under-curve
ASGPR	asialoglycoprotein receptor
ASO	Antisense oligonucleotide
CHE	cholesteryl hexadecylether
COC	Cyclin olefin copolymer
COP	Cyclin olefin polymer
CpG	Phosphorothioated unmethylated cytosine-guanine dinucleotide motif containing oligodeoxynucleotide
C_{max}	Maximum blood concentration
cryoTEM	cryogenic electron Microscopy
Dex	Dexamethasone
Dex-21-P	Dexamethasone-21-phosphate
DLinDAP	1,2-dilinoleoyl-3-dimethylaminopropane
DLinDMA	1,2-dilinoleyloxy-N,N-dimethyl-3-aminopropane
DLin-KC2-DMA	2,2-dilinoleyl-4-(2-dimethylaminoethyl)-[1,3]-dioxolane
DLin-MC3-DMA	(6Z,9Z,28Z,31Z)-Heptatriaconta-6,9,28,31-tetraen-19-yl4-(dimethylamino)butanoate (or dilinoleylmethyl-4-dimethylaminobutyrate)

DLS	Dynamic light scattering
DMAP-BLP	3-(dimethylamino)propyl(12Z,15Z)-3-[(9Z,12Z)-octadeca-9,12-dien-1-yl]henicosa-12,15-dienoate
DNA	deoxyribonucleic acid
DODAC	N,N-dioleoyl-N,N-dimethylammonium chloride
DODAP	1,2-dioleoyl-3-dimethylammonium propane
DOPE	1, 2 dioleoyl-*sn*-glycero-3-phosphoethanolamine
DOTMA	*N*-[1-(2,3-dioleyloxy) propyl]-*N*,*N*,*N*-trimethylammonium chloride
DSPC	1,2-distearoyl-*sn*-glycero-3-phosphocholine
DSPE	1,2-distearoyl-*sn*-glycero-3- phosphoethanolamine
ED_{50}	Median effective dose
EPR	enhanced permeability and retention
FDA	Food and drug administration
FRET	Forster (fluorescent) resonance energy transfer
FVII	Factor VII
GalNAc	N-acetylgalactosamine
GalNAc-PEG	N-acetylgalactosamine cluster conjugated to PEG-DSG
HBV	Hepatitis B virus
HDL	High-density lipoprotein
HEPES	4-(2-Hydroxyethyl) piperazine-1-ethanesulfonic acid
i.p.	intraperitoneal
i.v.	intravenous

IDL	Intermediate-density lipoprotein
KSP	kinesin spindle protein
LDL	Low-density lipoprotein
LNP	Lipid nanoparticle
LRB-DOPE	1,2-dioleoyl-sn-glycero-3-phosphoethanolamine-N-(lissamine rhodamine B sulfonyl)
MES	2-(N-Morpholino) ethanesulfonic acid
MPS	Mononuclear phagocyte system
mRNA	Messenger RNA
MTT	3-[4,5-Dimethylthiazol-2-yl]-2,5-diphenyl-tetrazolium bromide
MWCO	Molecular weight cut-off
NBD-DOPE	1,2-dioleoyl-sn-glycero-3-phosphoethanolamine-N-(7-nitro-2-1,3-benzoxadiazol-4-yl)
NMR	Nuclear magnetic resonance
ODN	oligodeoxynucleotide
PBS	Phosphate buffered saline
PC	Phosphatidylcholine
PCSK9	proprotein convertase subtilisin/kexin type 9
PDMS	polydimethylsiloxane
PdI	polydispersity indexes
PEG	Polyethylene glycol
PEG-Cer	Polyethylene glycol conjugated ceramide lipid

PEG-DMG	(R)-2,3-bis(octadecyloxy)propyl-1-(methoxy polyethylene glycol 2000) carbamate
PEG-DSG	(R)-2,3-bis(stearyloxy)propyl-1-(methoxy poly(ethylene glycol)2000 carbamate
PEG-s-DAG	PEG-succinoyl-diacylglycerols
PK/BD	pharmacokinetics and biodistribution
pK_a	acid dissociation constant
PLK1	Polo-like kinase 1
POPC	1-palmitoyl-2-oleoyl-sn-glycero-3-phosphocholine
RBC	Red blood cells (erythrocytes)
RISC	RNA-Induced Silencing Complex
RNA	Ribonucleic acid
s.c.	subcutaneous
s.d.	standard deviation
SALP	Stabilized antisense lipid particle
siRNA	Short-interfering RNA
SNALP	stable nucleic acid lipid particle
SPLP	Stabilized plasmid lipid particle
TNS	2-(p-toluidino)-6-napthalene sulfonic acid
TTR	Transthyretin
TX-100	Triton X-100
UHPLC	ultra high pressure liquid chromatography

v	volume
VEGF	vascular endothelial growth factor
VLDL	Very-low density lipoprotein
wt	weight

Acknowledgements

I would like to thank my supervisor, Dr. Pieter Cullis for giving me the opportunity to carry out my research in his laboratory. It is very fitting that the first time I worked with liposomes and lipid nanoparticles was at a company he started (one of many) as an undergraduate research student. Since then, Pieter took me into his lab and introduced to me the many facets of science which included things far beyond bench work. Pieter's resilience and passion is inspirational and contagious! I would also like to thank my supervisory committee members Drs. Marcel Bally and Christian Kastrup for their support and tolerance of my bad behaviour. They have always pulled through for me despite my ridiculous requests and I would not be here if they hadn't.

Next, I would like to thank my lab family (both past and present). My thesis was built on the shoulders of everyone in the lab and this would not have been possible if it weren't for them. I would like to especially thank Dr. Chris Tam for being a great mentor and friend. It was through her encouragement I pursued my PhD. I have been extremely lucky to have someone I can always depend on. I could go on about all that she has done for me and how she's not lazy but it would get horribly long and sappy. I would also like to thank Dr. Karen Lam for happily editing all my applications, manuscripts and even this dissertation. Many thanks to Drs. Mick Hope, Barb Mui and Terry Allen for always welcoming my silly questions and being my permanent go-to's. Along similar lines but less welcoming, caring and helpful are Drs. Ying Tam and Paulo Lin. Ying and Paulo frequently reminded me of the importance of never showing your weakness. I mustn't forget the research associates and post-doctoral fellows that I have had the pleasure to work with: Drs. Genc Basha, Souvik Biswas, Ismail Hafez, Roy van der Meel, Chen Wan, Lizzie Wang, Josh Zaifman and Igor Zhigaltsev. Thanks to Cayetana Schluter and Yan Liu for making my lab life easier. Nobody handles fires, pots, lids and packrats quite like Tania. Thanks to the current and

past graduate students, Dr. Justin Lee, Dr. Alex Leung, Mina Ordobadi, Joslyn Quick, Nisha Chander, Andrew Cottle and especially Jayesh Kulkarni for always being difficult and a complete pain. Thanks to my super talented and helpful minions Molly Sung, Sophie Sigurdson and Caitlin Wong for doing everything I did not want to!

I would also like to thank all the mentors and collaborators I've had that is/was not associated with liposomes and lipid nanoparticles. Many thanks to Dr. Masayuki Numata who was my first research supervisor. His enthusiasm made me fall in love with research. I would like to thank Ali McAfee (Foster Lab), Heather Denroche (Verchere Lab), Morgan Roberts (Harder Lab), Soroush Nasseri (Cheung Lab), Ursula Neumann and Michelle Kwon (Kieffer Lab) for being incredibly passionate and enthusiastic collaborators. These collaborations give purpose to the lipid nanoparticles we develop and I truly thank them for making my degree more interesting. I would also like to thank Julian and his team at the ARU for always being cheery and helpful.

To my friends, thank you for being patient and understanding over the years. Winnie Lam and Victoria Ng, thank you for tolerating my constant cold. Finally, I would like to thank my family for giving me the safe haven to return to. It hasn't been easy but as a family, we've endured and overcome numerous obstacles. I thank my parents for always emphasizing the importance of hard-work, compassion, dedication, integrity and responsibility. These core values will always be a part of me. To my brother Ernest, thank you for being as stubborn as you are even in the face of hardship! I've watched you overcome every obstacle in your way, big or small, since I can remember. Your stubbornness, although often unwelcomed, is a constant reminder to not give up. Nothing easy is ever worth your time.

Chapter 1: Introduction

1.1 Lipid-based Vehicles for Drug Delivery

1.1.1 Lipid Nanoparticles in Nature

Lipids are a diverse class of hydrocarbon-based biomolecules characterized by their solubility in organic solvents. In biological systems, lipids play numerous roles ranging from chemical signaling to energy storage. Amphipathic lipids such as glycerophospholipids are often structural components that allow cellular and sub-cellular compartmentalization. Due to the chemical complexity and biological importance of lipids, humans have evolved the ability to transport these biomolecules throughout the body, either from dietary sources or from the liver where most lipid biosynthesis occurs (Fielding and Fielding, 2008; Jonas and Phillips, 2008; Vance and Adeli, 2008). As all lipids are water-insoluble, their transport through circulation to various destinations in the body is enabled by assembly into nanoparticles as plasma lipoproteins. Lipoproteins consist of protein components, or apolipoproteins, which serve various functions such as emulsifying lipids, activating enzymes involved in lipid metabolism, targeting lipid cargo to its desired destination, and facilitating endocytosis into the cell. Several classes of apolipoproteins (ApoA, ApoB, ApoC, ApoD, ApoE, ApoH), along with the variants therein, exist to confer such functional diversity. Both apolipoprotein and lipid compositions of lipoproteins are dynamic, with a given lipoprotein constantly exchanging its content with the surrounding environment. Lipoproteins are generally classified based on their densities, protein component and/or particle diameter. A summary of the various lipoproteins and their properties are found in Table 1.1.

Lipoproteins are critical for transporting lipids, primarily cholesterol, phospholipids and triacylglycerols between tissues. In the context of energy and energy storage, such tissues include

muscles and adipose tissue. Chylomicrons, the least dense of lipoproteins due to its high triglyceride content, have a single copy of ApoB48 and are made up of lipids generally derived from dietary sources of fatty acids. Chylomicrons are formed and secreted from the small intestine and must transit through the lymphatic system before reaching the peripheral circulation. There, they deliver its lipid cargo to the liver, muscles or adipose tissue for further processing. When chylomicrons are depleted of their triglyceride content, the remnants are returned to the liver via an ApoE-mediated pathway.

Very low-density lipoproteins (VLDLs) are formed and secreted by the liver when excess fatty acids are available. VLDLs contain a single full length ApoB (or ApoB100) and transport triglycerides to peripheral tissues for energy storage. When depleted of some of its triglyceride content, VLDLs either return to the liver via an ApoB-mediated pathway or continue to circulate in the peripheral circulation as intermediate density lipoproteins (IDLs). As further loss of triglyceride occurs, these IDLs are converted to low-density lipoproteins (LDLs), which are cleared from the circulation by the liver (Brown and Goldstein, 1986).

Lipoproteins are also involved with the reverse process in which lipids, primarily cholesterol, are transported from peripheral tissues to the liver. This is often referred to as reverse cholesterol transport and involves high density lipoproteins (HDLs) (Miller, 1990). HDLs are first secreted as disk-like nanoparticles by the liver and intestines. These nascent HDLs primarily contain phospholipids and apolipoproteins with very little cholesterol or cholesteryl-ester. Transiting through peripheral circulation, the disk-like HDLs become spherical as they scavenge peripheral tissues and immune cells for cholesterol and cholesteryl-ester. Ultimately, HDLs return their lipid payload to the liver for further processing in either a lipid-transfer protein dependent mechanism or an ApoE dependent mechanism where the entire particle is endocytosed by

hepatocytes. It is important to note that lipoproteins are diverse and differ in apolipoprotein and lipid composition but invariably, these lipid-rich particles are coated with a surface monolayer of phospholipids surrounding a hydrophobic core of lipids such as triglycerides and cholesterol esterified to fatty acids. In essence, lipoproteins are nature's lipid nanoparticles (LNPs). Lipoprotein transport within the body has provided important insights on how therapeutic LNPs may behave *in vivo* (Section 1.2). However, the use of LNPs for drug delivery did not arise from the realization of how nature transports lipids throughout the body, but began with research on cell membranes and its ability to form permeability barriers. Current LNPs used for drug delivery have their roots traced back to the early work of pioneers in liposome research.

Table 1.1 Lipoprotein Composition and Characteristics*

	Chylomicrons	Very low density lipoproteins	Low density lipoproteins	High density lipoproteins
Density (g/mL)	< 0.94	0.94-1.006	1.006-1.063	1.063-1.210
Approximate diameter (nm)	>80	30-80	18-25	5-12
Total lipid (% wt)	98-99	90-92	75-80	40-48
Glycerolipids (% wt lipid)	81-89	50-58	7-11	6-7
Cholesteryl esters (% wt lipid)	2-4	15-23	47-51	24-45
Cholesterol (% wt lipid)	1-3	4-9	10-12	6-8
Phospholipids (% wt lipid)	7-9	19-21	28-30	42-51
Apolipoproteins	A1, A4, B48, C1, C2, C3, E	B100, C1, C2, C3, E	B100, C3, E	A1, A2, C1, C2, C3, D, E
Transport Function	Dietary triglyceride and cholesterol	Triglyceride to peripheral tissues	Cholesterol to peripheral tissues	Reverse cholesterol transport to liver

* Adapted from (Jonas and Phillips, 2008), (Fielding and Fielding, 2008), (Vance and Adeli, 2008) and (Mahley et al., 1984)

1.1.2 Traditional Liposomes: Model Membranes to Drug Delivery

A search of the term "liposome" on PubMed results in over 50,000 publications, all originating from the first description of multilamellar lipid vesicles entrapping an aqueous core in 1964 (Bangham and Horne, 1964). By negative staining electron microscopy, lecithin extracted from egg yolk formed lamellar structures when hydrated. These swollen phospholipid systems were capable of maintaining ion concentration gradients that were disrupted by detergents (Bangham et al., 1965). These enclosed bilayers quickly became model membrane systems to study the behaviours of lipids in nature. Liposomes were initially called "Banghasomes" in honour of Alec Bangham who first described these vesicles. Among the first applications of liposomes was a study of how anesthetics affected the permeability of model membranes, which have implications for the mechanism of action within cells. It was found that liposomes exposed to anesthetics became significantly more permeable to ions (Johnson et al., 1973).

It was soon recognized that biologically active compounds could also be entrapped within the lipid bilayer or the aqueous compartment of liposomes. In the 1990s, AmBisome, a liposomal formulation of amphotericin B, was approved in Europe and DOXIL, a liposomal formulation of doxorubicin, was approved in the United States. These were the first lipid nanoparticle formulations approved for human use. Some of these drugs and their indications are summarized in Table 1.2. Interestingly, the manner by which these two compounds incorporate into liposomes are distinct and highlight the two classes of molecules that can benefit from liposomal formulations: hydrophobic compounds that can associate with the lipids and hydrophilic weak base compounds that can be remotely loaded based on transmembrane gradients.

Fundamentally, drug carriers are used to improve disease site accumulation while reducing the exposure of healthy tissues to the deleterious effects of the entrapped compounds. A number

of critical nanoparticle properties and design parameters, including such factors as drug loading and circulation lifetime, have been identified by studying traditional liposomes.

Table 1.2 FDA Approved Lipid/Liposomal Drugs

Trade Name	Active Compound	Indications*
Abelcet	Amphotericin B	Invasive fungal infections
AmBisome	Amphotericin B	Invasive fungal infections Aspergillus, Candida, Cryptococcus infections Visceral leishmaniasis
Amphotec	Amphotericin B	Aspergillosis infection
DaunoXome	Daunorubicin	HIV-Associated Kaposi's Sarcoma
DepoCyt	Cytosine Arabinoside (Cytarabine)	Lymphomatous meningitis
DepoDur	Morphine Sulfate	Pain pre/post surgery
Diprivan	Propofol	Anesthesia
Doxil	Doxorubicin	Ovarian Cancer HIV-Associated Kaposi's Sarcoma Multiple Myeloma
Exparel	Bupivacaine	Postsurgical analgesia
Marqibo	Vincristine sulfate	Philadelphia chromosome-negative acute lymphoblastic leukemia
Onivyde	Irinotecan	Pancreatic adenocarcinoma
Visudyne	Verteporphin	Age-related macular degeneration, myopia or ocular histoplasmosis

*Indications from the FDA and https://dailymed.nlm.nih.gov/

1.1.3 Drug Loading and Controlled Release

Not all compounds can be entrapped and stably retained within liposomes. Hydrophobic compounds which embed within the lipid bilayer are prone to dissociate from the liposome upon interacting with serum proteins or lipophilic reservoirs such as circulating lipoproteins. Taxanes,

a family of potent antimicrotubule chemotherapeutics, are prime examples of such compounds where, despite favourable drug loading, the poor retention of the drug within liposomes greatly reduces the benefits of a liposomal formulation (Sharma et al., 1997; Soepenberg et al., 2004). Many researchers have addressed this and similar challenges by chemically modifying the active compound into a pro-drug form that enables efficient loading and entrapments.

Liposomes are permeability barriers for most hydrophilic compounds that are entrapped within the aqueous lumen. Lipid composition plays a critical role in the retention of water-soluble compounds. The use of more saturated phospholipids with higher phase transition temperatures (e.g., distearoylphosphatidylcholine versus dioleoylphosphatidylcholine or palmitoyloleylphosphatidylcholine) reduces permeability (Charrois and Allen, 2004; Gabizon et al., 1993). Cholesterol abolishes phase transition behaviours of phospholipid bilayers, and can tighten the bilayer and reduce permeability (Papahadjopoulos et al., 1973; Papahadjopoulos et al., 1972). Inclusion of sphingomyelin in the presence of cholesterol also stabilizes bilayer structures (Cullis and Hope, 1980) and reduces permeability (Webb et al., 1995). In addition to establishing stable and persistent permeability barriers, the retention of compounds can be further controlled by choosing compounds with appropriate physical properties. Anions, for example, exhibit higher rates of diffusion across the bilayer when compared to cations, while water remains freely permeable (Bangham et al., 1965). Furthermore, larger compounds diffuse across the bilayer more slowly than smaller compounds.

Loading technique is another factor that has significant impact on therapeutic potential. Some of the first applications of liposomes as drug carriers utilized passive loading techniques whereby the bilayer is formed in a bulk solution containing the compound of interest. This generally results in poor drug entrapment efficiencies, a serious limitation to realizing the

therapeutic potential of liposomes. The discovery that a stable transmembrane pH gradient can concentrate catecholamines within the lumen of the liposome was a major milestone in LNP drug delivery (Nichols and Deamer, 1976). When weak base compounds are exterior to the liposome, where the pH of the solution is greater than the compounds' acid dissociation constant (pKa), they exist in both protonated cationic and deprotonated neutral forms. The neutral form freely diffuses across the liposome membrane down its concentration gradient. Upon reaching the acidic interior of the liposome, the compound becomes protonated and is trapped within the liposome. As the concentration of the compound within the liposome increases, crystallization may occur, which further promotes the diffusion of the compound into the liposome down the concentration gradient. This established mechanism prompted researchers to attempt loading other weak base compounds using similar remote loading strategies involving pH gradients (Fenske et al., 1998; Haran et al., 1993; Madden et al., 1990; Mayer et al., 1986). Drugs like doxorubicin can accumulate at high concentrations and crystalize within the acidic interior of liposomes, resulting in the characteristic "coffee-bean" structures observed under electron microscopy (Abraham et al., 2005; Barenholz, 2012). In contrast to passive loading, active or remote loading can result in very efficient (> 80%) drug entrapment.

The therapeutic activity of a liposomal formulation depends on both drug retention and release. Retention is often dependent on a drug's chemical properties. For example, compounds that can precipitate or crystalize within the liposome tend to be retained well (eg: doxorubicin) in contrast to other compounds that do not readily precipitate (eg: ciprofloxacin (Maurer et al., 1998)). Furthermore, drugs that remain within the liposome carriers are not bioavailable and do not act therapeutically. Therefore, it is critical that liposomes accumulate at the disease site which

increases the local concentration, prior to releasing its payload. The drug must reach therapeutic local concentrations for an appropriate duration in order to maximize therapeutic effects.

1.1.4 Improving Circulation Parameters and Target Site Accumulation

In order for liposomes to reach target disease sites while avoiding healthy tissues, it must remain sufficiently long in the circulation. This allows it to capitalize on a natural targeting phenomena that occurs in regions with permeable vasculatures such as sites of inflammation or tumorigenesis. For tumors, the architecture of neovasculature is often defective and leaky, thereby allowing large macromolecules (> 40 KDa) or nanoparticles (< 200 nm) to permeate. Along with impaired lymphatic drainage, this results in the accumulation of particulates at the solid tumor. This phenomenon is termed the enhanced permeability and retention (EPR) effect (Fang et al., 2011; Maeda et al., 2000; Matsumura and Maeda, 1986).

Early liposomes were rapidly cleared from the circulation by the mononuclear phagocyte system (MPS) found in the liver and spleen, which limits the amount of liposomes that can accumulate at the site of disease. To overcome this, researchers "saturated" the MPS by using high or repeat dosing regimens or pre-dosing with large quantities of liposomes not carrying a therapeutic payload (Abra et al., 1980; Kao and Juliano, 1981). Consequently, the clearance of liposomes is dose dependent, with circulation lifetime increasing concomitantly with dosage (Allen and Hansen, 1991). An important breakthrough in this area came from the recognition that a likely mechanism for clearance by the MPS was opsonization of liposomes (Chonn et al., 1992; Hoekstra and Scherphof, 1979). This finding led to surface modifications of liposomes.

The first demonstration that surface modifications of liposomes resulted in improved circulation properties was the addition of the natural lipid monosialoglycoprotein GM1. It was

found that GM1 prolonged the circulation of liposomes and enhanced tumor uptake without the need to saturate the MPS. However, the difficulty associated with purifying or synthesizing GM1 at the time significantly limited its usefulness (Allen and Chonn, 1987; Gabizon and Papahadjopoulos, 1988). In the early 1990s, polyethylene glycol conjugated lipids (PEG-lipids) were described to extend circulation lifetimes of liposomes by several research groups (Allen et al., 1991; Blume and Cevc, 1990; Klibanov et al., 1990; Papahadjopoulos et al., 1991; Senior et al., 1991). Unlike natural lipids like GM1, these polymer-lipid conjugates can be easily and cost effectively synthesized and purified, enabling rapid adoption in the field. Liposomes containing PEG-lipids did not have dose-dependent blood clearance and also showed greater tumor accumulation. These PEGylated liposomes are referred to as "Stealth" or sterically stabilized liposomes. The extended circulation lifetimes was demonstrated in mice, dogs and humans (Gabizon et al., 1994; Gabizon et al., 1993), and ultimately led to the approval of DOXIL, a stealth liposomal formulation of doxorubicin.

1.2 Lipid Nanoparticles for Nucleic Acid Delivery

1.2.1 Challenges of Nucleic Acids Therapeutics

The use of lipid delivery vehicles such as conventional liposomes has dramatically improved the therapeutic potential of a variety of drugs. This is owing to the ability of the delivery vehicle to modify the pharmaocokinetics and biodistribution of the compounds entrapped, which has direct impacts on the toxicology of the compound. Small molecule drugs such as doxorubicin (Doxil, Caelyx, Myocet), vincristine (Marqibo), daunorubicin (DaunoXome) and amphotericin B (AmBisome, Amphotec, Abelcet) have all been clinically improved by being entrapped in or

associated with lipid delivery vehicles (Allen and Cullis, 2012). Similar improvements could apply to genetic drugs or nucleic acid based therapeutics.

Multiple barriers prevent the widespread therapeutic use of nucleic acids. To start, nucleic acid polymers tend to be susceptible to nucleases present in biological fluids. RNA (Tsui et al., 2002) and single stranded DNA (Eder et al., 1991) are more susceptible to degradation than double stranded DNA. Nevertheless, it has been shown that plasmid DNA exposed to whole blood can be completely degraded within minutes (Kawabata et al., 1995). Even if nuclease degradation is avoided, molecules less than 10 nm in diameter would be susceptible to rapid renal filtration or clearance given the glomerular pore size is approximately 8 nm. Shorter nucleic acid polymers like antisense oligonucleotides (ASO) or short-interfering RNA (siRNA) are only several nanometers in diameter and thus are subject to rapid clearance (Geary et al., 2001; Sands et al., 1994; van de Water et al., 2006). Therefore, free nucleic acid has very poor bioavailability. Notwithstanding the issue of clearance, there is no means for nucleic acids to extravasate the endothelium and reach disease causing tissues or preferentially accumulate at the site of disease. The polyanionic nature of nucleic acids prevent efficient cellular uptake at disease sites, since large and negatively charged molecules diffuse very slowly across the cell membrane (Whitehead et al., 2009). If internalization by endocytosis does occur, nucleic acids lack the means to disrupt the endosomal membrane and reach the cytoplasm, where nucleic acids such as siRNA and messenger RNA (mRNA) must reach in order to inhibit or induce gene expression. In the case of plasmid DNA, the nuclear membrane is an extra barrier that must be crossed in order to access transcriptional machinery (Roth and Sundaram, 2004). An additional overarching complication is that nucleic acids are potent activators of the innate immune response. Systemic administration of unmodified RNA can activate Toll-like receptors, leading to rapid increases in serum cytokine

levels (Barbalat et al., 2011; Judge et al., 2005; Sahin et al., 2014). In order to overcome these barriers, sophisticated delivery technologies for nucleic acids are necessary.

1.2.2 Early Attempts to Encapsulate Nucleic Acids in Lipid Nanoparticles

Early attempts to encapsulate nucleic acids in conventional liposomes without the use of cationic lipids or polymers generally resulted in poor encapsulation efficiencies (Wheeler et al., 1999) since entrapment within the aqueous lumen of the liposome is an entirely passive process. Thus, in order to get reasonable nucleic acid-to-lipid ratios, high concentrations of nucleic acids must be used. Because the majority of the nucleic acid remains exterior to the vesicles, most of the nucleic acid is removed and wasted. The use of cationic lipids to improve encapsulation efficiency was an important breakthrough, most notably enabling the transfection of plasmid DNA into cells. This was first described by Felgner and colleagues in 1987 using the cationic lipid N-[1-(2, 3-dioleyloxy)propyl]-N,N,N-trimethylammonium chloride (DOTMA) and membrane destabilizing lipid 1,2-dioleoyl-sn-glycero-3-phosphoethanolamine (DOPE) (Felgner et al., 1987). Through ionic interactions, the positively charged DOTMA would interact with negatively charged phosphates on the nucleic acid, resulting the formation of lipid-DNA complexes or lipoplexes with near complete encapsulation of the DNA (Felgner et al., 1993). To further improve on cationic lipid design, a series of novel lipids were synthesized and tested for transfection efficiency (Felgner et al., 1994). These lipids form the basis of lipid-based transfection reagents that are now commercially available and routinely used in the laboratory. Transfection efficiency as measured by plasmid gene expression is often higher than more traditional methods that use calcium phosphate or DEAE-dextran (Felgner et al., 1987). Although cationic lipoplexes have been very successful in transfecting cultured cells with nucleic acids, it has been less successful for *in vivo*

applications. This is largely due to its uncontrolled particle parameters (lipoplexes often have diameters in the micron range) and permanent cationic charge, which together result in rapid plasma clearance and hemolytic, coagulation, liver and complement related toxicities (Audouy et al., 2002; Litzinger et al., 1996; Tam et al., 2000; Zhang et al., 2005). More robust manufacturing methods were later employed to control LNP parameters (Section 1.2.3), and ionizable rather than cationic amino-lipids were developed to reduce systemic toxicities (Section 1.2.5).

1.2.3 Manufacturing of Lipid Nanoparticles for Nucleic Acid Delivery

1.2.3.1 Pre-formed Vesicle and Extrusion-based Methods

Early development of LNP for nucleic acid delivery was based on plasmid DNA and antisense oligonucleotides. Stabilized plasmid-lipid particles (SPLPs) were LNP composed of DOPE, dioleoyldimethylammonium chloride (DODAC), and PEG-ceramide lipid conjugate (Tam et al., 2000; Wheeler et al., 1999; Zhang et al., 1999). Plasmid DNA and lipids are solubilized and mixed in an aqueous solution of the detergent octylglucopyranoside. Removal of the detergent by dialysis results in the formation of SPLPs, which appear to be unilamellar liposomes of approximately 70 nm in diameter. DNA encapsulation efficiencies reached 50-70%. SPLPs exhibited a prolonged circulation half-life (6-7 hours in mice) and also accumulated at distal tumors resulting in gene expression (Fenske et al., 2001; Tam et al., 2000). Luciferase gene expression was observed primarily in tumor tissue with very little expression in the liver, spleen, lungs and kidneys. Despite these advantages, however, this detergent dialysis method is difficult to scale and manufacture.

Stabilized antisense lipid particles (SALP) LNP containing ASO and were composed of the ionizable lipid 1,2-dioleoyl-3-dimethyaminopropane (DODAP), cholesterol, distearoyl-

phosphatidylcholine (DSPC) and PEG-lipid. The lipid components were first dissolved in ethanol and slowly added to an acidic aqueous solution of ASO while under constant vortex mixing (Semple et al., 2001). Rather than using a detergent to solubilize all the components as in the case of SPLP production, ethanol was used instead. The acidic pH ensured that the ionizable amino-lipid, DODAP (pKa ~6.6) is protonated, thus promoting its interaction with the nucleic acid. This mixture was then extruded 10 times through three stacked polycarbonate membranes to ensure uniform size. The residual ethanol was removed and pH was raised to pH 7.0 by dialysis to ensure that SALP is electrostatically neutral in circulation. This method resulted in high nucleic acid encapsulation efficiencies (up to 70%) and particle sizes of approximately 100 nm.

A variation to this method was developed where large unilamellar liposomes containing the same lipids (DODAP, cholesterol, DSPC and PEG-lipid) were first formed by either lipid film hydration with an acidic aqueous buffer followed by extrusion and addition of ethanol, or slow addition of lipids dissolved in ethanol to the acidic buffer with constant vigorous mixing followed by extrusion (Maurer et al., 2001). Both procedures resulted in large unilamellar liposome dispersions in an acidic ethanol-aqueous solution. ASO was then slowly added under mixing, then incubated for one hour and finally dialyzed, removing the residual ethanol and raising the pH to deprotonate DODAP. The systems generated using these extrusion based methods exhibited multilamellar structures and had high nucleic acid encapsulation efficiencies (up to 80%). Mechanistically, it is proposed that the nucleic acids interact with DODAP on the surface of the unilamellar liposome, forming adhesion points between adjacent particles. Because of the high ethanol content, remodeling of the vesicles can occur, which facilitates the formation of multilamellar vesicles and the entrapment of the nucleic acid between concentric bilayers. These methods have been successfully adapted and employed for plasmid DNA and siRNA, but are,

unfortunately, not scalable and difficult to reproduce. Furthermore, the bulk mixing of solutions may result in batch-to-batch and user variability. This has led to the development of simpler and more robust rapid mixing methods of LNP formation.

1.2.3.2 Spontaneous Formation by Rapid Mixing Methods

Two forms of rapid mixing are commonly employed for the spontaneous formation of LNP. The first was developed as a more robust method to produce SPLP that does not require the use of detergents and, similar to the production of SALP, uses ethanol for lipid solubilization (Jeffs et al., 2005). Plasmid DNA is first prepared in an acidic buffer, while lipids are dissolved in ethanol. These two mixtures are then rapidly injected together with peristaltic pumps into a T-shaped mixing chamber resulting in the spontaneous self-assembly of LNP. The remaining ethanol is then removed by dialysis or tangential flow filtration (Figure 1.1). Because this method requires the injection of the two streams into a T-junction for mixing to occur, it is often referred to as T-tube or in-line mixing. In-line mixing was later adapted for use with siRNA and the resulting LNP-siRNA were termed stable nucleic acid lipid particle (SNALP). The high flowrates required for efficient mixing makes laboratory scale formulations difficult, but because of the scalability of in-line mixing, this is currently the method of choice for manufacturing LNP for clinical development (Section 1.3.1).

Numerous reports have demonstrated the efficacy of SNALP in rodents, non-human primates and humans. One of the earliest demonstrations of SNALP efficacy was in a mouse model of hepatitis B virus (HBV) infection. SNALPs containing siRNA against the HBV genome inhibited replication and greatly reduced serum HBV levels after three daily injections (Morrissey et al., 2005). Because chemically modified siRNA were used, the silencing effects were observed

for over a week with no immune stimulation detected. Shortly after, SNALP efficacy was again demonstrated in cynomolgus monkeys where circulating levels of apolipoprotein B (ApoB) was substantially reduced after a single intravenous (i.v.) administration of SNALP containing siRNA against ApoB (Zimmermann et al., 2006). At an siRNA dose of 2.5 mg/kg body weight, persistent gene silencing in the liver (> 90% mRNA reduction) was observed over 11 days, with concomitant reduction in total plasma cholesterol and LDL. No significant effects on HDL were observed. SNALP formulations were very well tolerated in this non-human primate model with no toxicities observed. Similar successes have been observed in clinical trials (Section 1.3.1).

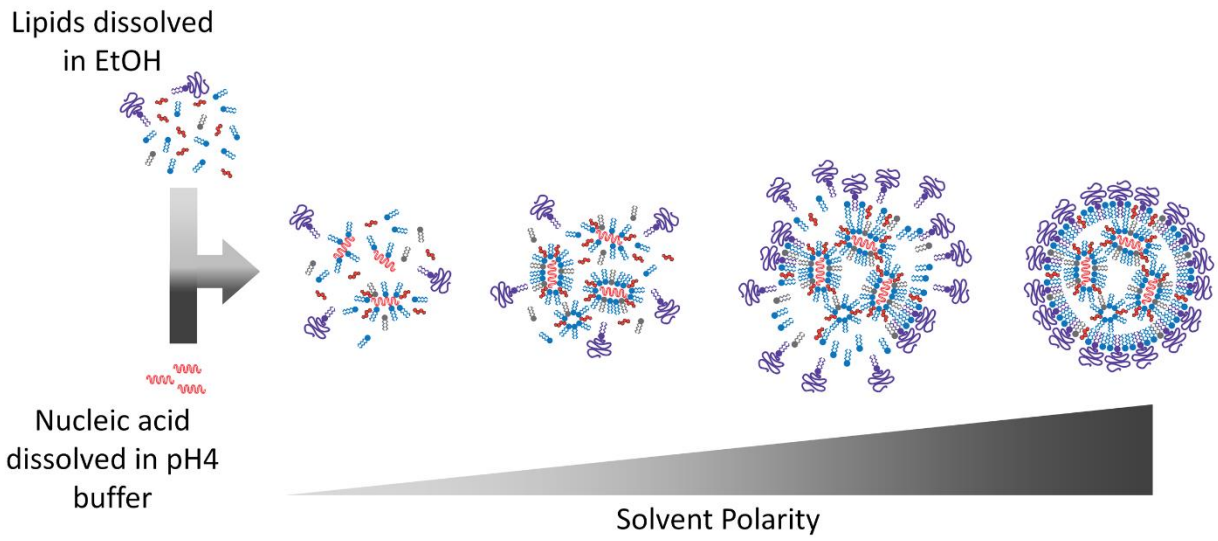

Figure 1.1 Diagrammatic Representation of the Spontaneous Formation of LNP by Rapid Mixing Methods.

It is currently believed that LNP spontaneously formed by rapid mixing methods are a result of lipids condensing nucleic acid based on ionic interactions and the increase in solvent polarity. As lipids dissolve in solvent, typically ethanol, rapidly mixes with nucleic acids dissolved in a low pH aqueous buffer, the amino-lipids become cationic and form ionic interactions with the anionic phosphates on the nucleic acids. These lipid-nucleic acid condensates form the nucleating core of the LNP. As the solvent polarity rapidly rises, the various lipid components precipitate according to their solubilities. The most polar PEG-lipid component falls out of solution last and coats the surface of the LNP.

More recently, as it became recognized that rapid and homogenous mixing is critical to the spontaneous formation or self-assembly of LNP, a microfluidic-based mixing method was developed. Whereas the variable local mixing of slower mixing methods may result in inconsistent compositions, heterogeneity and high particle polydispersities, rapid local mixing enables the lipid compositions of LNP to dictate the final physical properties. Similar to in-line mixing, nucleic acid is dissolved in a low pH buffer and lipids are dissolved in ethanol or other water-miscible solvents. These two solutions are injected into the micromixer or microfluidic chamber though a Y-shaped junction. The current microfluidic mixing chambers employed to make LNP-siRNA is a staggered herringbone micromixer (Figure 1.2). This herringbone architecture results in the two fluid streams folding and wrapping on itself which increases the total surface area of contact of the two streams and results in mixing by chaotic advection (Walsh et al., 2014). This promotes diffusion and allows for mixing on a millisecond timescale. Using the staggered herringbone micromixers at a total combined flowrate of 2 mL/min, complete mixing is achieved in 3 milliseconds (Belliveau et al., 2012). These micromixers were initially composed of polydimethylsiloxane (PDMS), a polymer that enables simple fabrication but has limited chemical compatibility. Current micromixers are composed of cyclic olefin polymers or copolymers (COP or COC) rather than PDMS, which allow for higher total flowrates (> 30 mL/min) and importantly, greatly improve chemical compatibility. One benefit of using microfluidic mixing to generate LNP is that very small volumes can be made, which drastically reduces the cost of research. Scale up of this procedure is possible by parallelization of micromixers.

Because of the efficient mixing enabled by the microfluidics-based formulation process, scalable production of LNP systems over the size range of 20-100 nm in diameter has been demonstrated (Belliveau et al., 2012; Zhigaltsev et al., 2012). As depicted in Figure 1.1, the rapid

mixing and consequent rapid rise in polarity cause the most hydrophobic components to fall out of solution first, creating nucleation sites where inverted micelles are formed by association of cationic lipids with the negatively charged macromolecule. This is followed by deposition of the more polar lipids and finally the most polar PEG-lipid component (Leung et al., 2012). This formulation concept was further extended to manufacturing of LNP that contain mRNA, plasmid DNA and anionic colloidal gold (Leung et al., 2015). In addition, "limit-size" particles can be generated by adjusting the core-to-surface lipid ratio. For example, in the case of triolein-1-palmitoyl-2-oleoyl-sn-glycero-3-phosphocholine (POPC) mixtures, the hydrophobic triolein falls out of solution first to be subsequently coated by the more polar POPC. By changing the ratio of surface lipid (POPC) to core lipid (triolein), LNP with sizes over the range of 20-100 nm can be readily generated (Zhigaltsev et al., 2012). These systems are "limit size" in the sense that they are the smallest possible systems that are compatible with the molecular makeup of the particle.

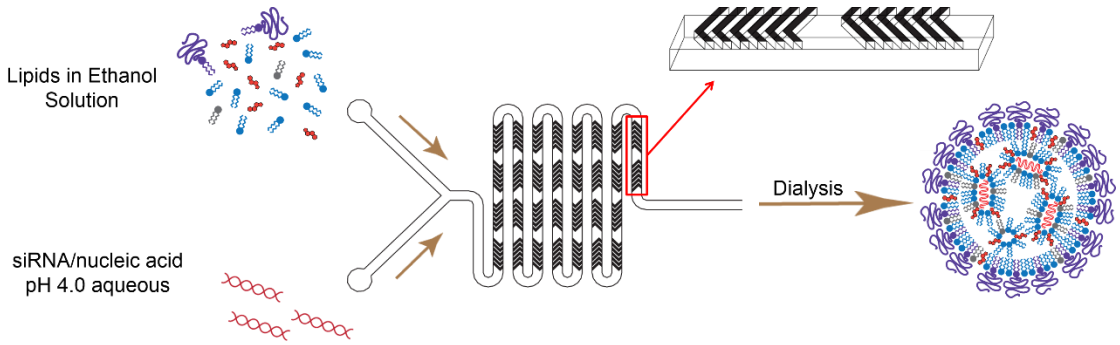

Figure 1.2 Spontaneous Formation of LNP by Rapid Mixing Through a Staggered Herringbone Microfluidic Mixer.

Schematic representation of the staggered herringbone microfluidic mixing chamber. Lipids dissolved in ethanol and nucleic acids dissolved in pH 4 aqueous buffer is injected into a Y-shaped junction. Upon reaching the staggered herringbone structure, the two streams fold on itself, drastically increasing the surface area of contact and promoting mixing by chaotic advection. Rapid mixing mediated by microfluidics occurs very rapidly on the millisecond timescale.

1.2.4 General Composition, Structure and Size

Currently, the most advanced LNP formulations contain siRNA and have diameters less than 100 nm as measured by dynamic light scattering and cryo-transmission electron microscopy (cryoTEM). They are generally composed of ionizable amino-lipids, a phospholipid such as DSPC, cholesterol and a surface PEG-lipid at a molar ratio of 50:10:38.5:1.5. Figure 1.3 depicts the most commonly used LNP components. The ionizable amino-lipid heptatriaconta-6,9,28,31-tetraen-19-yl 4-(dimethylamino)butanoate (DLin-MC3-DMA) is the most active among the amino-lipids depicted in Figure 1.3B. CryoTEM revealed that LNP systems formed by rapidly mixing an ethanol stream containing the lipid mixture with an aqueous stream containing the siRNA, by either a T-junction (Crawford et al., 2011) or microfluidic-based mixing (Belliveau et al., 2012; Leung et al., 2012), have an electron-dense core, which is in contrast to the less dense aqueous cores that are characteristic of conventional liposomes or vesicular structures (Leung et al., 2012; Zhigaltsev et al., 2006). Indeed, these LNP-siRNA systems have an interior lipid core containing siRNA complexed with ionizable cationic lipid, as shown by the absence of ^{31}P NMR signal from free phosphorothioate in the siRNA and the complete protection of siRNA degradation by external RNases (Leung et al., 2012). Computer simulation of the self-assembly of lipids suggests a nanostructured core in which siRNA is located in internal inverted micelles complexed with ionizable amino-lipid (Figure 1.4). Furthermore, DSPC interacts with siRNA phosphate through its choline-headgroup, cholesterol is dispersed evenly between the core and surface, and the PEG-lipid is distributed predominantly on the surface. It is postulated that the rapid mixing of lipid components with the siRNA allows for the formation of nucleating structures composed of siRNA and ionizable amino-lipid. Other LNP systems that contain ASO and a larger proportion of DSPC, which promote bilayer formation, exhibit multilamellar structures. In this case, the nucleic acid is

thought to be sandwiched or entrapped between the concentric bilayers (refer to Section 1.2.3.1). This further supports the hypothesis that, with appropriate mixing techniques, LNP structure and physical properties can be controlled by its lipid constituents. Indeed, a continuum of structures were observed based on varying lipid compositions and siRNA content (Leung et al., 2015). For example, reducing the amount of ionizable amino-lipid from 40 mol% to 20 mol% results in LNP-siRNA that contain lamellar structures. Increasing the saturation of the amino-lipid from linoleyl to oleyl promotes the formation of multilamellar structures within the LNP, while increasing nucleic acid content reduces multilamellar structures. These observations were further extended to other macromolecules such as mRNA, plasmid DNA and negatively charged colloidal gold.

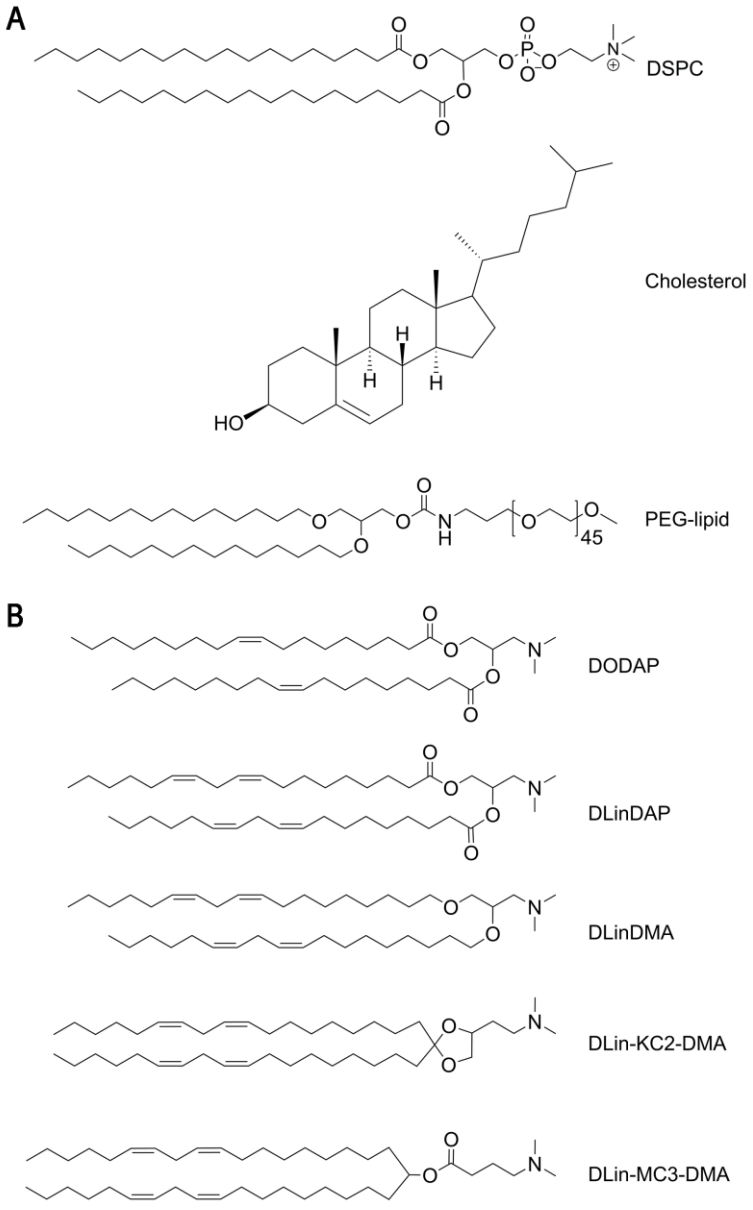

Figure 1.3 Typical Lipid Components Found in LNP.

LNP-siRNA systems are typically composed of four primary components including (A) phosphatidylcholine lipids such as DSPC, cholesterol, PEG-conjugated lipid and (B) an ionizable amino-lipid. Five examples of ionizable amino-lipids that are commonly used in LNP are shown. The amino-lipids are arranged by their ability to mediate gene silencing from top to bottom: DLin-MC3-DMA > DLin-KC2-DMA > DLinDMA > DLinDAP > DODAP.

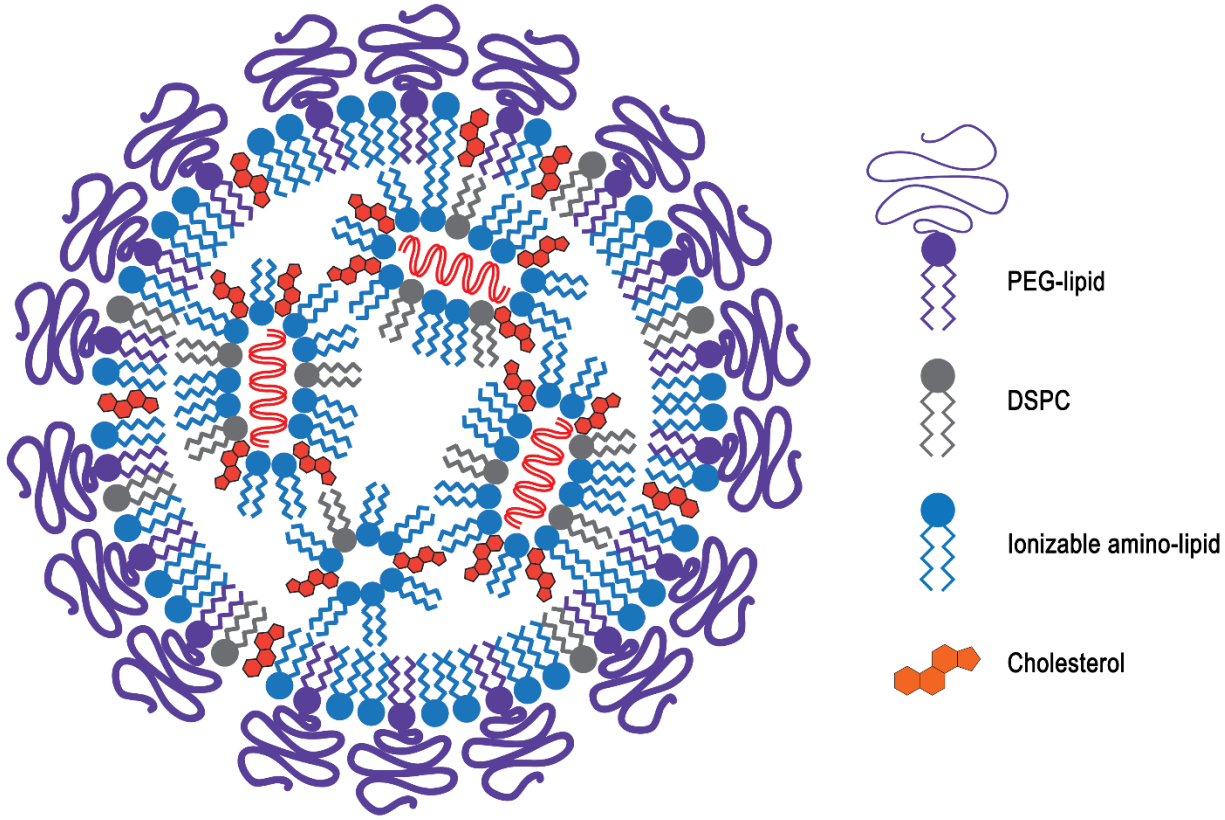

Figure 1.4 Schematic Representation of Lipid Nanoparticles Containing Nucleic Acids.

LNP are composed of four primary lipid components: polyethyleneglycol conjugated lipids (PEG-lipid, purple), structural or helper lipids such as distearoylphosphatidylcholine (DSPC, gray), cationic or ionizable amino-lipids (blue) and cholesterol (orange). During spontaneous formation by rapid mixing methods, the ionizable amino-lipid is cationic, which allows it to interact with the polyanionic nucleic acids. This forms inverted micelle structures which are further coated by other more polar lipid components such as PEG-lipid. Nucleic acid is completely entrapped within the core of the LNP, preventing nuclease access and immune detection.

1.2.5 Cationic and Ionizable Amino-lipids

A major advancement in the design of ionizable amino-lipids was the modulation of their pK_a. pK_a values of 7 and lower have been shown to be critical for encapsulation of nucleic acids and *in vivo* activity (Maurer et al., 2001; Semple et al., 2001). In environments where the pH is below the pK_a of the ionizable lipid (e.g., pH 4.0), the tertiary amino group is protonated and interacts with the negatively charged nucleic acids, thereby promoting the self-assembly of the formulation components. In physiological environments where the pH is above the pK_a of the ionizable lipid (e.g., pH 7.4), the surface of the LNP has an almost neutral charge, resulting in improved circulation and reduced toxicity. Subsequently, in the acidic environment of endosomes, the amino group of the ionizable lipid becomes protonated and associates with the anionic endosomal lipids. This interaction enables the destabilization of the endosomal membranes and promotes the release of siRNA into the cytosol (Hafez et al., 2001; Xu and Szoka, 1996).

The first ionizable amino-lipid that was used for nucleic acid encapsulation was DODAP, which has a pKa of 6.6-7 and one double bond in each of its acyl chains (Figure 1.3B) (Bailey and Cullis, 1994; Maurer et al., 2001; Semple et al., 2001). Subsequent work focused on the impact of the number of double bonds or the degree of unsaturation in the alkyl chain demonstrated that ionizable amino-lipids containing fully saturated alkyl chains showed no silencing of luciferase activity *in vitro,* whereas ionizable amino-lipids containing two or three double bonds per alkyl chain showed enhanced silencing activity (Heyes et al., 2005). Encapsulation efficiencies of siRNA seemed to be compromised using amino-lipids that contain three double bonds per alkyl chain. Therefore, the linoleyl moiety has become the alkyl chain configuration of choice in ionizable lipid development.

Structure-activity relationship studies have guided the synthesis and screening of a large number of ionizable amino-lipids with various types of linkers connecting the amino group and alkyl chains. These studies have identified DLin-KC2-DMA (2,2-dilinoleyl-4-(2-dimethylaminoethyl)-[1,3]-dioxolane) (Semple et al., 2010), and DLin-MC3-DMA (Jayaraman et al., 2012) to be 100-fold and 1000-fold more potent, respectively, in silencing of a hepatic gene (Factor VII) in comparison to the previous generation lipid DLinDMA (1,2-dilinoleyloxy-N,N-dimethyl-3-aminopropane) (Heyes et al., 2005). The ED_{50} (median effective dose) for LNP containing DLin-MC3-DMA to silence Factor VII in mice and TTR in non-human primates was 0.005 mg/kg and 0.03 mg/kg, respectively (Jayaraman et al., 2012). A key finding from these studies was that an optimal lipid pK_a value of 6.2-6.5 was a determining factor of hepatic gene-silencing activity *in vivo*. DLin-MC3-DMA, having a pKa of 6.44, is currently the most active ionizable lipid being used in clinical trials (Section 1.3.1).

In hopes of further promoting biocompatibility, a novel generation of ionizable amino-lipids was synthesized with biodegradable functionalities in the alkyl chains (Maier et al., 2013). These novel lipids were well tolerated and rapidly eliminated from plasma and tissues in animal studies. Importantly, they exhibited excellent potencies ($ED_{50} < 0.01$ mg/kg in mice, similar to that of DLin-MC3-DMA) in both rodent and non-human primate models. Although their relevance to human treatment remains to be proven, these preclinical results for biodegradable LNP-siRNA formulations show great promise for clinical applications.

1.2.6 Steric Barrier for Stability and Prolonged Circulation

Unprotected lipid-based delivery systems are rapidly cleared by the mononuclear phagocyte system (Allen, 1994; Ishida et al., 2002). To overcome this, hydrophilic polyethylene

glycol has been widely used to coat lipid-based delivery systems. The PEG coating prevents aggregation during the formulation process and provides "stealth" like characteristics post i.v. administration (refer to Section 1.1.4). The optimized PEG-lipid characteristics in current LNP-siRNA systems were largely derived from earlier work on PEGylated liposomes (Klibanov et al., 1990; Webb et al., 1998; Woodle and Lasic, 1992) and stabilized plasmid or antisense lipid particles (SPLP or SALP). It was found that the length of the ceramide lipid anchor dictated how long the PEG-lipid remained associated with the LNP. For instance, SPLP or SALP containing PEG-ceramide with C_{20} anchors (PEG-CerC_{20}) exhibited poor transfection efficiency in cultured cells compared to shorter anchor counterparts such as PEG-CerC_{14} or PEG-CerC_8 (Mok et al., 1999; Song et al., 2002; Wheeler et al., 1999). PEG-lipids with longer acyl anchors remain associated with the LNP longer, thus preventing LNP interaction with cells and subsequently with the endosomal membranes. They also provide the LNP with a more durable coat, which extends circulation lifetime (Monck et al., 2000; Tam et al., 2000). Consistent findings were observed when PEG-ceramides were replaced with PEG-succinoyl-diacylglycerols (PEG-s-DAG) that have various acyl anchor lengths (Ambegia et al., 2005). Due to the ease of synthesis and purification, PEG-s-DAG replaced PEG-Cer in later SPLP formulations, and long acyl chain versions of PEG-s-DAG such as PEG-s-distearoylglycerol (PEG-s-DSG) were used to increase circulation lifetime in hopes of exploiting the EPR effect at tumor sites.

Unfortunately, despite being efficacious and non-toxic after a single bolus injection, PEGylated LNP with long acyl anchors (PEG-DSPE (1,2-distearoyl-*sn*-glycero-3-phosphoethanolamine), PEG-s-DSG, or PEG-CerC_{20}) were rapidly cleared upon repeated administration as a result of a robust immune response to the PEG component (Judge et al., 2006; Semple et al., 2005). The use of rapidly dissociating, shorter anchor PEG-lipids such as PEG-s-

dimyristoyl (DMG) or PEG-CerC_{14}, however, mitigated this immunogenic response. Coincidentally, it was also observed that LNP containing PEG-s-DAG progressively lost the PEG moiety due to hydrolysis of its succinate linker, leading to particle aggregation and a reduced shelf-life. In response to this, the succinate linker was replaced with a carbamate linker to confer improved chemical stability without affecting efficacy (Heyes et al., 2006). PEG-lipids containing carbamate linkages are now used in the most advanced LNP-siRNA systems in the clinic.

1.2.7 Promoting Cellular Uptake with Endogenous and Exogenous Ligands

Neutral liposomes have been shown to bind to proteins in serum, exchange components with lipoproteins and acquire factors that can potentially target them to specific cell types (Chonn et al., 1992; Cullis et al., 1998). In particular, they interact with ApoE and ApoA1 (Mendez et al., 1988; Rensen et al., 1997). ApoE, but not ApoA1 or ApoA4, was further found to enhance uptake of neutral liposomes in HepG2 cells and primary hepatocytes (Bisgaier et al., 1989). The role of ApoE in LNP uptake into hepatocytes was confirmed *in vivo* using ApoE-deficient mice (Yan et al., 2005), which cleared LNP more slowly from the circulation and showed at least 20-fold less LNP take up by hepatocytes when compared to wild-type animals. Similarly, LNP-siRNA systems containing ionizable amino-lipids require ApoE for activity (Akinc et al., 2010). Silencing of Factor VII was compromised in mice lacking ApoE or LDL receptor, suggesting that ApoE acts as an endogenous ligand for LNP-siRNA systems that facilitates uptake into hepatocytes via the LDL receptor. The ApoE and LDL receptor dependence is reminiscent of how natural lipoprotein transport occurs within the body (Section 1.1.1). Figure 1.5 depicts the current model for LNP uptake into hepatocytes.

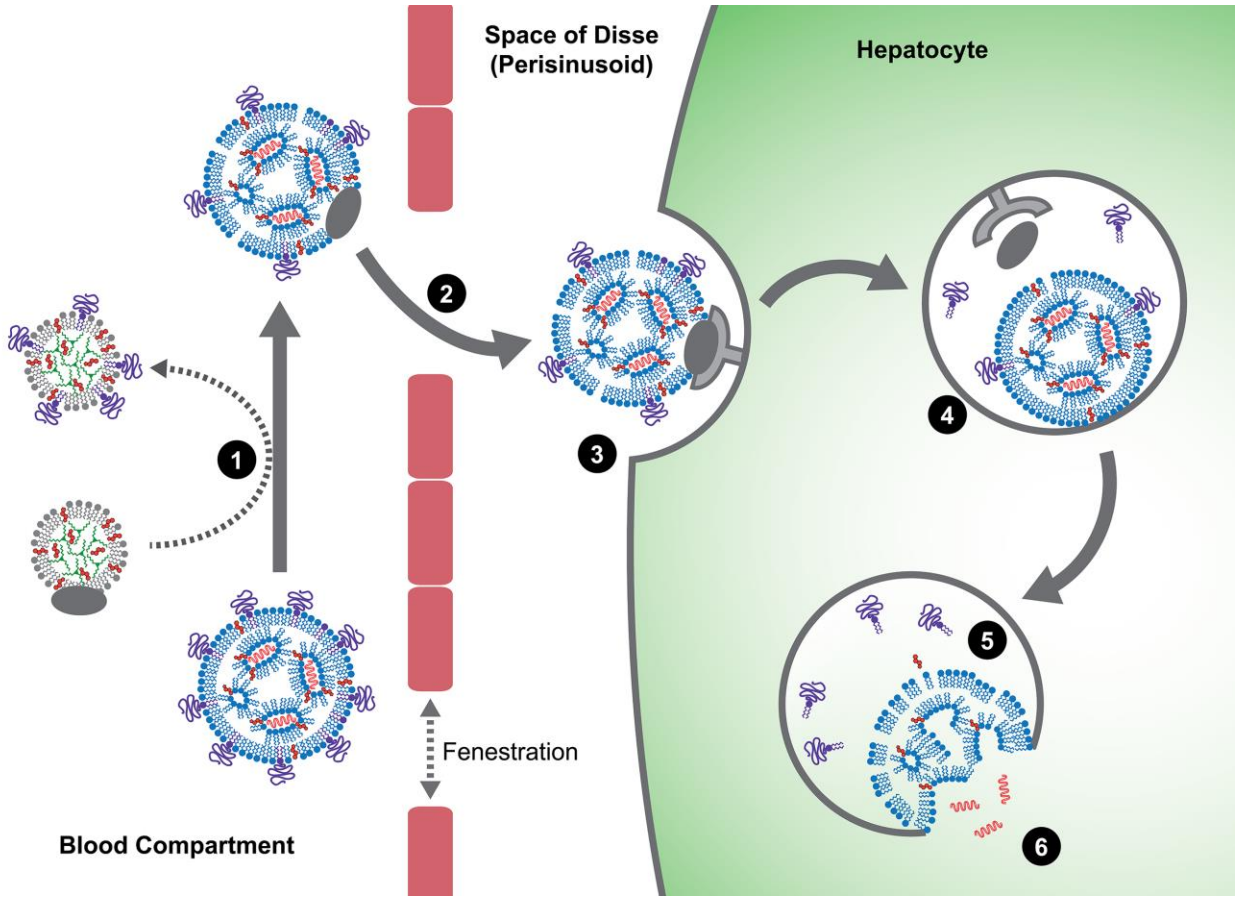

Figure 1.5 Current Model of LNP-siRNA Delivery to Hepatocytes

Following i.v. administration, LNPs rapidly lose its PEG-lipid coat and are opsonized by apolipoproteins such as ApoE (1). LNP are able to extravasate from the circulation and enter the liver sinusoids where there is a significant reduction in blood flow. Here, LNP are able to cross the fenestrated vasculature and enter the Space of Disse where it can directly interact with hepatocytes (2). The ApoE bound to the LNP interact with LDL-receptors found on the surface of hepatocytes, triggering endocytosis (3). As the endosome acidifies, the ionizable amino-lipids become protonated, facilitating the interaction of the now positively charged LNP with the negatively charged endosomal lipids (4). The now cationic amino-lipids disrupt the endosomal membrane (5), resulting in the release of siRNA into the cytoplasm of the hepatocyte (6) where it

is free to interact with the RNA-Induced Silencing Complex (RISC) and cause sequence specific degradation of mRNA and suppression of protein production.

When endogenous ligands are not available, exogenous ligands can be used to enhance uptake of LNP-siRNA systems into target cells. Exogenous ligands such as antibodies, antibody fragments and peptides have been widely used in the field of liposome technology (Allen et al., 2002b; Cressman et al., 2009; Di Paolo et al., 2011; Sapra and Allen, 2003). However, they are expensive and difficult to manufacture, as well as potentially immunogenic. In contrast, small molecule ligands conjugated to the distal end of PEG-lipids can be synthesized and formulated into LNP in a straightforward manner (Akinc et al., 2010; Li and Huang, 2006; Tam et al., 2013). N-acetylgalactosamine (GalNAc), which binds with high affinity to the asialoglycoprotein receptor (ASGPR) found on hepatocytes, have been shown to rescue gene-silencing activity of LNP-siRNA systems in ApoE deficient mice (Akinc et al., 2010). Other exogenous small molecule ligands have shown utility in non-hepatic cells. Anisamide, which interacts with sigma receptors, increases delivery and activity of siRNA containing nanoparticles in lung tumors and metastases (Chen et al., 2009; Li et al., 2008; Li and Huang, 2006). Furthermore, strophanthidin, a cardiac glycoside that binds to the ubiquitously expressed cell surface receptor Na^+/K^+ ATPase, has been shown to enhance delivery of LNP-siRNA to various cell types originating from the ovary, breast, pancreas, lung and prostate (Tam et al., 2013). While the delivery of LNP using a promiscuous ligand may be non-specific, target specificity can be conferred using siRNA against tissue specific disease causing genes.

1.3 Clinical Evaluation of siRNA Delivered by Lipid Nanoparticles

1.3.1 LNP-siRNA in the Clinic

Because LNP have preferential affinity for the liver, there are several LNP-siRNA in development for disorders such as hepatocellular carcinoma, hypercholesterolemia and transthyretin-mediated amyloidosis. LNP formulations with similar composition and structures (refer to Section 1.2) under clinical evaluation utilize either DLinDMA (first generation LNP) or DLin-MC3-DMA (second generation LNP).

One of the first demonstrations of LNP-siRNA activity in humans is by Alnylam Pharmaceuticals (Cambridge, MA). Alnylam's ALN-VSP is an LNP that targets kinesin spindle protein (KSP) and vascular endothelial growth factor (VEGF); it utilizes DLinDMA and contains two siRNAs at a 1:1 molar ratio (Tabernero et al., 2013). In preclinical murine orthotopic liver tumor models, a single i.v. administration of ALN-VSP into mice with established hepatocellular carcinoma resulted in dramatic reductions (up to 50%) of both KSP and VEGF mRNA levels. Within 48 hours of the injection, phenotypic changes as a result of KSP knockdown were observed and tumor cells were arrested in mitosis. Reductions in microvascular density and intratumoral hemorrhaging were also observed and is thought to be a result of VEGF knockdown. After 3 weeks of repeated administration (6 injections at siRNA dose of 4 mg/kg body weight), an approximate improvement of 50% in mean survival was observed in tumor bearing mice. These results in addition to non-human primate data warranted a Phase I clinical study in 2009, with an enrollment of 41 cancer patients. This study successfully demonstrated siRNA-mediated mRNA degradation in the liver and that biweekly administration was generally safe and well tolerated with dose-limiting toxicities (e.g.: thrombocytopenia, hypokalemia, hepatic failure) observed at 1.25 and 1.5 mg/kg. Due to the disease progression in the enrolled patients and the heterogeneity of the tumor

biopsies, it was difficult to determine if KSP and VEGF were downregulated in tumors, but both KSP and VEGF siRNA were present. Prolonged disease stabilization of up to 1.5 years was also observed in one patient with extensive metastasis who showed complete response to treatment.

In 2011, another LNP-siRNA formulation developed by Alnylam Pharmaceuticals entered Phase I clinical trials (Fitzgerald et al., 2014). ALN-PCS targets the proprotein convertase subtilisin/kexin type 9 (PCSK9) for the treatment of familial hypercholesterolemia. PCSK9 is primarily expressed in the liver and intestine, and loss-of-function mutations result in reduced plasma LDL levels and consequently reduced risks for heart disease. Other than the lower LDL levels, humans and mice with reduced PCSK9 are generally healthy (perhaps arguably healthier), making this an attractive target for siRNA therapeutics. With a single i.v. administration of ALN-PCS at an siRNA dose of 0.4 mg/kg body weight, serum PCSK9 levels were reduced by approximately 70% by day 3 post-injection and LDL-cholesterol was reduced by 40%. The duration of PCSK9 and LDL-cholesterol reduction was also dose-dependent with higher doses resulting in more persistent reductions. Not surprisingly, the Phase I results agree with non-human primate preclinical studies. In favour of the novel and propriety Enhanced Stabilization Chemistry platform, chemically modified siRNA against PCSK9 conjugated to a GalNAc-targeting moiety has been developed to largely replace the LNP-based ALN-PCS.

One of the most advanced LNP formulations is a therapeutic that utilizes DLin-MC3-DMA and carries siRNA against transthyretin (TTR). TTR is a serum transport protein that is primarily synthesized in the liver and carries thyroxine and retinol binding protein. Mutations in TTR causes misfolding, which promotes the formation of fibrils that can eventually deposit in various tissues as amyloid plaques (Sekijima et al., 2008; Ueda and Ando, 2014). These amyloid deposits prevent tissues and organs from functioning properly and often manifest as cardiomyopathies or

neuropathies. There is evidence suggesting that a reduction of 50% in disease-causing or fibril forming protein can result in positive clinical outcomes (Lachmann et al., 2003). Currently, Alnylam Pharmaceuticals is developing ALN-TTR02, also known as Patisiran, which targets both wild-type and mutant TTR to reduce serum TTR levels and prevent the progression of amyloid formation. Preclinical studies in non-human primates show that > 80% reduction in serum TTR can be achieved with a single i.v. dose of LNP-siRNA (with an siRNA dose of 0.3 mg/kg body weight) (Coelho et al., 2013). At an siRNA dose of 0.1 mg/kg body weight, ALN-TTR02 is able to reduce serum TTR by approximately 70% whereas ALN-TTR01 (which utilizes DLinDMA) is only able to reduce serum TTR by 45% at a much higher siRNA dose of 10 mg/kg. This dramatic improvement in LNP-siRNA potency again demonstrates the importance of the ionizable amino-lipid. Furthermore, a dose dependent reduction in TTR was observed, indicating that ALN-TTR02 is indeed responsible for mediating gene silencing. At the siRNA dose of 0.3 mg/kg, persistent gene silencing can be observed for over a month, and repeated i.v. injections every 4 weeks results in repeated reduction in serum TTR. It is important to note that at 0.3 mg/kg, Phase I clinical trial data matches that of the non-human primate pre-clinical data, providing confidence for this LNP-siRNA strategy. Phase II multi-dose studies show that administration of ALN-TTR02 at 0.3 mg/kg every three weeks was generally well tolerated and led to a rapid, dose dependent reduction of both wildtype and mutant (Val30Met) TTR (Suhr et al., 2015). The maximum knockdown achieved was impressive at 96%. Preliminary Phase II open label extension studies show that sustained TTR knockdown of ~80% is achieved after 168 days. Neurological symptoms due to amyloid buildup stabilized and improvements were seen over 6 months. Currently, Phase III development of ALN-TTR02 (Patisiran) is underway.

Other LNP-based therapeutics currently under Phase I/II clinical development include TKM-PLK1 (TKM-080301) and ARB-1467, both of which are developed by Arbutus Biopharma, formerly Tekmira Pharmaceuticals. TKM-PLK1 contains siRNA against polo-like kinase 1, a protein involved in tumor cell proliferation. TKM-PLK1 is currently being evaluated for three indications: gastrointestinal neuroendocrine tumors, adrenocortical carcinoma and hepatocellular carcinoma. ARB-1467 contains multiple siRNA against the hepatitis B virus (HBV) to ensure that all variants of HBV are targeted.

1.3.2 Observations, Challenges and Limitations of Current LNP Systems for Nucleic Acid Delivery

Mild infusion related reaction (IRRs) have been observed following administration of LNP-siRNA (Barros and Gollob, 2012; Coelho et al., 2013; Fitzgerald et al., 2014; Suhr et al., 2015; Tabernero et al., 2013). These mild reactions have been fairly well controlled by co- or pre-administration with glucocorticoids such as dexamethasone. Because siRNA are short 19-21mer nucleic acids, it is relatively easy to modify the bases to mask it from immune detection. Significant progress has been made in the chemical modification of RNA such that it is immune silent. These improvements, however, are limited to shorter nucleic acid species like ASO or siRNA. Longer nucleic acid polymers such as plasmid DNA or mRNA are both difficult and costly to modify, and require delivery vehicles such as LNP (refer to Section 1.2.1). In addition, given that IRRs for LNP containing chemically modified, immune silent siRNA are still observed, more severe reactions are suspected to occur for LNP containing longer nucleic acid polymers. This continues to be a significant clinical obstacle for the development of nucleic acid therapeutics.

Another challenge is the ease of administration of LNP-based drugs. LNP systems were designed for systemic delivery and require slow i.v. infusions to reduce the IRRs. Although i.v. injection is the most direct route of administration and results in the greatest bioavailability, it also requires the help of trained professionals. This is a burden to existing health care systems and may result in compliance issues. This route of administration may be tolerable for more life threatening and debilitating conditions such as cancer; however, it is less appealing for manageable metabolic disorders such as moderate high cholesterol (not to be confused with more sever hypercholesterolemia). Indeed, in the development of siRNA therapeutics for liver applications, there is a preference for novel chemical modifications of nucleic acids that allow for direct subcutaneous (s.c.) administration of the siRNA (Nair et al., 2014; Sehgal et al., 2015). These modifications not only prevent rapid degradation but also integrates a liver targeting aspect. Although much higher siRNA doses are required to achieve similar degrees of gene silencing when compared to the i.v. administered LNP-siRNA, s.c. injections enable patient self-administration and reduces the costs of manufacturing. Advances in chemical modifications to enhance stability, evade immune detection and target the liver have drastically increased the therapeutic index of siRNA despite the need for much higher doses. At the moment, this technology is only available for siRNA and short nucleic acid species.

1.4 Thesis Objectives

Recent advances in LNP systems for *in vivo* delivery of siRNA have dramatically improved the potency of siRNA-mediated gene silencing and are undergoing clinical development for various diseases, as discussed in Section 1.3.1. The overall objective of this thesis is to build on

the existing LNP technologies and develop more effective and safer delivery vehicles of nucleic acid therapeutics.

As noted, current LNP-siRNA formulations are optimized for activity in the liver after i.v. administration. There are, however, compelling reasons to develop LNP-siRNA that can be s.c. administered. These include the potential for self-administration, a prolonged therapeutic window (due to a depot effect and access to cell types that are in contact with the lymphatic system, such as immune cells), and increased tissue availability through the circulation. In order to reach distal tissues beyond the local lymph nodes, LNP must drain from the site of injection to the lymphatic system and subsequently enter the arterial circulation. In Chapter 3, two key properties were explored to develop LNP for s.c. administration: 1) Particle size and effect on tissue penetration and 2) Degree and robustness of PEG-coating. We hypothesized that having a persisting PEG-coat prevents opsonization and particle destabilization and therefore immune-related clearance, while small particle sizes allow the LNP to better traverse the loose connective tissue and promote lymphatic drainage and systemic delivery. The ability of existing LNP-siRNA to mediate gene silencing at the liver was explored. The effects of size and PEG-coating on the rate of drainage from the injection site, pharmacokinetics and biodistribution (PK/BD), and the duration and reproducibility of gene silencing was determined for LNP formulations administered subcutaneously.

In the work presented in Chapter 3, we found that small LNP (< 45 nm in diameter) are able to reach the circulation after s.c administration and indeed others have shown that small particles better penetrate into tumor tissue (Cabral et al., 2011; Dreher et al., 2006; Huo et al., 2013; Popovic et al., 2010). Interestingly, it was shown that small LNP-siRNA were less efficacious at hepatic gene silencing post s.c. administration. Continuing the efforts to develop

highly potent small LNP-siRNA, in Chapter 4 we sought to understand this size-related impairment. In order to remove confounding effects due to s.c. administration such as the need to drain from the site of injection, hepatic gene silencing of LNP with sizes ranging from 30-100 nm was characterized following i.v administration. It was shown that the decreased potency of small 30 nm LNP-siRNA systems can be attributed, at least in part, to a pronounced instability of LNP-siRNA systems as their size is reduced below 45 nm diameter. Here, we demonstrated that improvements in activity and stability can be achieved with proper LNP design.

Finally, motivated by the observations that LNP-siRNA administered subcutaneously results in skin irritations likely as a result of local immune stimulation (Chapter 3) and that the potency of small LNP-siRNA cannot be further improved with existing components of the LNP (Chapter 4), lipophilic pro-drugs that can efficiently incorporate into LNP were designed. Recognizing that most LNP-siRNA systems used in the clinic require co- or pre-dosing of corticosteroids to ameliorate infusion-related reactions and that the skin irritations post s.c. administration of LNP are likely caused by immune stimulation, the first series of compounds synthesized is a pro-drug of a potent corticosteroid, dexamethasone, that is currently used to reduce IRRs for LNP drugs. In Chapter 5, we demonstrate that incorporation of dexamethasone directly into LNP can greatly reduce the level of proinflammatory cytokines induced compared to co-administration of free dexamethasone with LNP. Various versions of these pro-drugs were synthesized and tested to better understand the requirements for effective incorporation, the ability for esterases to access the pro-drug, the tolerability, and the ability of these pro-drugs to mitigate cytokine induction by using LNP containing immune stimulatory DNA or *in vitro* transcribed mRNA.

Chapter 2: Material and Methods

2.1 Materials

(R)-2,3-bis(octadecyloxy)propyl-1-(methoxy polyethylene glycol 2000) carbamate (PEG-DMG) and (R)-2,3-bis(stearyloxy)propyl-1-(methoxy poly(ethylene glycol)2000 carbamate (PEG-DSG) were provided by Alnylam Pharmaceuticals or synthesized as previously described (Akinc et al., 2008). N-acetylgalactosamine cluster conjugated PEG-DSG (GalNAc-PEG) were provided by Alnylam Pharmaceuticals. 3-(dimethylamino)propyl(12Z,15Z)-3-[(9Z,12Z)-octadeca-9,12-dien-1-yl]henicosa-12,15-dienoate (DMAP-BLP) and (6Z,9Z,28Z,31Z)-Heptatriaconta-6,9,28,31-tetraen-19-yl4-(dimethylamino)butanoate (DLin-MC3-DMA) were provided by Alnylam Pharmaceuticals or synthesized by BioFine International (Vancouver, BC) (Jayaraman et al., 2012; Rungta et al., 2013). 1,2-distearoyl-sn-glycero-3-phosphocholine (DSPC) was purchased from Avanti Polar Lipids (Alabaster, AL) and cholesterol was purchased from Sigma-Aldrich (St. Louis, MO). The sense and antisense strand sequences of siRNA against Factor VII (siFVII) are 5′-GGAucAucucAAGucuuAcT*T-3′ and 5′-GuAAGAcuuGAGAuGAuccT*T-3, respectively (Akinc et al., 2009; Akinc et al., 2008; Semple et al., 2010). 2'-Fluoro-modified nucleotides are represented in lower case and phosphorothioate linkages are represented by asterisks. All siRNA were either provided by Alnylam Pharmaceuticals or purchased from Integrated DNA Technologies (San Diego, CA). Phosphorothioated unmethylated cytosine-guanine containing oligonucleotides (CpG) complementary to the initiation codon region of the human/mouse c-myc proto-oncogene (5'-AACGTTGAGGGGCAT-3') was purchased from TriLink Biotechnologies (San Diego, CA). This sequence has been previously identified as highly immunostimulatory when administered to mice due to the presence of the CpG dinucleotide motif

(de Jong et al., 2007; Mui et al., 2001; Semple et al., 2005; Wilson et al., 2007). *In vitro* transcription of luciferase mRNA was carried out as described previously (Wang et al., 2013).

2.2 Preparation of Lipid Nanoparticle-siRNA by Rapid Mixing Techniques

Ionizable amino-lipid (either DMAP-BLP or DLin-MC3-DMA), DSPC, cholesterol and PEG-DMG were dissolved in ethanol at the mole ratio of 50:10:(39.75-x):(0.25+x), respectively where the quantity of cholesterol and PEG-DMG are altered accordingly to ± x. The lipids in ethanol and siRNA prepared in 25 mM acetate buffer (pH 4.0) was then injected into microfluidic mixers (Precision Nanosystems, Vancouver, BC) at a flow rate ratio of 1:3 respectively with a combined final flow rate of 4 mL/min. The LNP-siRNA mixtures were immediately dialyzed for 4 hr against a pH 6.7 buffer containing 50 mM MES and 50 mM citrate followed by phosphate buffered saline overnight (12-14 kD MWCO dialysis tubing, Spectrum Labs, Rancho Dominguez, CA). LNP-siRNA were then filtered through a 0.2 µm filter (Pall, Ville St. Laurent, Quebec) and concentrated to approximately 1 mg/mL siRNA using Amicon Ultra centrifugal filters (Millipore, Billerica, MA). The theoretical siRNA-to-lipid ratios for all formulations were maintained at 0.056 mg siRNA per µmole lipid which results in N/P charge ratios (ratios of the charge on the cationic lipid, assuming it is in the positively charged protonated form, to the negative charge on the siRNA oligonucleotide) of 3. Formulations that deviated more than 10% from the theoretical target were not used. In experiments requiring radiolabelled LNP, ^{3}H-cholesteryl hexadecylether (^{3}H-CHE, Perkin Elmer; Boston, Massachusetts) was incorporated at the ratio of 3.9 µCi/µmol total lipid. All LNP preparation work was carried out at room temperature.

Similarly, LNP containing CpG were prepared by rapid mixing methods as described previously (Belliveau et al., 2012; Jeffs et al., 2005; Semple et al., 2010). Briefly, DMAP-BLP,

DSPC, cholesterol and PEG-DMG were dissolved in ethanol at the mole ratio of 50, 10, 38.5 and 1.5 respectively. Dexamethasone pro-drugs were incorporated at 0, 1, 4 or 10 mol% at the expense of DMAP-BLP. CpG were dissolved in 25 mM sodium acetate buffer at pH 4.0 such that the final mixture would have a CpG-to-lipid weight ratio of 0.1. Ethanolic and aqueous mixtures were mixed together at a 1:3 volume and flow rate ratio with final flow rates > 2 mL/min at room temperature with a t-junction. Resulting mixtures were dialyzed against phosphate buffered saline (PBS) overnight.

For LNP containing *in vitro* transcribed mRNA, DLin-MC3-DMA was used instead of DMAP-BLP and the mRNA-to-lipid ratio was maintained at 0.028 mg mRNA per µmole lipid. CpG concentration and entrapment efficiency were determined by measuring the absorbance at 260 nm after lipids were extracted using the Bligh and Dyer method (Bligh and Dyer, 1959). Lipid concentrations were determined by measuring the cholesterol content (Cholesterol E Assay, Wako Chemicals, Richmond, VA).

2.3 Analysis of Lipid Nanoparticles

LNP size and morphology were determined using cryogenic-transmission electron microscopy (cryoTEM) as described previously (Belliveau et al., 2012; Leung et al., 2012). LNP size (number weighting) was further confirmed by dynamic light scattering (DLS) using the Malvern Zetasizer NanoZS (Worcestershire, UK). LNP formulations generally had polydispersity indexes (PdI) below 0.05. Formulations with PdI > 0.1 were not used for further studies. siRNA encapsulation efficiency was determined using the Quant-iT Ribogreen RNA assay (Life Technologies, Burlington, ON). Briefly, LNP-siRNA was incubated at 37°C for 10 min in the presence or absence of 1% Triton X-100 (Sigma-Aldrich, St. Louis, MO) followed by the addition

of the ribogreen reagent. The fluorescence intensity (Ex/Em: 480/520 nm) was determined and samples treated with Triton X-100 represent total siRNA while untreated samples represent unencapsulated siRNA. Total lipid was determined by measuring the cholesterol content using the Cholesterol E assay (Wako Chemicals, Richmond, VA) and the siRNA concentration was determined by measuring the absorbance at 260 nm. mRNA encapsulation efficiency was determined similarly with Quant-iT Ribogreen RNA assay. CpG concentration and entrapment efficiency were determined by measuring the absorbance at 260 nm after lipids were extracted using the Bligh and Dyer method (Bligh and Dyer, 1959).

2.4 *In Situ* Determination of the Apparent Acid Dissociation Constant of LNP-siRNA

Apparent acid dissociation constant (pKa) of LNP-siRNA was determined as previously described (Jayaraman et al., 2012). Briefly, 2-(p-toluidino)-6-napthalene sulfonic acid (TNS, Sigma-Aldrich, St. Louis, MO) was dissolved in water to a working concentration of 0.6 mM and LNP-siRNA was diluted with PBS to 0.05-0.1 mM total lipid. 0.12 mL of diluted LNP-siRNA was mixed with 20 µL of diluted TNS to a final volume of 2 mL with pH 2.5-11 buffer containing 10 mM HEPES, 10 mM MES and 10 mM ammonium acetate. Samples were mixed thoroughly and the fluorescence intensity was measured (Ex/Em: 321/445 nm) using a Perkin Elmer LS55. A sigmoidal best fit analysis was applied using Sigma Plot and the pKa was measured as the pH at half-maximal fluorescence intensity.

2.5 *In Vitro* Lipid and siRNA Dissociation

LNP were prepared with 0.5 mol% of ^{14}C labelled DSPC (American Radiolabeled Chemicals, Saint Louis, MO) and 0.25 mol% of ^{3}H labelled PEG-DMG (Alnylam

Pharmaceuticals, Cambridge, MA) or 0.5 mol% of ^{14}C labelled dilinoleylmethyl-4-dimethylaminobutyrate (DLin-MC3-DMA, Alnylam Pharmaceuticals) and 0.002 mol% of ^{3}H-CHE. The ^{3}H:^{14}C ratios were maintained at approximately 3:1. For siRNA dissociation studies, siRNA conjugated to Quasar 570 fluorophore (Alnylam Pharmaceuticals) was used. LNP were incubated for 0, 0.25, 1, 2, 4 and 8 hr at 37°C in 200 µL of sterile mouse plasma (Cedarlane, Burlington, Ontario) at a final lipid concentration of 0.3 mM. At the various time-points, samples were loaded onto a 1.5 × 27 cm Sepharose CL-4B column (Sigma-Aldrich, St. Louis, MO). 30 × 2 mL fractions were collected and analyzed by liquid scintillation counting. To determine the amount of siRNA remaining in the LNP fractions, 135 µL of each fraction was incubated with 0.5 mM hexaethylene glycol monodecyl ether (Sigma-Aldrich, St. Louis, MO) and the fluorescence at 590 nm was measured. All dissociation rates were estimated from a linear fit of the first four timepoints. For experiments monitoring Forster Resonance Energy Transfer (FRET) as a measure of particle stability, LNP were prepared as described previously with the addition of 1 mol% each of 1,2-dioleoyl-sn-glycero-3-phosphoethanolamine-N-(7-nitro-2-1,3-benzoxadiazol-4-yl) (NBD-DOPE) and 1,2-dioleoyl-sn-glycero-3-phosphoethanolamine-N-(lissamine rhodamine B sulfonyl) (LRB-DOPE). LNP were incubated at 37°C in mouse plasma for up to 24 hr at a final lipid concentration of 0.3 mM. Fluorescence of NBD-DOPE was measured (Ex/Em: 485/530 nm) in the presence or absence of 1.5% Triton X-100.

2.6 Pharmacokinetics and Biodistribution

^{3}H-CHE-labelled LNP (based on siRNA concentration) were injected by i.v. or s.c. under the loose interscapular skin at the back of the neck of female CD1 mice (Charles River Laboratories, Wilmington, MA). Mice were euthanized 15 min to 48 hr post-injection and tissues

were collected. To determine LNP concentration, approximately 600 mg of tissue was homogenized using the FastPrep homogenizer from MP Biomedicals (Santa Ana, CA) and incubated with 0.5 mL of Solvable (Perkin Elmer) at 50°C overnight. Samples were cooled then decolourized with the addition of 200 uL of 30% (v/v) hydrogen peroxide followed by the addition of 5 mL of Pico-Fluor Plus scintillation fluid (Perkin Elmer). To determine LNP concentration in blood, 100 µL of whole blood was added directly to solvable and hydrogen peroxide and allowed to decolourize overnight before the addition of Pico-Fluor Plus. All samples were read on a Beckman LS 6500 liquid scintillation counter. All procedures were approved by the Animal Care Committee at the University of British Columbia and were performed in accordance with guidelines established by the Canadian Council on Animal Care.

2.7 *In Vivo* LNP-siRNA Activity in Mouse Factor FVII Model

LNP-siRNA were diluted with PBS such that injection volumes were maintained at 10 mL/kg body weight and administered (based on siRNA concentration) either i.v. or s.c. under the loose interscapular skin in 6-8 weeks old female C57Bl/6 mice (Charles River Laboratories, Wilmington, MA). Animals were euthanized after 24 hr and blood was collected via intracardiac sampling. Serum was separated from whole blood using Microtainer Serum Seperator tubes (Becton Dickinson, Franklin Lakes, NJ). To study FVII knockdown over time, at 1, 2, 4, 7, 11, 15, 21 and 28 days post-injection, 20-30 µL of blood was collected from the lateral saphenous vein. Blood samples were allowed to coagulate at 4°C overnight and the serum was separated followed by centrifugation for 15 min at 12,000 rpm. The residual serum FVII levels were determined using the Biophen VII chromogenic assay (Aniara, Mason, OH) according to manufacturer's protocol and normalized to that of control mice injected with PBS.

2.8 Synthesis of Dexamethasone Pro-drugs

Log P (or Log D) values were predicted using MarvinSketch v6.1.2 following modified parameters previously described (Viswanadhan et al., 1989). Detailed descriptions of the synthesis of LD001-005 used in Chapter 5 can be found in Appendix A.

2.9 *In Vitro* Degradation of Dexamethasone Pro-drugs

To determine the biodegradability of the LD001-005, 1 mg/mL LNP was incubated in mouse plasma (Cedarlane, Burlington, Ontario) or PBS supplemented with 10U of purified porcine esterase (Sigma-Aldrich, St. Louis, MO) for up to 4 hours at 37°C. Post incubation, four volumes of chloroform/methanol (2:1) were added and the mixture was vortex mixed. Samples were centrifuged at 13,000g for 5 minutes and the upper phase was discarded. The remaining organic phase was dried down under vacuum and the resulting lipid extract was dissolved in methanol/acetonitrile (1:1). Quantity of parent dexamethasone pro-drug was determined by ultra high pressure liquid chromatography (UHPLC) on a Waters Acquity H-Class UHPLC System equipped with a BEH C18 column (1.7 µm, 2.1×100 mm) and a photodiode array detector. Separation was achieved at a flow rate of 0.5 mL/min, with a mobile phase consisting of a linear methanol-water gradient (85:15 to 100:0) over 5 minutes at a column temperature of 55ºC. The absorbance at 239 nm was measured and the analyte concentration was determined using calibration curves.

2.10 *In Vitro* LNP Tolerability by MTT and Hemolysis

In vitro LNP tolerability was determined by performing an MTT cell proliferation assay on cultured HeLa cells. Briefly, 10,000 cells/well were seeded in 96-well plates, grown overnight and treated with various concentrations of LNP (5×10^{-7} to 5 mg/mL, with or without pro-drug) for 24 h. Cells were then incubated with 1 mg/mL of 3-[4,5-Dimethylthiazol-2-yl]-2,5-diphenyl-tetrazolium bromide (MTT, Sigma-Aldrich, St. Louis, MO) in 100 µL of complete media for 2 h followed by an overnight incubation with 100 µL of 20% sodium dodecyl sulfate dissolved in dimethylformamide/water (1:1) at pH 4.7 at 37°C. Absorbance at 570 nm was measured after the overnight incubation and % viability was determined by normalizing the absorbance of LNP treatment with PBS controls.

The ability of LNP to cause hemolysis was. Briefly, human erythrocytes (RBC) (Innovative Research, Novi, MI) were washed three times with cold isotonic saline (0.9% w/v NaCl in water) and resuspended in pH 7.4 PBS to a final concentration of 4% vol/vol. LNP (made with varying amounts of PEG-lipid or with dexamethasone pro-drug) were then incubated with the RBC solution at a final lipid concentration of 0.15 mg/mL for 1 hour at 37°C. RBC solutions incubated with saline or 0.2% vol/vol Triton X-100 were used as controls. Samples were then cooled and centrifuged for 5 minutes at 1000×g at 4℃ and the supernatant was removed and the absorbance at 562 nm was determined. % hemolysis was determined by normalizing the absorbance at 562 nm to Triton X-100 treated samples.

2.11 *In Vivo* Immune Suppression by LNP with Dexamethasone Pro-drugs.

6-8 Weeks old female C57Bl/6 mice (Charles River Laboratories, Wilmington, MA) were injected intravenously with Dex-LNP containing CpG (10 mg/kg) or mRNA (3 mg/kg). Animals

were euthanized 2 and 4 hours post-injection and blood was collected via intracardiac sampling. Plasma was separated from whole blood by centrifugation and analyzed for proinflammatory cytokines using the Mesoscale Proinflammatory Multiplex kit (Rockville, MD). All procedures were approved by the Animal Care Committee at the University of British Columbia and were performed in accordance with guidelines established by the Canadian Council on Animal Care.

Chapter 3: Development of Lipid Nanoparticle Formulations of siRNA for Hepatocyte Gene Silencing Following Subcutaneous Administration

3.1 Synopsis

Recently developed lipid nanoparticle (LNP) formulations of siRNA have proven to be effective agents for hepatocyte gene silencing following intravenous administration with at least three LNP-siRNA formulations in clinical trials. The aim of this work was to develop LNP-siRNA systems for hepatocyte gene silencing that can be administered subcutaneously (s.c.). Three parameters were investigated, namely LNP size, residence time of the polyethylene glycol (PEG)-lipid coating and the influence of hepatocyte-specific targeting ligands. LNP sizes were varied over the range of 30 to 115 nm in diameter and PEG-lipid that dissociates rapidly (PEG-DMG) and slowly (PEG-DSG) were employed. In mice, results show that large (~80 nm) LNP exhibited limited accumulation in the liver and poor Factor VII (FVII) gene silencing at 1 mg siRNA/kg body weight. Conversely, small (~30 nm) LNP systems showed maximal liver accumulation yet still had minimal activity. Interestingly, intermediate size (~45 nm) LNP containing PEG-DSG exhibited nearly equivalent liver accumulation as the smaller systems following s.c. administration but reduced FVII levels by 80% at 1 mg siRNA/kg body weight. Smaller systems (~35 nm diameter) containing either PEG-DMG or PEG-DSG were less active, however addition of 0.5 mol% of a GalNAc-PEG lipid to these smaller systems improved activity to levels similar to that observed for the ~45 nm diameter systems. In summary, this work shows that appropriately designed LNP-siRNA systems can result in effective hepatocyte gene silencing following s.c administration and has been published (Chen et al., 2014).

3.2 Results

3.2.1 LNP-siRNA Systems Containing PEG-DSG Exhibit Maximum Delivery to Liver Following Subcutaneous Administration

Previous investigations have shown that the diameter of LNP-siRNA systems can be modulated over the range of 25-100 nm by varying the proportion of PEG-lipid in the formulation using a microfluidic mixing process (Belliveau et al., 2012). As the lipid composition employed here is different than used previously, we examined the size distribution achieved for LNP-siRNA systems composed of DMAP-BLP, DSPC, cholesterol and PEG-DMG in the molar ratios 50:10:(39.75-x):(0.25+x), where x was varied from 0 to 4.75, encapsulating siRNA at a N/P (+/-) charge ratio of 3. The total amount of PEG-lipid was therefore varied from 0.25 to 5.0 mol%. The size and structure of these LNP-siRNA systems were determined by cryoTEM and DLS (Figure 3.1). LNP-siRNA systems of sizes ranging from 30 nm to 115 nm in diameter were generated that exhibited electron dense cores as previously described (Belliveau et al., 2012; Leung et al., 2012) (Figure 3.1 A-D). Particle sizes determined using DLS were consistent to those determined using cryoTEM (Figure 3.1E). Size differences compared to previous reports (Belliveau et al., 2012) can be attributed to the different lipid compositions employed. Hereafter for simplicity, reported particle sizes are rounded to the nearest multiple of five and based on DLS measurements.

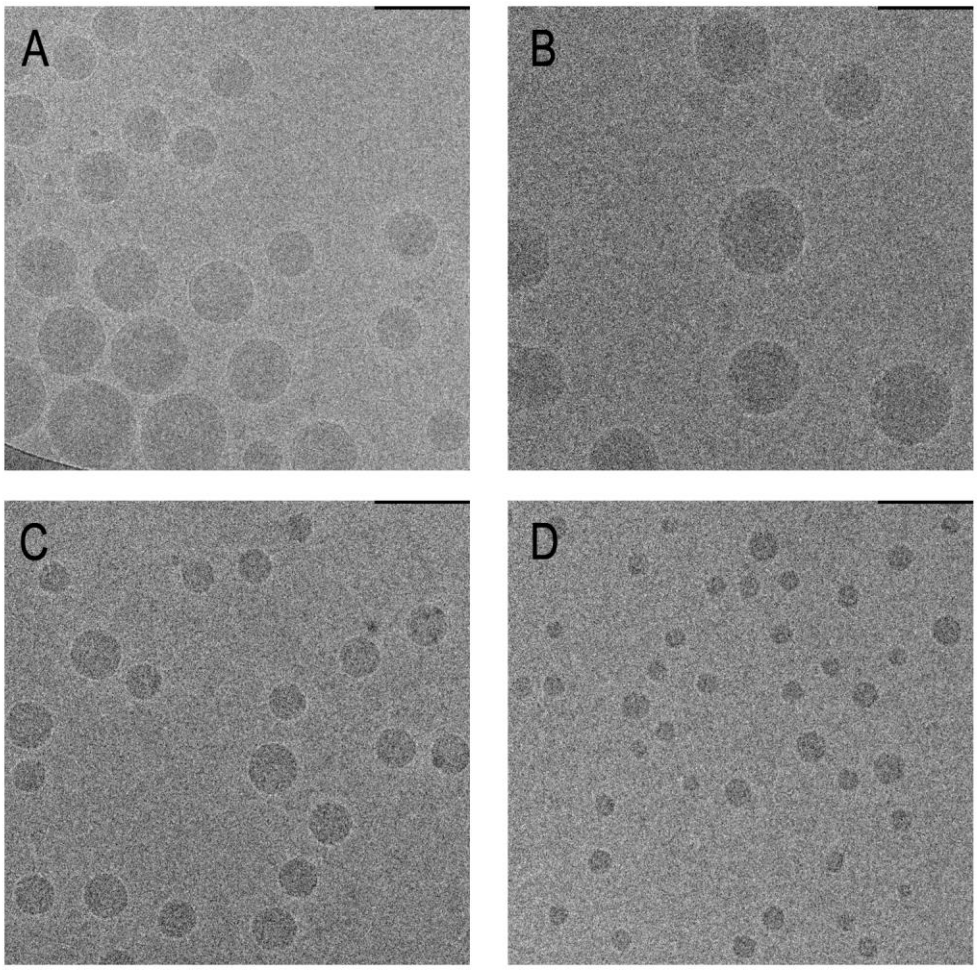
A
B
C
D

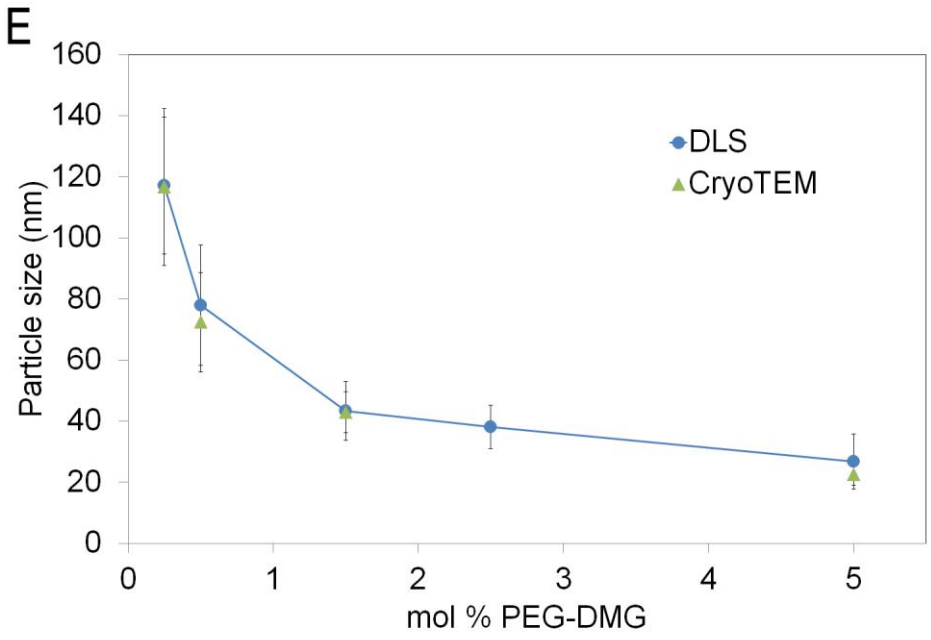
E
160
140
120
100
80
60
40
20
0
Particle size (nm)
0
1
2
3
4
5
mol % PEG-DMG
DLS
CryoTEM

Figure 3.1 LNP Size is Correlated with Amount of PEG-lipid.

LNP of various sizes were made using microfluidics by varying PEG-DMG content. Representative cryoTEM micrograph of LNP containing PEG-DMG at 0.25 mol% (A), 0.5 mol% (B), 1.5 mol% (C) and 5 mol% (D) were shown. (E) Size and polydispersity of LNP formulations in A-D were determined using cryoTEM images and DLS. Sizes determined by cryoTEM for LNP containing 0.25, 0.5, 1.5 or 5 mol% PEG-DMG were 117, 72, 43 and 23 nm respectively. By DLS, LNP containing 0.25, 0.5, 1.5, 2.5, or 5 mol% PEG-DMG were 117, 78, 43, 37, 28 nm respectively. Results shown represent the mean diameter ± s.d. of ~200 LNP for cryoTEM and 3 independent formulations for DLS. Scale-bar represents 200 nm in A and 100 nm in B-D.

Previous studies have shown that particle size can affect liposome drainage and biodistribution following s.c. administration (Allen et al., 1993; Oussoren and Storm, 2001). In order to investigate the impact of LNP-siRNA size on the drainage from the injection site and the accumulation at the local draining lymph nodes, LNP-siRNA of either ~30 nm or ~80 nm in diameter were fluorescently labeled with DiR or radiolabelled with trace amounts of the non-exchangeable ^{3}H-CHE (Semple et al., 2005) and administered s.c. at 1 mg/kg in the inter-scapular region of mice. Mice injected with fluorescently labeled LNP were imaged 24 hours post-injection (Figure 3.2A) while the axial and brachial lymph nodes were collected and analyzed for residual LNP from mice injected with radiolabelled LNP (Figure 3.2B). Qualitatively, more of the ~80 nm LNP was retained at the inter-scapular injection site compared to the ~30 nm LNP 24 hours post-injection. While no significant difference in brachial lymph node accumulation was observed over 24 hours, approximately five times more ~30 nm LNP (~2.5% injected dose) was detected in the brachial lymph nodes compared to the larger ~80 nm particle (~0.5% injected dose) by 48 hours

post administration. Not surprisingly, very little (less than 0.1% injected dose) of either formulation was detected in the axial lymph nodes (data not shown) since the inter-scapular site of injection drains almost exclusively to the brachial lymph nodes (Tilney, 1971).

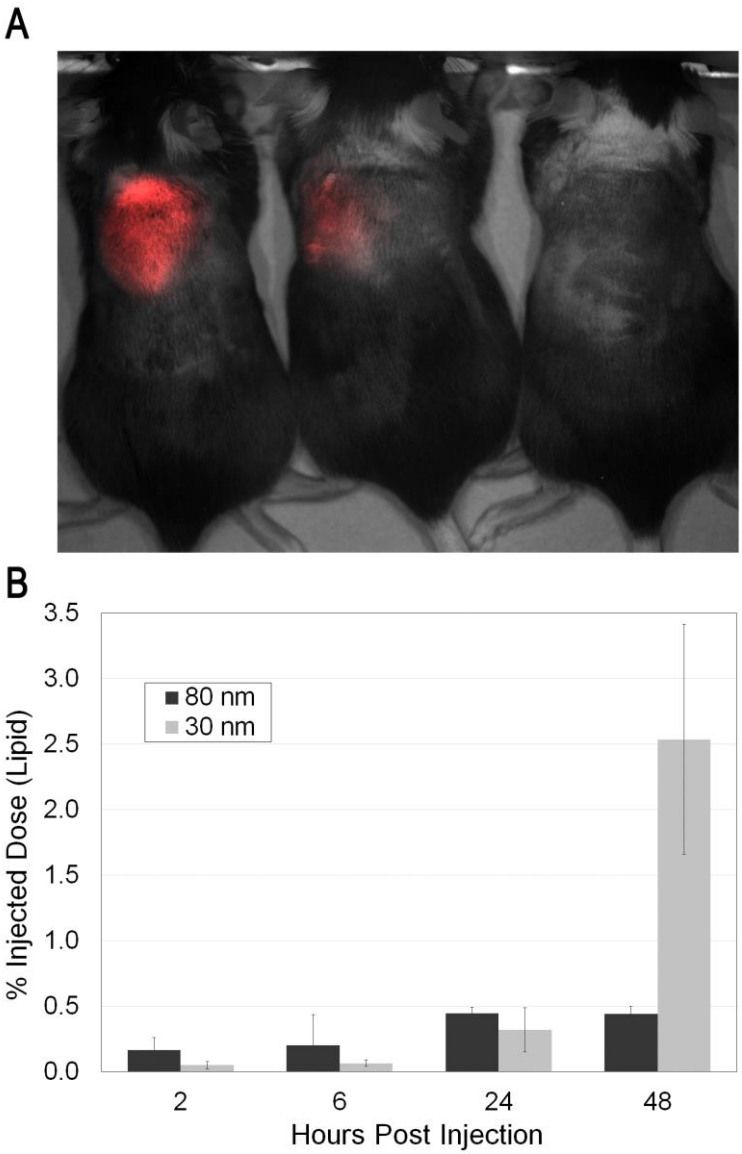

Figure 3.2 A Greater Proportion of Small LNP Drain from the Site of Injection and Accumulate at Brachial Lymph Nodes Following s.c. Administration.

(A) Mice injected with DiR-labelled LNP that were either ~80 nm (left), ~30 nm (center) or PBS (right) were imaged 24 post-injection. (B) ^{3}H-labelled LNP containing PEG-DSG that were ~80 nm (black) and ~30 nm (gray) in diameter were administered s.c. at 1 mg/kg body weight. Brachial lymph nodes were harvested at 2, 6, 24 and 48 hours post injection. Results shown represent the mean ± s.d. of four animals.

In order to investigate the impact of particle size and PEG coating on the distribution of s.c. administered LNP-siRNA to blood and subsequently to the liver, radiolabelled LNP-siRNA were tracked for 48 hours post s.c. injection. PEG-lipids containing either the rapidly dissociating C_{14} (PEG-DMG) or the non-dissociating C_{18} (PEG-DSG) acyl anchors were tested. As shown in Figure 3.3A, the small systems containing 5% PEG-DSG exhibited by far the highest circulating concentration (C_{max}) of LNP (17.1% of the injected dose) following s.c. administration (Table 3.1). However, this did not result in higher levels of accumulation in the liver. Instead, equivalent levels of accumulation corresponding to approximately 15% of the total dose were observed 48 hours post injection for small (~30 nm) LNP containing either 5% PEG-DMG or PEG-DSG (Figure 3.3B). Furthermore, these levels were equivalent to those observed for large (~80 nm) and intermediately sized (~45 nm) LNP with PEG-DSG. The fact that the small LNP containing 5% of the non-exchangeable PEG-DSG do not exhibit greater liver accumulation despite achieving a higher maximum concentration in the blood can be attributed to their long circulation lifetimes following penetration to the blood compartment which facilitates distribution to tissues other than the liver (Allen et al., 1991; Cullis et al., 1998; Woodle and Lasic, 1992). At the maximum concentration of LNP appearing in the blood, no hemolysis-induced toxicity is expected since LNP-siRNA showed no hemolytic activity at pH 7.4 (Figure 3.4). Less than 5% of the ~45 nm and ~80 nm PEG-DMG LNP was found in the liver.

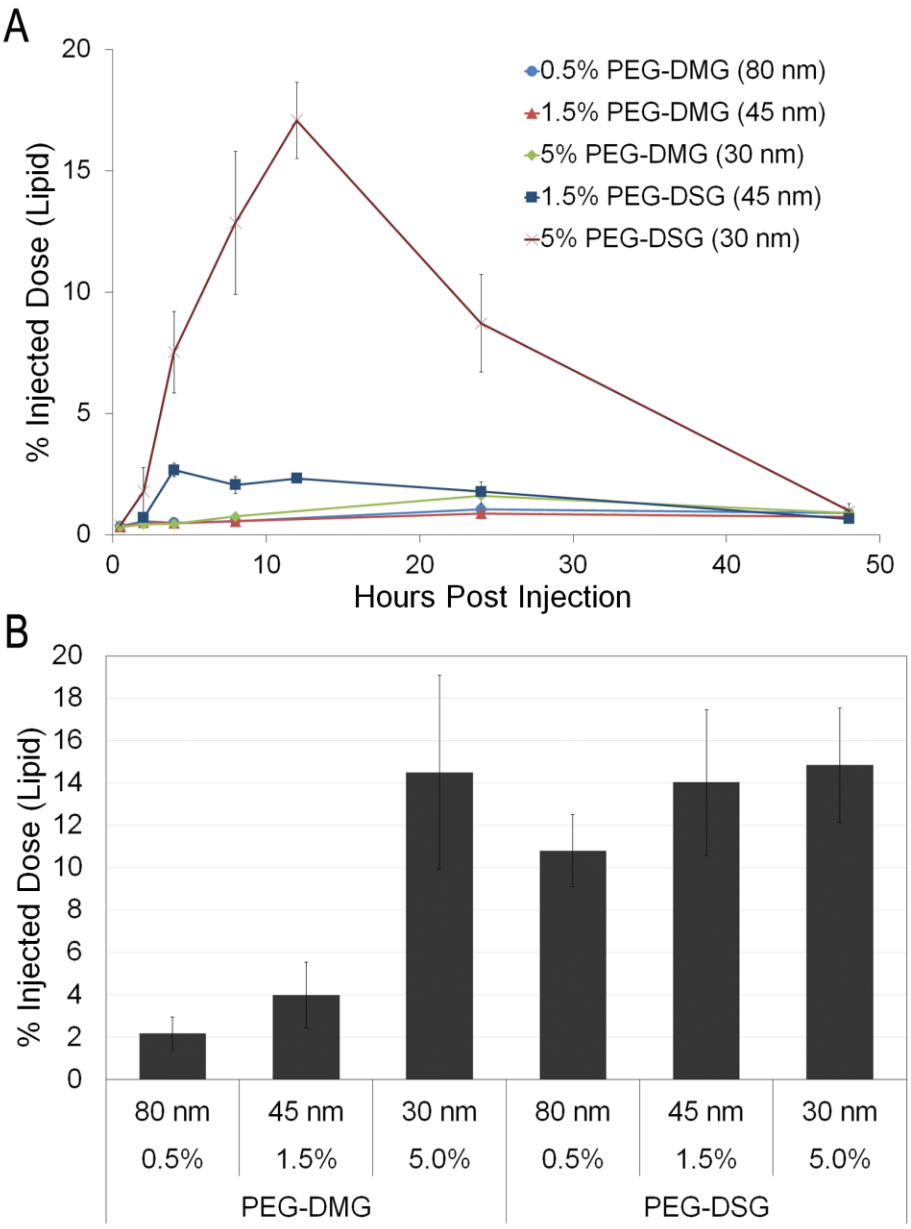

Figure 3.3 LNP with Non-dissociating PEG Coating Drain More Quickly into the Blood and Exhibit Enhanced Accumulation in the Liver Following s.c. Administration.

^{3}H-CHE labelled LNP containing 0.5%, 1.5%, 5% PEG-DMG, 1.5% or 5% PEG-DSG were administered s.c. at 1 mg/kg of body weight. Blood and livers were collected at various time points.

(A) Clearance of LNP from blood over a period of 48 hr. (B) Amount of LNP found in liver at 48 h. Results shown represent the mean ± s.d. of four animals.

Table 3.1 Area-under-curve (AUC) and Maximum Blood Concentration (C_{max}) of LNP with Varying Sizes.

LNP	Size (diameter, nm)	AUC (% inj. dose·hour)	C_{max} (% injected dose)
0.5% PEG-DMG	80	39.0	1.0±0.2
1.5% PEG-DMG	45	33.6	0.9±0.1
5% PEG-DMG	30	51.6	1.6±0.6
1.5% PEG-DSG	45	75.3	2.7±0.3
5% PEG-DSG	30	376.1	17.1±1.6

Note: AUC and C_{max} determined from blood clearance data presented in Figure 3.3

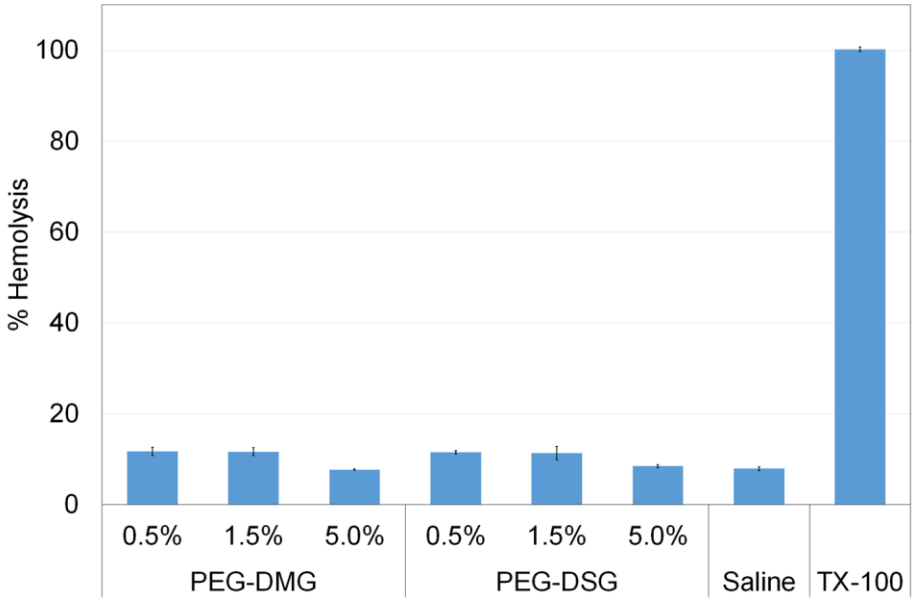

Figure 3.4 LNPs are not hemolytic at physiological pH.

LNPs containing 0.5, 1.5 or 5 mol% of PEG-DMG or PEG-DSG were incubated with human RBC for 1 hour at 37℃. Samples were centrifuged at 1000×g and the absorbance of the supernatant was measured at 562 nm. Data is expressed as % hemolysis relative to the Triton X-100 control (TX-100).

3.2.2 Intermediate Sized (45 nm) LNP–siRNA Systems Exhibit Maximal Hepatic Gene Silencing Following Subcutaneous Administration

We next investigated the effect of LNP size on hepatocyte gene silencing upon s.c. administration. Experiments were performed to compare LNP ranging from ~30 nm to ~100 nm in diameter with either the rapidly dissociable PEG-DMG (Figure 3.5A) or the more stable PEG-DSG (Figure 3.5B). Animals were injected s.c. with LNP loaded with siRNA against FVII, a protein produced and secreted by hepatocytes, at 1 or 5 mg/kg siRNA. Serum FVII levels were determined 48 hours post injection. While the largest LNP tested showed no gene silencing at the 1 mg/kg dose, 5 mg/kg siRNA induced a 40% reduction in protein levels in animals treated with PEG-DSG LNP but not PEG-DMG LNP. Since the PEG-DSG LNP were approximately 15 nm smaller than the PEG-DMG counterpart, it is unclear whether this improvement in gene silencing was a result of size or the PEG-lipid. On the other end of the size spectrum, LNP of diameter ~30 nm composed of 5 mol% of either PEG-lipid were unable to silence FVII regardless of the injected dose. Interestingly, the most potent LNP for either PEG-lipid were those with intermediate diameters (~45 nm). We observed that FVII levels were reduced by 60% and 80% at 1 mg/kg and 90% and 95% at 5 mg/kg for PEG-DMG LNP and PEG-DSG LNP, respectively. These results suggest that hepatic gene silencing via s.c. administration requires LNP of a specific size which, in the case of these particles, is ~45 nm.

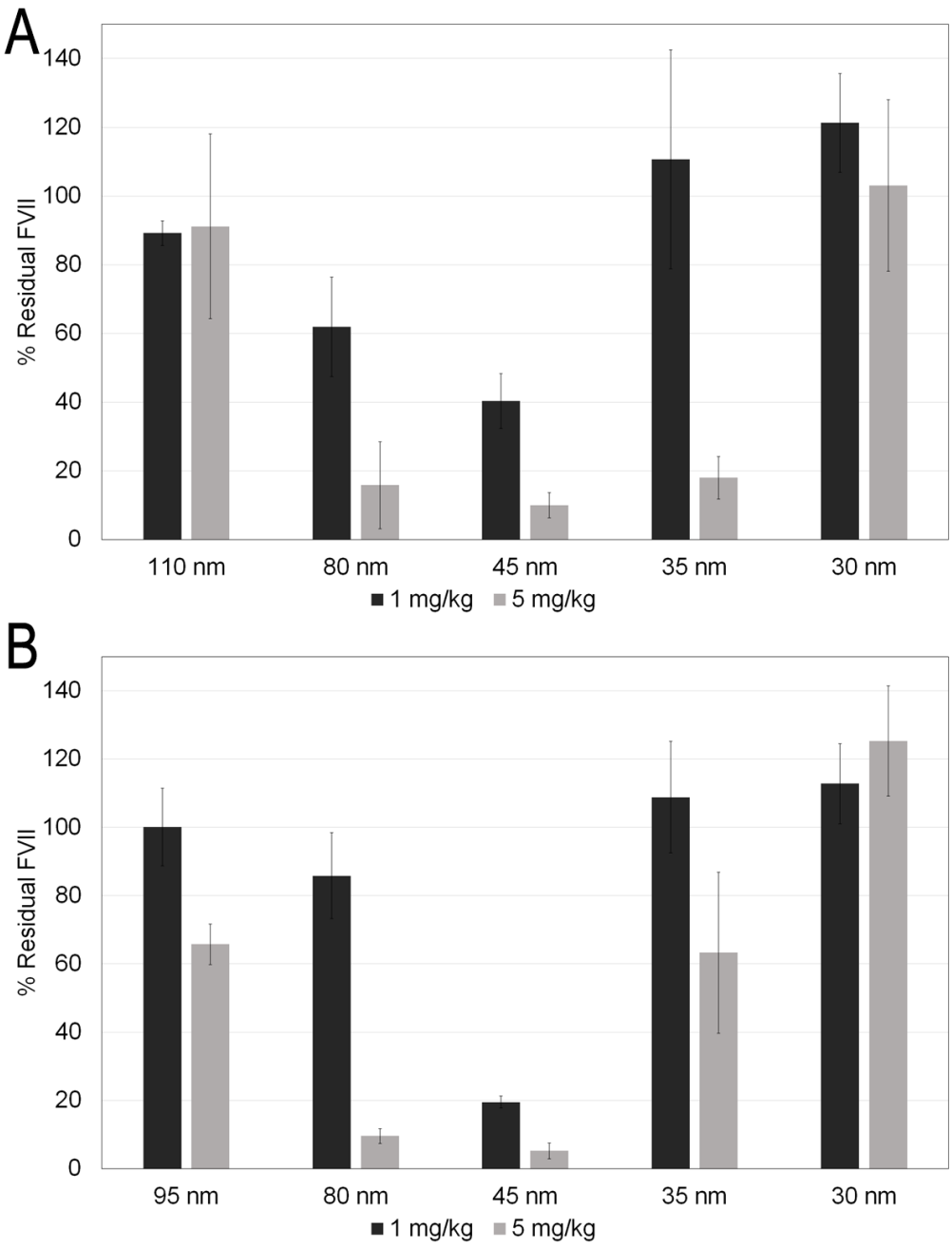

Figure 3.5 ~45 nm LNP Exhibit Maximum Gene Silencing Post s.c. Injection.

(A) PEG-DMG or (B) PEG-DSG LNP were s.c. administered at 1.0 (black) or 5.0 mg/kg (gray) of body weight and the serum FVII was determined 48 hours post-injection. Results shown represent the mean ± s.d. of four animals.

To explore the duration of gene silencing following s.c. administration, blood was collected from animals injected with the most active LNP-siRNA formulation (~45 nm diameter) over 28 days and serum FVII levels were determined (Figure 3.6). A single injection of 1 mg/kg led to greater than 50% FVII protein reduction which persisted for at least 4 days for PEG-DMG LNP and 7 days for PEG-DSG LNP (Figure 3.6A). This result implicates the importance of a stable PEG coat for gene silencing using LNP administered s.c. The higher hepatic gene silencing ability of PEG-DSG LNP can be attributed, at least in part, to the fact that they accumulated at least 3-fold more in the liver than PEG-DMG LNP of a similar size (Figure 3.3B). When the mice were dosed at 5 mg/kg, a reduction in FVII of approximately 90% was observed for a minimum of 4 days and protein levels were reduced below 50% for at least 11 days (Figure 3.6B). There was no significant difference in the degree or duration of silencing between LNP containing PEG-DMG or PEG-DSG likely due to fact that the dosage was high enough to mask any potency differences.

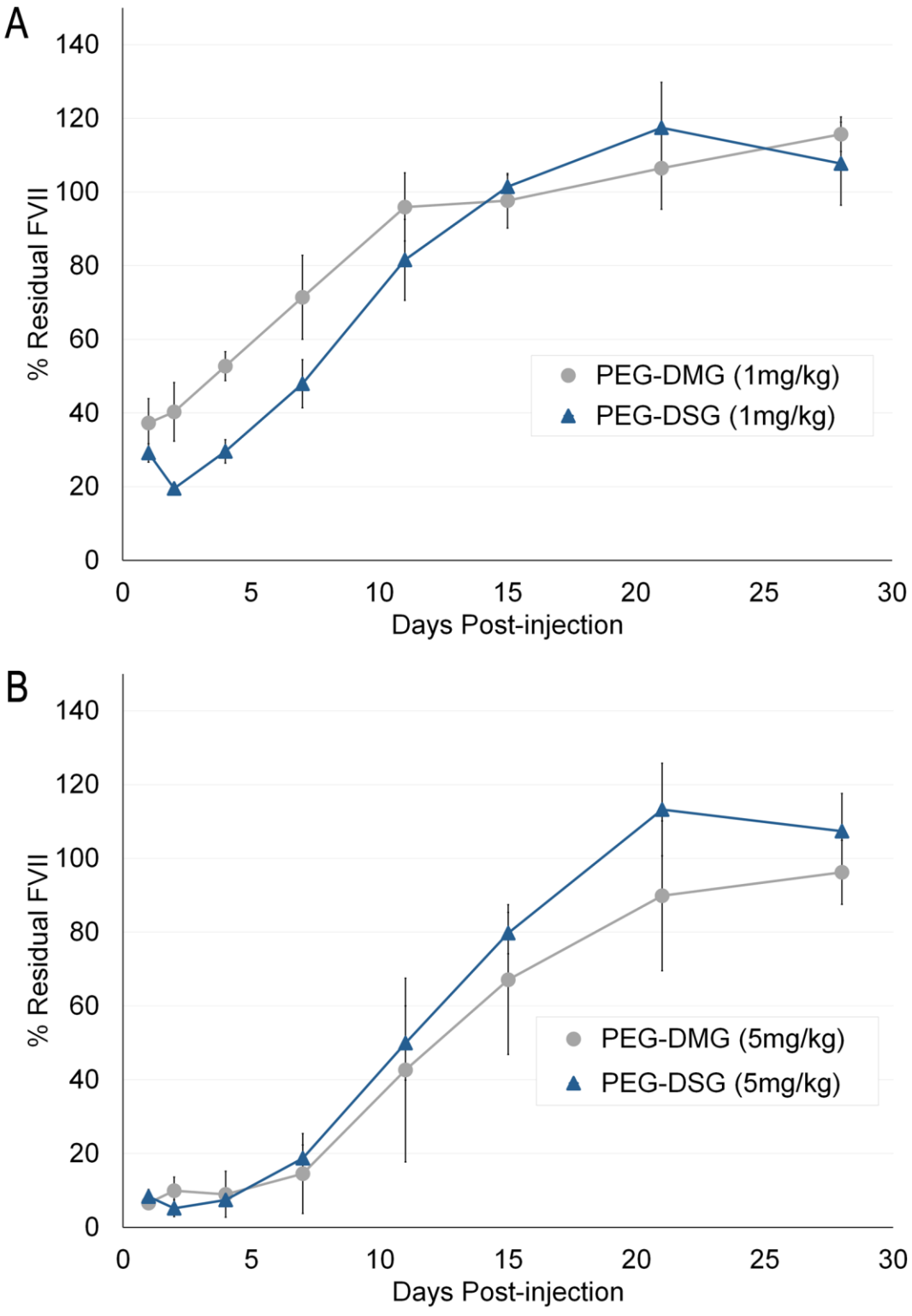
A
% Residual FVII
140
120
100
80
60
40
20
0
0
5
10
15
20
25
30
Days Post-injection
PEG-DMG (1mg/kg)
PEG-DSG (1mg/kg)
B
% Residual FVII
140
120
100
80
60
40
20
0
0
5
10
15
20
25
30
Days Post-injection
PEG-DMG (5mg/kg)
PEG-DSG (5mg/kg)

Figure 3.6 Persistent Gene Silencing (< 50% protein) is Observed Over 11 Days Following s.c. Administration of ~45 nm Diameter LNP.

LNP of similar sizes (~45 nm) but different PEG-lipids were administered s.c. in C57Bl/6 mice at 1 mg/kg or 5 mg/kg of body weight. Blood was collected over 28 days. Serum factor VII silencing was determined and normalized to that of control mice treated with PBS. Residual FVII levels were plotted against time for (A) 1 mg/kg and (B) 5 mg/kg siRNA. Results shown represent the mean ± s.d. of four animals.

It is surprising that small ~30 nm LNP with the stable PEG-DSG coat were less active in gene silencing given that they showed favourable blood exposure and liver accumulation. We speculated that the reduced gene silencing was likely the result of inadequate uptake of LNP into hepatocytes since the stable PEG-DSG coat has been shown to inhibit opsonization in circulation and delay LNP clearance to the liver. In order to explore this possibility, GalNAc conjugated PEG-lipid (GalNAc-PEG) that targets asialoglycoprotein receptor expressed on the surface of hepatocytes was used as a targeting lipid (Akinc et al., 2010). Two PEG-DSG LNP compositions resulting in approximately 45 nm and 35 nm in diameter were tested with or without GalNAc-PEG lipid. Interestingly, no significant improvement on activity was observed at 48 h post administration when 0.5 mol% GalNAc-PEG was incorporated into 45 nm LNP (Figure 3.7A). This is not surprising since these formulations were the most active as shown in Figure 3.5 and were likely able to utilize ApoE-mediated endocytosis. However, when 0.5 mol% of GalNAc-PEG was incorporated into the smaller ~35 nm PEG-DSG LNP, a dramatic improvement in FVII silencing was observed (Figure 3.7B). Targeted LNP (containing GalNAc-PEG) showed almost 90% FVII knockdown for at least 7 days whereas only ~50% protein reduction was observed using

non-targeted LNP. Furthermore, the duration and degree of gene silencing of GalNAc-PEG LNP was similar to PEG-DMG LNP.

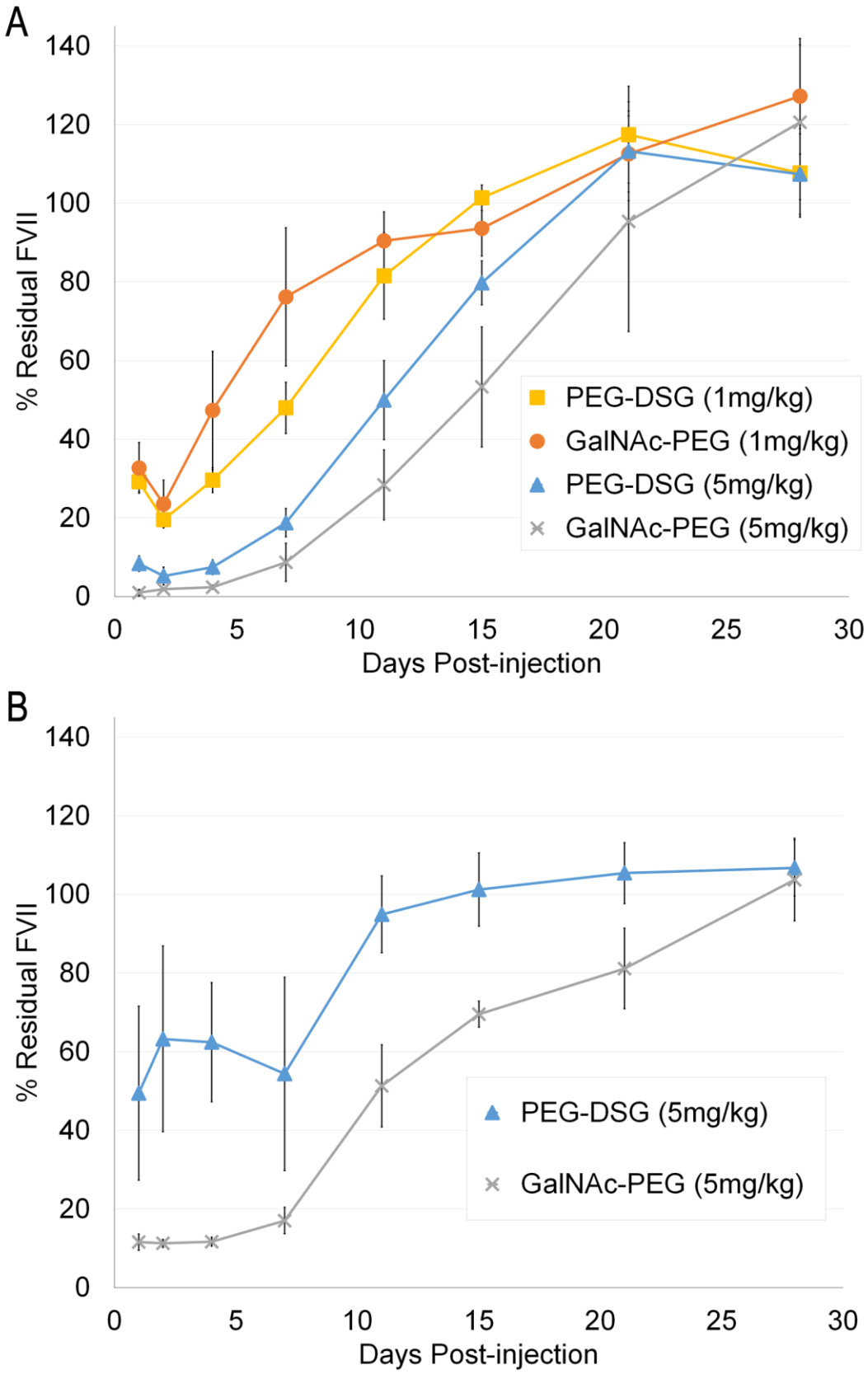
A
% Residual FVII
140
120
100
80
60
40
20
0
0
5
10
15
20
25
30
Days Post-injection
PEG-DSG (1mg/kg)
GalNAc-PEG (1mg/kg)
PEG-DSG (5mg/kg)
GalNAc-PEG (5mg/kg)
B
% Residual FVII
140
120
100
80
60
40
20
0
0
5
10
15
20
25
30
Days Post-injection
PEG-DSG (5mg/kg)
GalNAc-PEG (5mg/kg)

Figure 3.7 Hepatic Gene Silencing Can be Enhanced Using s.c. Administered LNP-siRNA Containing GalNAc-PEG lipid.

(A) Mice were s.c. injected with ~45 nm PEG-DSG LNP with or without 0.5% GalNAc-PEG at 1 or 5 mg/kg siRNA. Residual FVII was monitored for 28 days. (B) Residual FVII was monitored over 28 days for animals injected with ~35 nm PEG-DSG or PEG-DSG with 0.5% GalNAc-PEG LNP. Results shown represent the mean ± s.d. of four animals.

3.3 Discussion

To our knowledge, this is the first report on s.c. administration of LNP-siRNA for *in vivo* gene silencing. It was hypothesized that particle size and PEG steric barrier are crucial factors in determining the potency of s.c. administered LNP-siRNA since the particles must traverse through the meshwork of loose connective tissue to reach the local lymph nodes and drain into the lymphatic system and subsequently into the peripheral circulation. Consistent with this hypothesis, it was found that small LNP-siRNA with a stable PEG coat had a much greater AUC in blood (Table 3.1) than other formulations tested indicating that they were made available to access tissues such as the liver. We also demonstrated the importance of the stability of the PEG coat and particle size on the potency of s.c. administered LNP-siRNA. We discuss the implications of this study for the development of next generation LNP-siRNA systems with improved potency following s.c. administration.

The utility of liposomes as small as 40 nm in diameter for s.c. administration have been previously explored; however, these were bilayer systems manufactured by sonication and are poorly suited for carrying a therapeutic payload such as siRNA (Hope et al., 1986; Oussoren et al., 1997). For the non-bilayer “solid core" LNP-siRNA systems described here (Belliveau et al., 2012;

Leung et al., 2012), an inverse relationship between LNP size and the ability to drain from the site of injection and enter the blood following s.c. administration was observed. This is consistent with previous literature indicating that smaller LNP are able to drain faster into the circulation than their larger counterparts (Oussoren and Storm, 2001; Oussoren et al., 1997). At the brachial lymph nodes where the s.c. injected LNP are expected to drain to, ~2.5% of the small (~30 nm) PEG-DSG LNP was detected 48 hours following s.c. administration, compared to only < 0.5% of the larger (~80 nm) LNP (Figure 3.2). This suggests that the larger PEG-DSG LNP remain at the site of injection and slowly permeate into the circulation, whereas the small PEG-DSG LNP reach the lymph node at a faster rate resulting in a greater accumulation at the lymph node and subsequent release into the circulation. This is also supported by our observation that large and small LNP exhibit low and high C_{max} in blood, respectively (Figure 3.3A and Table 3.1).

For all LNP containing the rapidly dissociable PEG-DMG, the maximum dose appearing in the blood was less than 2% of the total injected dose (Figure 3.3A and Table 3.1). This low C_{max} may be the result of the PEG-DMG lipid being rapidly dissociated from the LNP leading to insufficient steric barrier necessary for the LNP to avoid immune clearance or particle aggregation, both of which could result in a build-up of LNP at the injection site and cause local toxicities. Any quantity that reaches the peripheral circulation will be rapidly cleared by the liver because PEG-DMG LNP administered i.v. have a circulation lifetime of less than 1 hour (Mui et al., 2013). It is estimated that less than 5% of the ~45 and ~80 nm PEG-DMG LNP administered s.c. reached the circulation and virtually all of this material is subsequently accumulated in the liver, resulting in the levels observed 48 hours post injection (Figure 3.3B). It is noteworthy that although the ~30 nm PEG-DMG LNP had a low C_{max} and AUC in the blood, they showed relatively high accumulation in the liver further supporting a rapid hepatic clearance of PEG-DMG LNP that were

drained into the blood. It is likely that at least 14% of the injected dose of the 30 nm PEG-DMG LNP reached the peripheral circulation. The rapid dissociation of PEG-DMG favours hepatocyte uptake while hindering drainage from the injection site. This may prove to be a useful aspect of LNP-siRNA *in vivo* behaviour as others have used particle aggregation as a strategy to promote liposome retention in lymph nodes (Phillips et al., 2000). It may be possible to modulate the rate of PEG-lipid dissociation by using different acyl anchor lengths such that an adequate quantity of LNP drains from the injection site while facilitating aggregation on reaching the lymph node.

When PEG-DMG was substituted with a more stable PEG-DSG, liver accumulation of LNP-siRNA was greatly enhanced. In the case of the ~45 nm diameter LNP, PEG-DSG LNP accumulated to levels three times higher than PEG-DMG LNP. This indicates that a stable PEG coating is an important factor, in addition to size, in allowing extravasation from the s.c. injection site to reach the liver, at least for the 30-80 nm size range tested here (Figure 3.3B). Furthermore, all LNP made with PEG-DSG accumulate to similar levels (~15% of the injected dose) in the liver 48 hours post injection while having drastically different maximum blood concentrations (2.7% for ~45 nm and 17.1% for ~30 nm). Finally, despite similar liver accumulation for PEG-DSG LNP systems (Figure 3.3B), differences in gene silencing were observed (Figure 3.5B) suggesting that other factors in addition to tissue localization such as cellular uptake and endosome destabilization are involved in dictating LNP activity.

While a stable PEG-coat may prevent unwanted protein interactions and promote lymphatic drainage and circulation lifetimes, it is likely that this coat will impair LNP uptake into hepatocytes since this process requires the association of LNP with ApoE (Akinc et al., 2010; Yan et al., 2005). In this case, an exogenous targeting ligand such as GalNAc used in this study, can be tethered to the distal end of the PEG-lipid to enhance LNP uptake into target cells (Akinc et al.,

2010). The incorporation of 0.5 mol% of GalNAc-PEG greatly improved the activity of ~35 nm PEG-DSG LNP suggesting that inefficient cellular uptake was, in part, responsible for the reduction in activity of LNP containing PEG-DSG (Figure 3.7B). Interestingly, the addition of GalNAc-PEG to larger ~45 nm systems did not improve the activity to the same extent as for smaller systems (Figure 3.7A). This is presumably because LNP with 1.5 mol% PEG-lipid are still able to associate with ApoE and the incorporation of an additional targeting ligand confers little additional benefit.

It is important to note that, regardless of the type of PEG-lipid coating, small LNP of size ~30 nm showed a reduction in activity compared to their larger counterparts (Figure 3.5) despite showing favourable blood and liver accumulation following s.c. administration (Figure 3.3). This presumably is due, in part, to inefficient release of the siRNA cargo from the endosome or a reduced siRNA and/or ionisable lipid payload per particle. Work is underway to investigate these factors and methods to improve efficacy of these small LNP-siRNA systems.

In addition to having rapid access to the circulation, small LNP, or LNP that have a stable PEG coating, also have the advantage of minimizing local immune responses at the site of injection. Indeed, signs of immune stimulation at the site of injection was observed for ~80 nm LNP containing the rapidly dissociable PEG-DMG. Mice injected with these relatively large particles showed lesions on the skin around the injection site (data not shown). Although the lesions resolved after one week, these possible immune-related responses raise concerns especially if high or repeat doses are required. It is possible that immunosuppressants could be co-administered to reduce the immune responses to LNP (Abrams et al., 2010).

The work described in this study has significant implications for the development of LNP-siRNA to silence disease-causing genes *in vivo* following s.c. administration. An important reason

for developing s.c. administrable drugs is the possibility of self-administration by patients. Previous work has shown that LNP-siRNA systems are well tolerated with therapeutic indices close to 1000 in rodents following i.v. injection (Jayaraman et al., 2012; Maier et al., 2013). However, the potency of LNP-siRNA systems delivered i.v. are significantly greater (~0.01 mg siRNA/kg body weight for 50% protein reduction) than achieved here for LNP-siRNA delivered s.c. (~1 mg siRNA/kg body weight for 50% protein reduction). As shown here, a major reason for this difference in potency is that a majority of s.c. administered material does not access the circulation. Smaller systems with stable PEG coatings that more readily extravasate to the circulation are less potent because of the presence of the stable PEG coat and an inherent lack of potency of smaller LNP-siRNA systems. To some extent this can be rectified by the inclusion of a targeting ligand such as GalNAc, however further gains in potency, in the range of a factor of 10, are necessary before s.c. administration of LNP-siRNA systems has clinical potential. This is because an injection volume of 10 mL/kg in rodents would translate to 800 mL for an 80 kg person. Assuming the maximum s.c. injection volume is ~2 mL, this would require 400 separate injections. To achieve an siRNA dose of 1 mg/kg for 2 mL injection volumes of the formulations employed here (0.1 mg siRNA/mL), the formulation would have to be concentrated to a lipid concentration of over 400 mg/mL, which is impractical.

As shown in this study, an important aspect of s.c. administration concerns enhanced delivery to the regional lymph nodes, particularly by small (~30 nm) systems. Methods of enhancing the gene silencing potency of these small LNP-siRNA systems are of interest and successful silencing of genes in immune cells in regional lymph could lead to treatments for inflammatory and autoimmune diseases as well as organ rejection (Hill et al., 2003; Ichim et al., 2003; Zheng et al., 2009). Also, tumour therapy would be expected to benefit from small LNP-

siRNA systems of ~30 nm. Others have shown that small ~30 nm particles are able to penetrate into poorly permeable tumor tissue (Cabral et al., 2011; Huo et al., 2013).

In summary, the work presented here is the first demonstration of LNP-siRNA mediated gene silencing in the liver following s.c. administration of LNP-siRNA systems over the size range of 30-80 nm with dissociable or stable PEG coatings. LNP-siRNA that are intermediate in size and ~45 nm in diameter exhibit maximum efficacy and with a dose as low as 1 mg/kg, greater than 50% hepatic gene silencing is observed and maintained over one week. Since small LNP size and a stable PEG coat appear to be essential for s.c. administration, future work will focus on improving the activity of small stably shielded LNP-siRNA. Other potential issues remain to be addressed to enable pre-clinical and clinical development of s.c. administered LNPs. These include potential injection site reactions caused by the LNPs or their components and the high injection volumes required.

Chapter 4: Influence of Particle Size on the *In Vivo* Potency of Lipid Nanoparticle Formulations of siRNA

4.1 Synopsis

Lipid nanoparticles (LNP) can provide a clinically effective method for delivering small interfering RNA (siRNA) to silence pathological genes in hepatocytes. The gene silencing potency of these LNP-siRNA systems has been shown to depend on a variety of factors including association with serum factors such as ApoE and the pKa of component ionizable lipids. Here we investigate the influence of LNP size, an important parameter affecting tissue penetration of LNP systems, on the pharmacokinetics, biodistribution, and hepatic gene silencing potency of LNP-siRNA systems following intravenous administration. For LNP systems stabilized by a polyethylene glycol (PEG)-lipid that can dissociate from the LNP following injection it is shown that small (diameter $\leq$ 30 nm) systems are considerably less potent than their larger counterparts. This is attributed in part to the ability of other lipid components, particularly the ionizable amino-lipid, to dissociate from the LNP following dissociation of the PEG-lipid. Small LNP stabilized by PEG-lipids with slow dissociation rates exhibited much reduced amino-lipid dissociation rates, however such systems are relatively impotent due to the continued presence of the PEG coating. These results demonstrate the delicate balance between the *in vivo* potency of LNP-siRNA systems and the residence times of component lipids in the LNP particle itself and suggest new directions to optimize the *in vivo* gene silencing potency of small LNP-siRNA systems. The work summarized in this Chapter has been accepted for publication (Chen et al., 2016).

4.2 Results

4.2.1 LNP-siRNA Systems with Diameter ~80 nm Exhibit Maximum Hepatic Gene Silencing Following i.v. Injection

We previously reported that LNP-siRNA with a diameter of ~45-50 nm exhibited most potent hepatic gene silencing following s.c. administration (refer to Chapter 3) (Chen et al., 2014). However, the influence of size on LNP potency in the s.c. model is complicated by the need to drain from the site of injection into the circulation, which favours smaller systems. We therefore examined the influence of LNP size on hepatic gene silencing following i.v. injection, the most direct route of administration. LNP-siRNA systems were produced with different diameters (27 to 117 nm) by varying the PEG-DMG content from 0.25 to 5 mol% lipid. The siRNA was designed to silence coagulation factor VII (siFVII), which is expressed in and secreted by hepatocytes (Akinc et al., 2008; Semple et al., 2010).

Mice were injected i.v. over the dose range of 0.01 to 3 mg siRNA/kg and FVII levels in blood were determined 24 hr post-injection. As shown in Figure 4.1A the 78 nm LNP systems exhibited the maximum gene silencing potency. A plot of the siRNA dose required to achieve 50% gene silencing (ED_{50}) versus particle size shows that both the smallest (27 nm) and the largest (117 nm) systems were relatively impotent (Figure 4.1B). The poor activity of the 117 nm LNP is likely due to an inability to penetrate the fenestrations in the liver vasculature, which are approximately 100-140 nm in diameter in mice (Braet and Wisse, 2002; Snoeys et al., 2007). However, the lack of potency of the 27 nm diameter LNP (ED_{50} of 0.8 mg/kg), which are more than 20 times less potent than the 78 nm diameter LNP (ED_{50} of 0.04 mg/kg), cannot be so readily rationalized. For clarity, particle diameters are rounded to the nearest multiple of five herein.

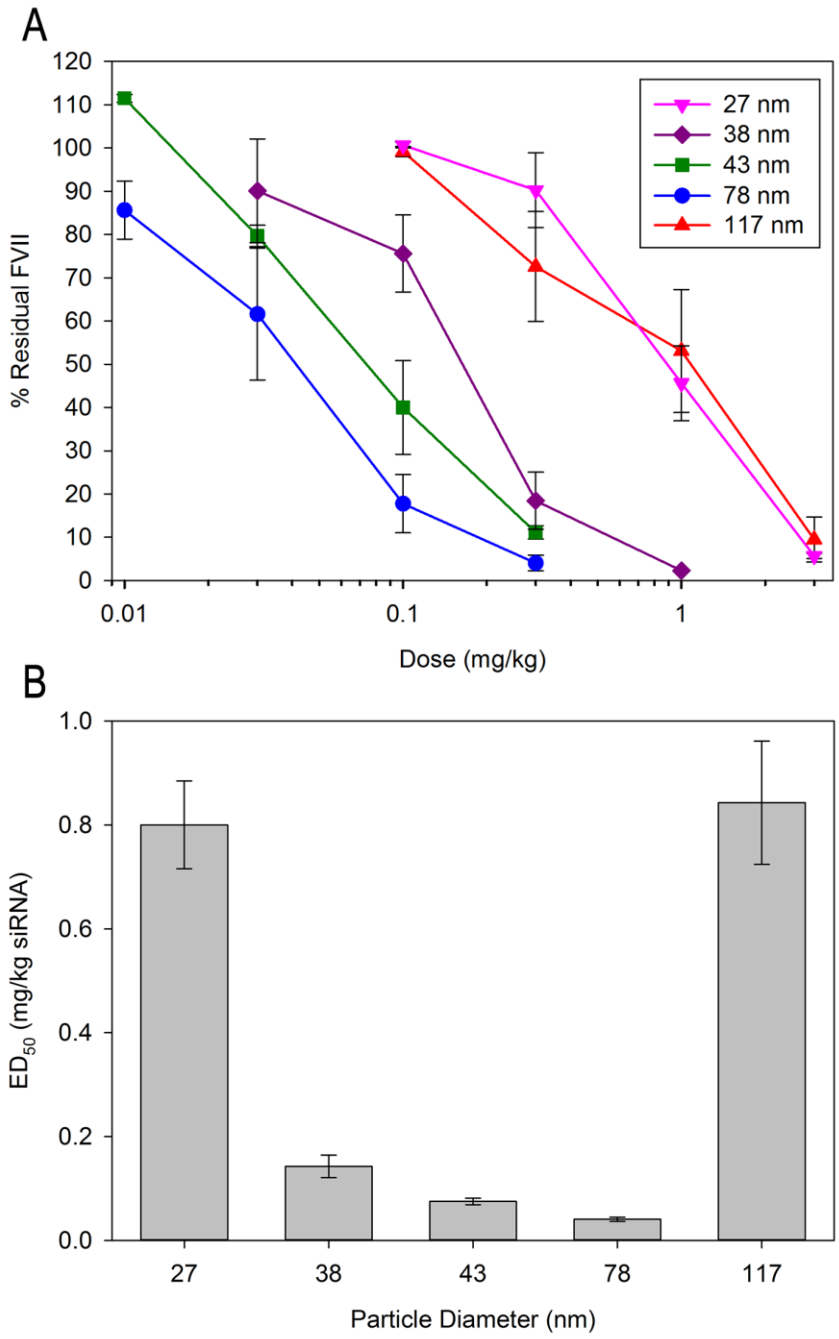

Figure 4.1 Hepatocyte Gene Silencing Following i.v. Injection of LNP-siRNA Systems is Dependent on LNP Size.

LNP-siFVII of various sizes were made by titrating the amount of PEG-DMG lipid present during the formulation process. (A) FVII gene silencing of LNP containing 0.25%, 0.5%, 1.5%, 2.5% or

5% PEG-DMG lipid which resulted in LNP with diameters ranging from 117 to 27 nm. Blood was collected at 24 hr post-injection of LNP and FVII levels were determined and normalized to that of control mice injected with PBS. Results shown represent the mean ± s.d. of three animals. (B) The dose required to achieve 50% reduction (ED_{50}) of factor VII protein expression for LNP with different diameters. ED_{50} values are extrapolated from the dose titration curve presented in Figure 4.1A. ED_{50} ± s.e. are calculated from the dose titration curve presented in Figure 4.1A.

4.2.2 LNP of Different Sizes All Distribute Rapidly to the Liver Following i.v. Administration

The size-dependent differences in LNP-siRNA activity could result from changes in *in vivo* characteristics such as pharmacokinetics (PK) and biodistribution (BD). To investigate the PK/BD of small (~30 nm diameter), medium (~45 nm diameter) and large (~80 nm diameter) LNPs, trace amounts of ^{3}H-CHE were incorporated into the LNP formulations and concentrations in various tissues were tracked over 24 hr in mice post i.v. administration. ^{3}H-CHE was used as a marker for LNP as it has been shown to be non-exchangeable and non-metabolizable (Semple et al., 2005; Stein et al., 1980). As shown in Figure 4.2A, the 30 nm and 45 nm LNP were very rapidly cleared from the blood compartment with a circulation half-life of < 15 min, whereas the larger 80 nm LNP were longer lived with a half-life of ~1.2 hr. At 24 hr post-injection, the vast majority of the LNP were found in the liver, regardless of size (Figure 4.2 B and C). Accumulation of LNP in the spleen, kidney, pancreas, lung, femur and heart was also examined. Less than 1% of any formulation was found in these tissues, with the exception of the spleen in which 10% of the 80 nm LNP was found at 24 hr (Figure 4.2C).

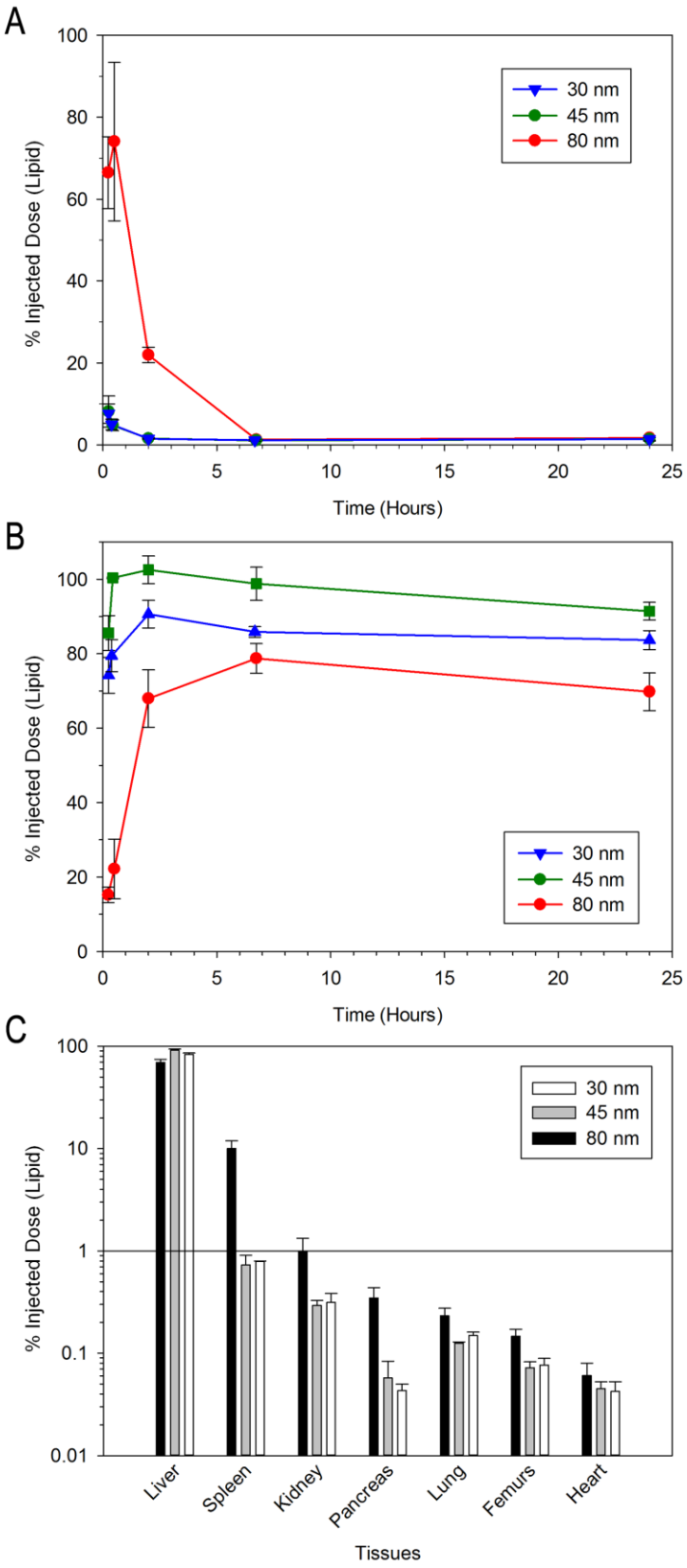
A
% Injected Dose (Lipid)
Time (Hours)
30 nm
45 nm
80 nm
B
% Injected Dose (Lipid)
Time (Hours)
30 nm
45 nm
80 nm
C
% Injected Dose (Lipid)
30 nm
45 nm
80 nm
Liver
Spleen
Kidney
Pancreas
Lung
Femurs
Heart
Tissues

Figure 4.2 Circulation Lifetime and Biodistribution of Small, Medium and Large LNP. Small (30 nm diameter), medium (45 nm diameter) or large (80 nm diameter) LNP labelled with trace amounts of ^{3}H-CHE were injected into mice at 0.3 mg siRNA/kg body weight. Blood and tissues were collected at indicated time points and ^{3}H-CHE levels were determined using liquid scintillation counting. (A) Clearance of LNP from blood over 24 hr post i.v. injection. (B) Accumulation of LNP in liver over 24 hr post injection. (C) Accumulation of LNP in various tissues at 24 hr post injection. Results shown represent the mean ± s.d. of four animals.

4.2.3 The Stability of LNP-siRNA Systems is Size Dependent

Given the fact that liver accumulation is not dramatically affected by LNP size and therefore is not likely to account for the difference in activity between 30 nm and larger systems, the question is what other effects could be reducing the potency of the smaller systems. Smaller nanoparticles exhibit larger surface to volume ratios with the attendant possibility of increased dissociation rates of LNP components (Hope et al., 1986; Scherphof et al., 1984). In order to examine the dissociation rates of the PEG-DMG, DSPC, amino-lipid and siRNA, radiolabelled versions of these compounds were obtained and studies were performed to ascertain the ability of these components to exchange out of LNP-siRNA systems when incubated with mouse plasma. It was found that larger LNP-siRNA systems (45 and 80 nm diameter) could be separated from serum components using a Sepharose CL-4B size exclusion column (data not shown). Unfortunately this technique could not be applied to smaller (30 nm diameter) systems because the LNP eluted in the same fraction as lipoproteins in the mouse plasma.

LNP-siRNA systems of 45 and 80 nm diameter were formulated with radiolabelled lipids and were incubated with mouse plasma at 37°C for up to 8 hr and then separated from plasma

using size exclusion chromatography as described in Methods. As shown in Figure 4.3A, the ^{3}H-CHE remained in the LNP fractions for at least 8 hr for both LNP systems. This is expected for this non-exchangeable marker (Semple et al., 2005). PEG-DMG is designed to dissociate from LNP systems (Akinc et al., 2010; Semple et al., 2010) to render them transfection competent, however, as shown in Figure 4.3B, the ^{3}H-PEG-DMG in the 45 nm diameter LNP dissociated at a significantly faster rate than for the 80 nm diameter LNP. The halftime ($t_{1/2}$) of dissociation for PEG-DMG from the 45 nm diameter LNP can be estimated to be 1.1 hr, as compared to 1.7 hr for the 80 nm LNP. Furthermore, even the DSPC dissociates from the 45 nm diameter LNP at an appreciable rate ($t_{1/2}$ = 6.2 hr) as compared to 80 nm LNP ($t_{1/2}$ = 43 hr) (Figure 4.3C).

In order to monitor the dissociation of the ionizable amino-lipid, ^{14}C-labelled DLin-MC3-DMA was used as a surrogate for DMAP-BLP. DLin-MC3-DMA is structurally very similar to DMAP-BLP (Figure 4.4) and results in similar particle parameters and *in vivo* FVII silencing activity when incorporated into LNP-siRNA systems (Jayaraman et al., 2012; Rungta et al., 2013). As shown in Figure 4.3D, DLin-MC3-DMA dissociated over two times faster from the 45 nm LNP ($t_{1/2}$ = 4.9 hr) than from the larger 80 nm system ($t_{1/2}$ = 12 hr) (Figure 4.3D). It is interesting to note the relatively little loss of the siRNA cargo on plasma incubation for either the 45 or 80 nm diameter LNP systems. There is an initial loss of approximately 20%, possibly corresponding to siRNA adsorbed to the LNP surface, however the remainder of the siRNA cargo remained associated with the LNP for up to 8 hr regardless of the initial particle size (Figure 4.3E).

The ability of the DSPC and particularly the amino-lipid to dissociate more rapidly from the 45 nm diameter LNP than from the 80 nm diameter system suggests that the relatively poor transfection potency of the 30 nm LNP system could arise from rapid dissociation of the amino-lipid from these systems following *in vivo* administration. In order to corroborate the observation

that smaller LNP sizes lead to increased desorption rates of component lipids, a fluorescence resonance energy transfer (FRET)-based assay using NBD-DOPE and LRB-DOPE was developed (Figure 4.3F). When these two lipid species are in close proximity, the fluorescence of NBD is quenched by LRB. Thus when NBD or LRB dissociate from the LNP, the NBD fluorescence will recover and can be used to assay for the dissociation of (fluorescent) lipids from the LNP. The relative dissociation rates of these fluorescent lipids should be influenced by particle size in a similar way as other lipid components. LNP-siRNA systems of 30, 45 and 80 nm diameter containing NBD and LRB were incubated with mouse plasma and the NBD fluorescence recovery was measured at 530 nm over 24 hr. It was found (Figure 4.3F) that NBD and/or LRB dissociated more slowly from the 80 nm LNP (NBD fluorescence recovery $t_{1/2}$ = 4.9 hr) than from the 45 nm LNP (NBD fluorescence $t_{1/2}$ = 3.4 hr) which was in turn slower than that observed for the 30 nm LNP (fluorescent recovery $t_{1/2}$ = 2.9 hr). This observation is consistent with the chromatography-based lipid exchange studies showing that lipids dissociated more slowly from the 80 nm LNP than the 45 nm diameter LNP and suggests that lipids dissociate from the 30 nm LNP even more rapidly.

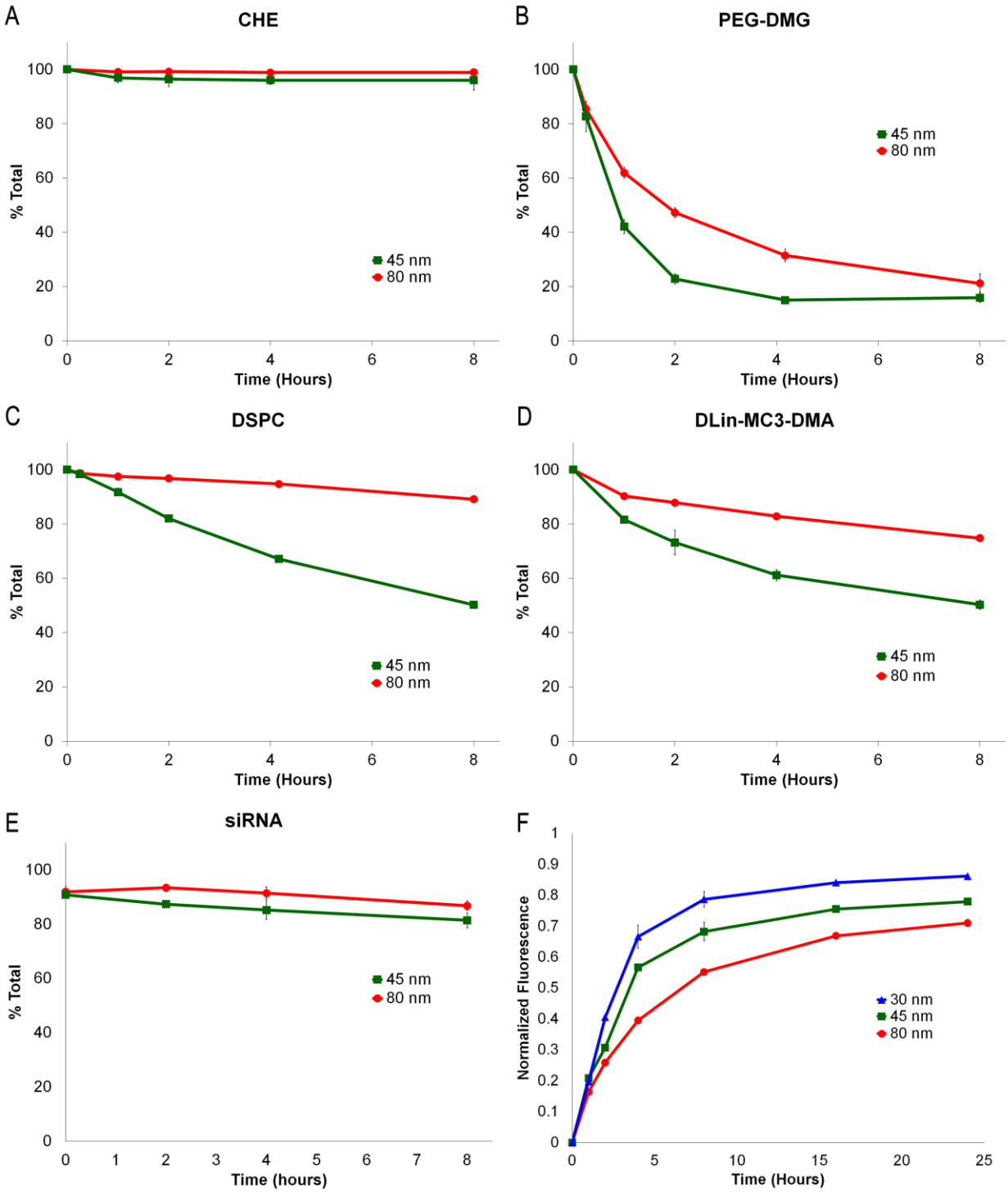
A
CHE
% Total
Time (Hours)
45 nm
80 nm
B
PEG-DMG
% Total
Time (Hours)
45 nm
80 nm
C
DSPC
% Total
Time (Hours)
45 nm
80 nm
D
DLin-MC3-DMA
% Total
Time (Hours)
45 nm
80 nm
E
siRNA
% Total
Time (hours)
45 nm
80 nm
F
Normalized Fluorescence
Time (Hours)
30 nm
45 nm
80 nm

Figure 4.3 The Rate at which Component Lipids Dissociate from LNP is a Sensitive Function of LNP size.

^{3}H-PEG-DMG, ^{14}C-DSPC LNP, ^{14}C-DLin-MC3-DMA or ^{3}H-CHE were formulated with either 0.5 mol% or 1.5 mol% PEG-DMG to produce 80 nm or 45 nm diameter LNP and were incubated for 0, 0.25, 1, 2, 4 and 8 hr at 37°C in mouse plasma and separated by size exclusion chromatography. The amounts of each lipid species that remained associated with the LNP fractions were determined over time and the rates of dissociation were determined by fitting to the first four time-points. (A) The amount of CHE remaining in the LNP fractions over 8 hr. As expected, CHE is non-exchangeable and remains with the LNP over the 8 hr time course for both particle sizes. (B) PEG-DMG dissociates at a rate of 26%/hr from 80 nm diameter LNP and at a rate of 36%/hr from 45 nm diameter LNP. (C) DSPC dissociates at a rate of 8%/hr from 45 nm diameter LNP and 1%/hr for 80 nm diameter systems. (D) DLin-MC3-DMA dissociates from 80 and 45 nm diameter LNP at 3%/hr and 6%/hr respectively. (E) 45 nm and 80 nm diameter LNP were formulated with siRNA conjugated to the Quasar 570 fluorophore, incubated with mouse plasma and separated by size exclusion. The amount that remained associated with LNP fractions was monitored for up to 16 hr. Over 80% of the siRNA remained associated with the LNP fractions for at least 8 hr. (F) LNP (30, 45 and 80 nm diameter) formulated with NBD and LRB –DOPE were incubated in plasma for up to 24 hr. The NBD fluorescence intensity was measured as a readout of dissociation of DOPE from the LNP and normalized to the fluorescence intensity of samples incubated with 1.5% Triton X-100. The rates of dissociation were found to be correlated with particle size (dissociation rates for 80 nm diameter < 45 nm diameter< 30 nm diameter).

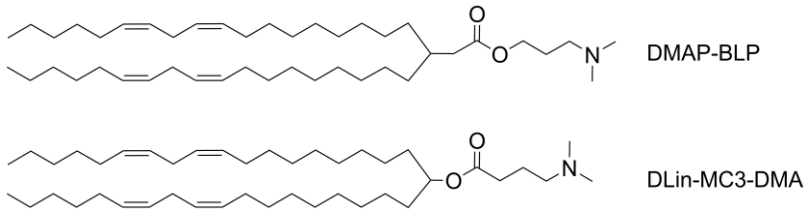

Figure 4.4 Chemical Structures of DMAP-BLP and DLin-MC3-DMA.

Top depicts 3-(dimethylamino)propyl(12Z,15Z)-3-[(9Z,12Z)-octadeca-9,12-dien-1-yl]henicosa-12,15-dienoate (DMAP-BLP) and the bottom depicts (6Z,9Z,28Z,31Z)-Heptatriaconta-6,9,28,31-tetraen-19-yl4-(dimethylamino)butanoate (DLin-MC3-DMA) which is also known as dilinoleylmethyl-4-dimethylaminobutyrate.

4.2.4 Increasing Ionizable Amino-lipid Content Improves Small LNP-siRNA Activity

The lipid dissociation studies suggest that a possible reason for the low potency of the small 30 nm LNP-siRNA systems is that a significant amount of the amino-lipid dissociates from the particle before it reaches or enters the target hepatocytes. The amino-lipid is critical for endosomal destabilization and release of siRNA into the cytoplasm (Hafez et al., 2001; Jayaraman et al., 2012; Semple et al., 2010). If reduced levels of amino-lipid are causing the low potency of the small (30 nm diameter) systems, then higher initial proportions of amino-lipid in the LNP should improve potency. The amine-to-phosphate charge ratio (positive charge on the ionized amino-lipid to the negative charge on the phosphates found on the siRNA), was therefore increased by decreasing the amount of siRNA encapsulated in the LNP and the *in vivo* potency was determined using the FVII assay. When the amine-to-phosphate ratio was increased from 1 to 12 in the 30 nm PEG-DMG LNP-siRNA, a progressive improvement in potency as indicated by the ED_{50} value was observed up to an amine-to-phosphate ratio of 6, with little improvement in LNP activity beyond

this point (Figure 4.5A). This suggests that a critical amount of excess amino-lipid is necessary for maximum endosome destabilization and that beyond this amount there is little additional benefit.

The amount of amino-lipid was also increased by increasing the molar fraction in the LNP formulation. Previous work has shown that 50 mol% amino-lipid provides optimum activity for systems of 50 nm or greater in diameter (Jayaraman et al., 2012). When 60 mol% of DMAP-BLP was incorporated into 30 nm LNP-siRNA systems at an amine-to-phosphate ratio of 6, FVII gene silencing potency improved by approximately a factor of two (at 0.3 mg siRNA/kg) over LNP-siRNA that contained 50 mol% DMAP-BLP (Figure 4.5B). By increasing the amine-to-phosphate ratio from 3 to 6 and increasing the mole fraction of DMAP-BLP in the LNP from 50 to 60 mol%, the activity of 30 nm LNP-siRNA systems was increased at least three times from an ED_{50} of 0.8 mg/kg to < 0.3 mg/kg. It is important to note that changes in particle size, amount of amino-lipid or amine-to-phosphate charge ratios do not result in changes in pKa (Figure 4.6) which is a critical parameter that dictates LNP-siRNA activity (Jayaraman et al., 2012). This strongly supports the proposal that the activity of smaller systems is compromised by the rapid dissociation of the amino-lipid component.

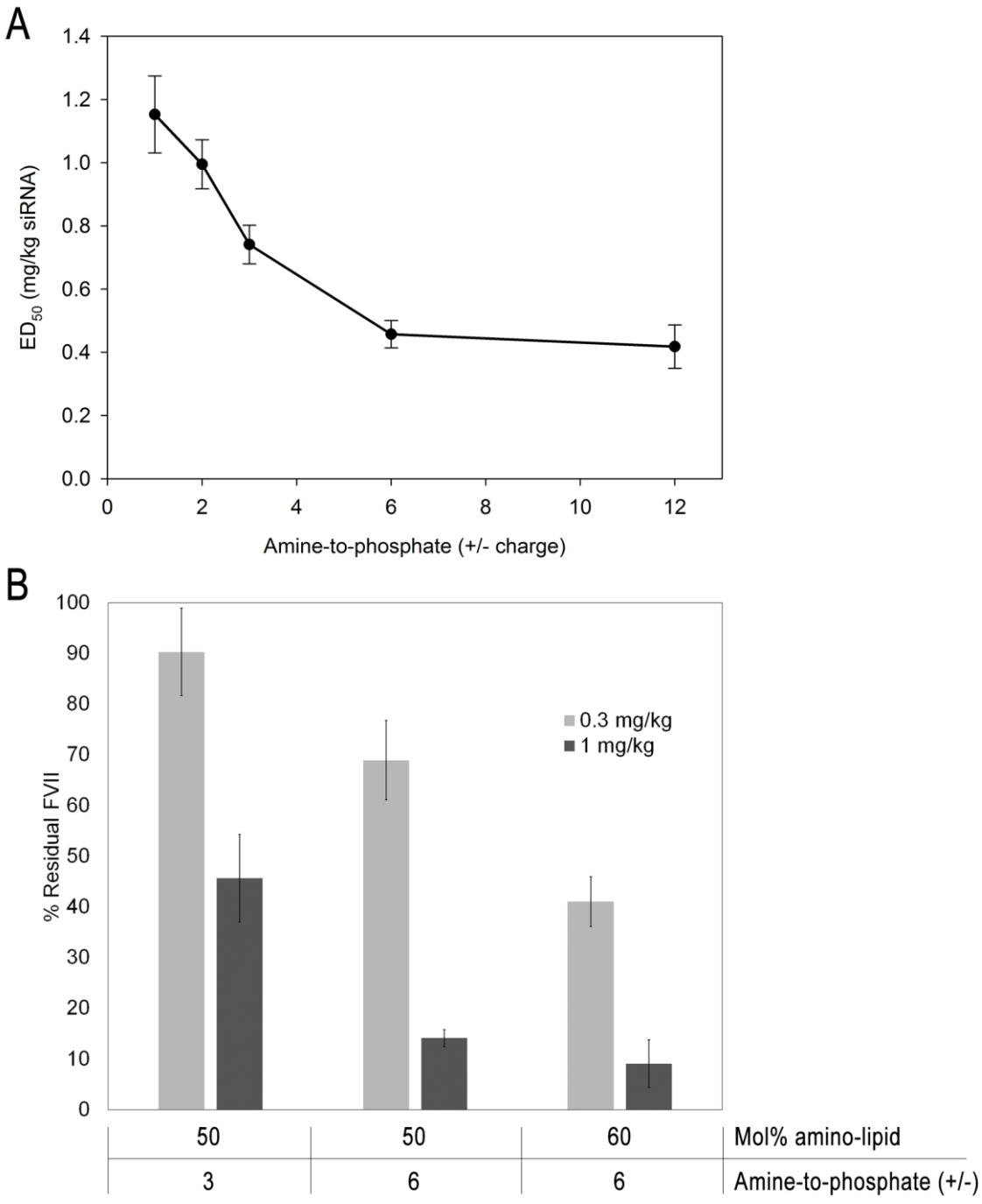
A
1.4
1.2
1.0
0.8
0.6
0.4
0.2
0.0
ED50 (mg/kg siRNA)
0
2
4
6
8
10
12
Amine-to-phosphate (+/- charge)
B
100
90
80
70
60
50
40
30
20
10
0
% Residual FVII
0.3 mg/kg
1 mg/kg
50
50
60
Mol% amino-lipid
3
6
6
Amine-to-phosphate (+/-)

Figure 4.5 The Gene Silencing Potency of Small LNP-siRNA Systems Can be Improved by Increasing the Amount of Amino-lipid in the LNP.

(A) Small 30 nm diameter LNP-siFVII containing 50 mol% DMAP-BLP were formulated at amino-lipid-to-siRNA phosphate charge ratios of 1-12 and injected into mice at doses of 0.3, 1 and 3 mg siRNA/kg body weight. The ED_{50} for FVII gene silencing is plotted against the amine-to-phosphate charge ratios. ED_{50} ± s.e. are calculated from dose titration curves. (B) Small 30 nm diameter LNP-siRNA containing 50 mol% DMAP-BLP at an amine-to-phosphate ratio of 3 or 6 and 60 mol% DMAP-BLP at an amine-to-phosphate ratio of 6 were injected into mice at 0.3 and 1 mg/kg body weight. The residual FVII (%) is normalized to control mice. Results shown represent the mean ± s.d. of three animals.

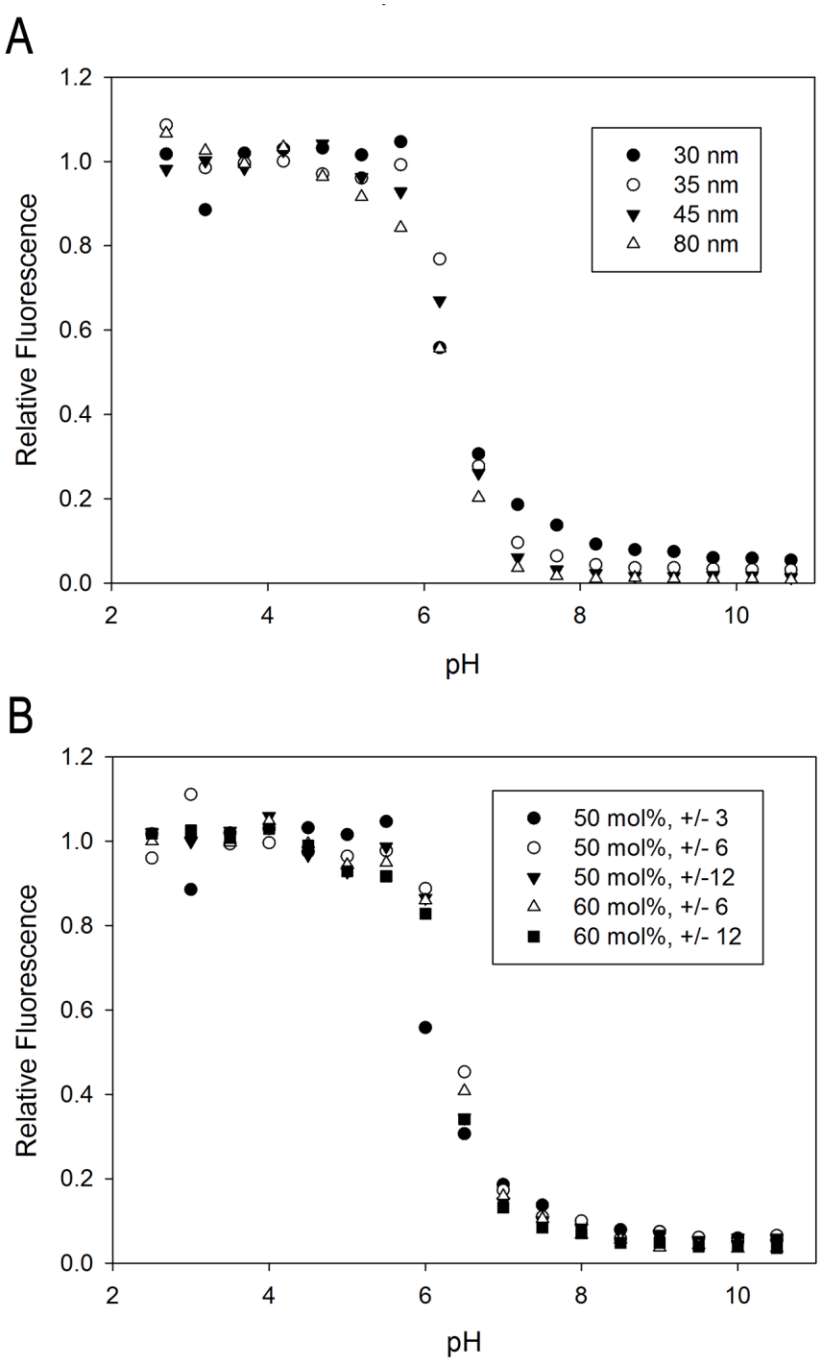

Figure 4.6 pKa of LNP are Not Affected by Particle Size, Quantity of Amino-lipid or Amine-to-phosphate Charge Ratios.

pKa of LNP-siRNA were determined by measuring the fluorescence intensity (Ex/Em: 321/445 nm) after mixing with TNS at pH 2-11.5 and applying a sigmoidal fit. (A) The pKa of 30-80 nm

LNP were determined to be between 6.2 and 6.4. (B) The pKa of 30 nm LNP with 50 or 60 mol% DMAP-BLP and an amine-to-phosphate charge ratio of 3, 6 or 12 were determined to also be between 6.2 and 6.4. Representative plots from three independent measurements are shown.

4.2.5 A PEG Coating that Dissociates Slowly Dramatically Improves Particle Stability

PEG-lipids with longer carbon chains dissociate from LNP more slowly than those with shorter acyl chains (Mui et al., 2013; Wheeler et al., 1999). Since the PEG-lipid comprises the coat lipid of the LNP (Leung et al., 2012) its loss would likely enhance the dissociation of other lipid components with the LNP. In order to improve particle stability, PEG-DSG, which has alkyl chains of 18 carbons was used in place of PEG-DMG. Figure 4.7 shows the dissociation rates of all lipid components in PEG-DSG LNP following incubation in mouse plasma. As expected, no measurable dissociation of the non-exchangeable ^{3}H-CHE was detected (Figure 4.7A). PEG-DSG did dissociate from the LNP over time but at a significantly lower rate (24 and 47 hr $t_{1/2}$ for 45 and 80 nm LNP) in comparison to PEG-DMG (1.1 and 1.7 hr) (Figure 4.7B). Similarly, the dissociation rate for DSPC was reduced with $t_{1/2}$ of 55 and 200 hr for 45 and 80 nm LNP (Figure 4.7C). Furthermore, as seen in Figure 4.7D, DLin-MC3-DMA dissociation was also reduced (dissociation $t_{1/2}$ of 15 and 19 hr). The siRNA cargo remained stably associated with the LNP fractions (> 90%) for up to 16 hr regardless of the initial particle size (Figure 4.7E).

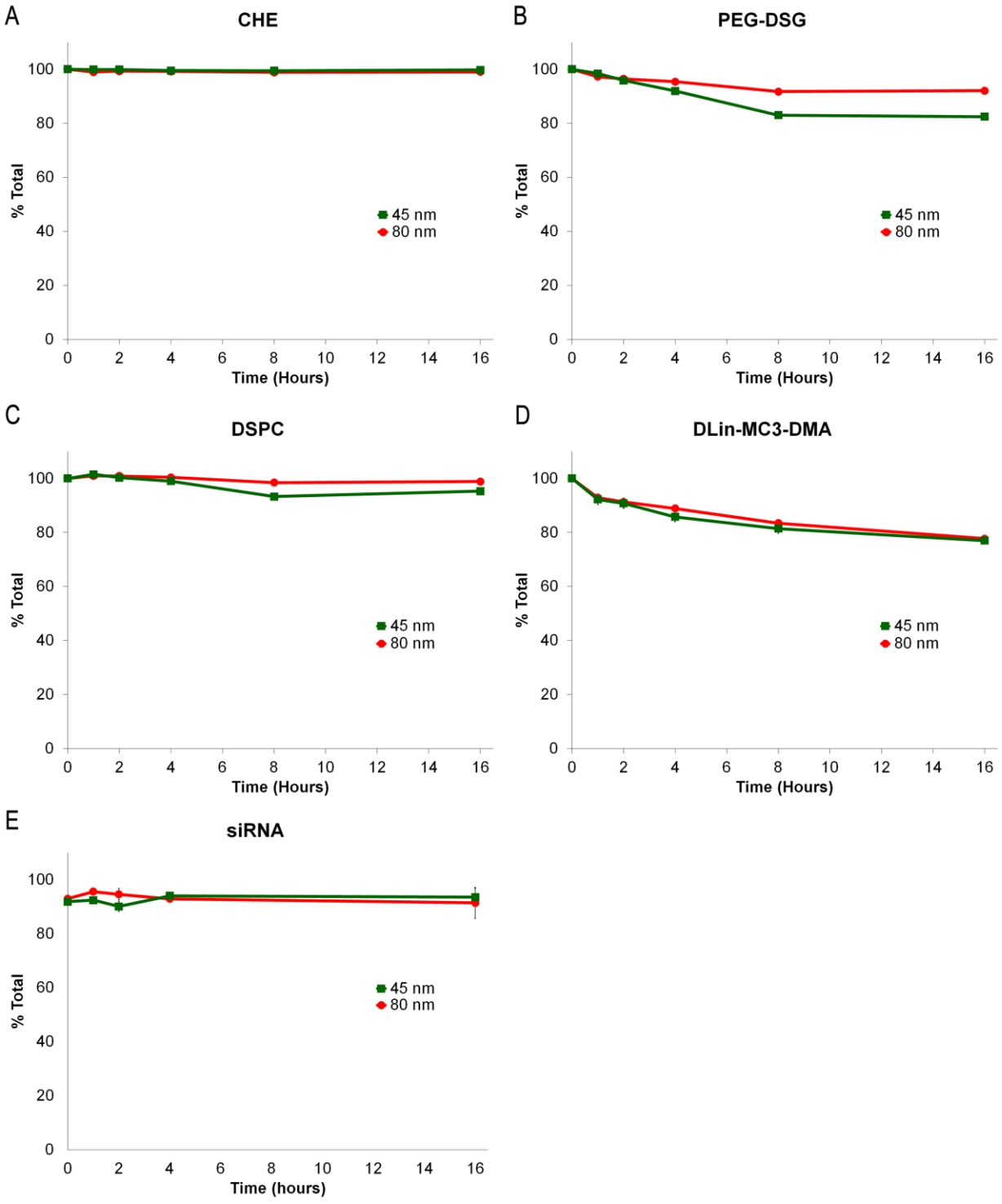
A
CHE
% Total
Time (Hours)
45 nm
80 nm
B
PEG-DSG
% Total
Time (Hours)
45 nm
80 nm
C
DSPC
% Total
Time (Hours)
45 nm
80 nm
D
DLin-MC3-DMA
% Total
Time (Hours)
45 nm
80 nm
E
siRNA
% Total
Time (hours)
45 nm
80 nm

Figure 4.7 Substitution of PEG-DSG for PEG-DMG Greatly Decreases the Dissociation Rates of Component Lipids.

^{3}H-PEG-DSG, ^{14}C-DSPC, ^{14}C-DLin-MC3-DMA or ^{3}H-CHE formulated with either 0.5 mol% or 1.5 mol% PEG-DSG were incubated for 0, 1, 2, 4, 8 and 16 hr at 37°C in mouse plasma and isolated by size exclusion chromatography. The rate of lipid dissociation from the LNP fractions was determined by using a linear fit for the first four time-points. (A) CHE remains associated with LNP. (B) PEG-DSG dissociates from 80 nm LNP at 1.2 %/hr and 2.2 %/hr for 45 nm LNP. (C) DSPC dissociates at less than 1 %/hr from both 80 and 45 nm diameter LNP. (D) DLin-MC3-DMA dissociates from 80 and 45 nm LNP at 2.6 %/hr and 3.3 %/hr respectively. (E) Over 90% of the siRNA remained associated with 45 and 80 nm diameter LNP for up to 16 hr as assayed for siRNA conjugated to Quasar 570 fluorophore, incubated with mouse plasma and resolved by size exclusion.

4.2.6 The Presence of PEG-DSG Extends LNP-siRNA Circulation Lifetimes and Reduces Hepatic Localization

A stable PEG coating on LNP systems results in long circulation lifetimes following i.v. administration and enhanced distribution to disease sites such as tumour sites (Allen et al., 2002a; Allen, 1994) and thus the LNP-siRNA systems containing PEG-DSG would be expected to exhibit different pharmacokinetics and biodistribution compared to systems containing PEG-DMG. Small, medium and large (~ 30, 45, 80 nm diameter) PEG-DSG LNP containing trace amounts of ^{3}H-CHE were formulated and blood levels assayed over 24 hr in mice following i.v. administration. LNP containing PEG-DSG exhibited dramatically increased circulation lifetimes (Figure 4.8A) compared to their counterparts containing PEG-DMG (Figure 4.2A). The greatest

difference is observed for 30 nm diameter PEG-DSG LNP, which has a circulation half-life of ~10.9 hr compared to < 0.25 hr for PEG-DMG LNP of similar size. The 45 and 80 nm diameter PEG-DSG LNP have approximate circulation half-lives of 0.5 and 3 hr, respectively. The relatively long circulation lifetime of 30 nm LNP can be attributed to the high PEG-lipid density on the surface which inhibits ApoE adsorption and cellular accumulation (Akinc et al., 2010; Mui et al., 2013).

Liver localization of LNP-siRNA was also affected by PEG-DSG. Not surprisingly, the rate of liver accumulation mirrors that of blood clearance (Figure 4.8B). At 24 hr post-injection, 70% of the total injected 45 nm LNP was found at the liver, whereas only 30% and 50% of the 30 nm and 80 nm LNP were found, respectively. Accumulation of LNP in the spleen, kidney, pancreas, lung, femurs and heart was also examined. Similar to the biodistribution profile of PEG-DMG LNP, less than 1% of the injected dose of any formulation was found in the pancreas, lung, femurs or heart (Figure 4.8C). Interestingly, only 5% of the injected 80 nm PEG-DSG LNP accumulated in the spleen, compared to 10% for PEG-DMG LNP (Figure 4.2C). Furthermore, there is an overall increase in the injected dose found in the kidney.

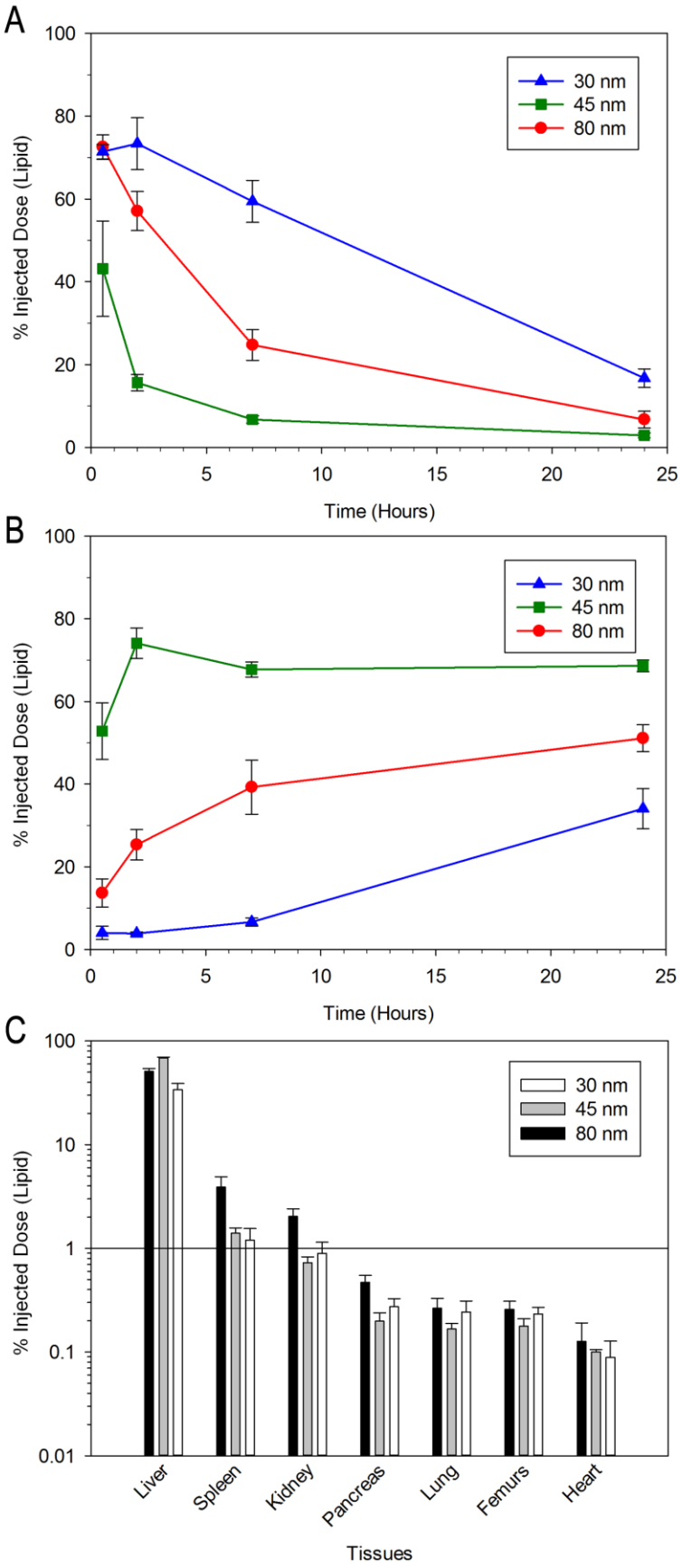
A
100
80
60
40
20
0
% Injected Dose (Lipid)
0
5
10
15
20
25
Time (Hours)
30 nm
45 nm
80 nm
B
100
80
60
40
20
0
% Injected Dose (Lipid)
0
5
10
15
20
25
Time (Hours)
30 nm
45 nm
80 nm
C
100
10
1
0.1
0.01
% Injected Dose (Lipid)
30 nm
45 nm
80 nm
Liver
Spleen
Kidney
Pancreas
Lung
Femurs
Heart
Tissues

Figure 4.8 Substitution of PEG-DMG for PEG-DSG Results in Increased LNP-siRNA Circulation Lifetimes.

Small (30nm), medium (45nm) or large (80nm) LNP formulated with PEG-DSG and labelled with trace amounts of ^{3}H-CHE were injected into mice at 0.3 mg siRNA/kg of body weight. Blood and tissues were collected at various time points and the amount of ^{3}H-CHE was determined. (A) Clearance of LNP from blood over a period of 24 hr. (B) Accumulation of LNP in liver over 24 hr. (C) Accumulation of LNP in various tissues at 24 hr. Results shown represent the mean ± s.d. of four animals.

4.3 Discussion

Small LNP with diameters of 30 nm or less exhibit enhanced penetration into diseased tissues such as tumours following i.v. administration (Cabral et al., 2011; Huo et al., 2013; Jain and Stylianopoulos, 2010). Similarly, we have recently shown that small LNP-siRNA are better able to reach regional lymph nodes and enter the circulation after being administered subcutaneously (Chapter 3)(Chen et al., 2014). However, we show here that small LNP-siRNA systems that contain rapidly dissociating PEG-lipids are less potent than their larger counterparts, possibly because the amino-lipid component also rapidly dissociates from the smaller particles. This reduced potency can be partially rescued by increasing the mole fraction of amino-lipid in the LNP or by increasing the amine-to-phosphate charge ratio. Although these results relate to the liver, the overall activity of small LNP-siRNA likely translates to tissues that require deeper penetration such as in tumors. The mouse FVII gene silencing model used here represents a measure for LNP-siRNA activity (Akinc et al., 2008; Jayaraman et al., 2012; Love et al., 2010; Semple et al., 2010). The ability of LNP-siRNA to penetrate into tissues require other models such

as 3D cell cultures or *in vivo* solid tumors which are currently being investigated in our laboratory. There are three aspects of this work that require discussion. The first concerns whether the time taken for the LNP-siRNA systems to reach the liver is long enough for appreciable loss of amino-lipid and second, whether factors other than amino-lipid content could be contributing to the poor potency of the smaller systems. The third topic concerns the delicate interplay between LNP size, amino-lipid content and the type of PEG-lipid employed and the biodistribution and gene silencing potency of LNP-siRNA systems, leading to questions regarding methods for improving the potency of LNP systems with diameters less than 50 nm. We discuss these areas in turn.

In this work we have demonstrated a correlation between the reduced potency of small (~30 nm diameter) LNP-siRNA systems and the increased rate of dissociation of lipid components, particularly the amino-lipid, for the smaller systems (Figure 4.3). The first question to be asked is whether there is adequate time following i.v. administration for the amino-lipid to dissociate to the extent that activity is compromised. It may be noted that the large majority of 30 and 45 nm diameter PEG-DMG LNP accumulate in the liver within 30 min post-injection (Figure 4.2B), however lipid dissociation likely continues after extravasation into the space of Disse in the liver and during the early stages of endocytosis into hepatocytes. It was recently reported that siRNA-gold conjugates delivered by LNP systems were found in the hepatocyte cytosol 1.5-2 hr post-administration (Gilleron et al., 2013). As noted, the $t_{1/2}$ for amino-lipid in the 30 nm diameter LNP could not be measured directly however it can be extrapolated from the $t_{1/2}$ measured for the 45 and 80 nm diameter systems assuming that the proportion of lipid dissociating per unit time is proportional to the surface area/particle volume, or 1/radius. Under this assumption, and using the measured dissociation $t_{1/2}$ of DLin-MC3-DMA from 45 nm (4.9 hr) and 80 nm diameter LNP (12 hr) (Figure 4.3D), the dissociation $t_{1/2}$ of DLin-MC3-DMA from 30 nm diameter LNP should be

in the range of 3.9 hr. Thus if it takes 2 hr for the LNP to effectively deliver its cargo to the cell interior it can be estimated that the proportion of amino-lipid in the LNP would be reduced from 50 mol% to 46 mol% for 80 nm LNP, 40 mol% for 45 nm diameter LNP and 37 mol% for 30 nm LNP. As noted elsewhere pronounced reductions in LNP-siRNA gene silencing activity have been noted for >50 nm diameter LNP containing less than 50 mol% amino-lipid (Belliveau et al., 2012; Jayaraman et al., 2012; Semple et al., 2010), consistent with the possibility that the limited activity of the 30 nm diameter systems arises at least in part from reduced levels of amino-lipid. It is important to note that despite being the most active LNP-siRNA, the 80 nm system had the lowest liver accumulation (~70% injected dose). Because the liver fenestrae are ~100 nm in diameter and 80 nm is the mean diameter of the size distribution, a small population of 80 nm LNP beyond 100 nm in diameter is likely excluded.

The second question is whether the reduction in potency of the smaller LNP-siRNA systems can be entirely attributed to enhanced lipid dissociation rates for smaller LNP. As shown in this work, a modest improvement in gene silencing potency was observed on increasing the LNP amino-lipid-to-siRNA ratio and a 3-fold improvement in potency was observed when the proportion of amino-lipid was increased to 60 mol% (Figure 4.5B). Both these observations are consistent with loss of amino-lipid contributing to the reduced potency of the 30 nm systems. However even with increased proportions of amino-lipid and reduced siRNA content, gene silencing activity cannot be raised to levels observed for the 80 nm diameter systems (ED_{50} 0.04 mg siRNA/kg vs ED_{50} of 0.3 mg siRNA/kg), suggesting that inefficient endosomal release resulting from diminished amino-lipid content cannot fully explain the overall reduction in potency of small LNP-siRNA systems. The difference in activity between large and small systems could arise due to differences in liver accumulation. However small and medium-sized (~30 and 45 nm

diameter) PEG-DMG LNP exhibit similar clearance and liver accumulation kinetics (Figure 4.2) yet have markedly different gene silencing potencies (Figure 4.1). It is also conceivable that the higher initial PEG-lipid content for smaller LNP could have some influence on LNP-siRNA activity. Because particle size is directly related to the amount of PEG-lipid used, these variables are difficult to evaluate independently. Differential protein adsorption could also explain the difference in activity since it has been shown that the efficacy of LNP-siRNA requires the adsorption of ApoE (Akinc et al., 2010). LNP that differ in size also differs in surface curvature which could directly affect the type and amount of protein adsorbed. This is currently being investigated. Another possibility is that the reduced activity of smaller systems is related to the reduced amino-lipid or siRNA payload for smaller LNP systems. For example, a 30 nm diameter LNP would only deliver ~1/20 as many siRNA copies as compared to an 80 nm diameter system.

The third topic for discussion concerns alternative ways of improving the gene silencing potency of small LNP-siRNA systems. We show here that the dissociation of lipid components from LNP can be dramatically reduced by utilizing the PEG-DSG coat lipid during formulation rather than the rapidly dissociating PEG-DMG lipid. However these systems are markedly less potent than systems containing PEG-DMG due to the long-lived PEG coat, which inhibits ApoE adsorption and prolongs circulation (Akinc et al., 2010; Mui et al., 2013), illustrating the complex interplay between particle size, amino-lipid content and the type of PEG-lipid employed to achieve LNP-siRNA systems with high potencies *in vivo*. It is also interesting to note that in contrast to 30 nm LNP that contain PEG-DMG, those that contain PEG-DSG exhibit the longest circulation lifetimes. The reason for the long circulation lifetime for the smaller LNP can be attributed to the fact that this system contained 5mol% PEG-DSG (which does not dissociate from the LNP) leading to long residence times in the circulation. The reduced circulation lifetimes of the 45 nm

diameter system can be attributed to the much lower PEG-DSG levels (1.5 mol%). The surprising observation that the 80 nm diameter system (which contained 0.5 mol% PEG-DSG) exhibits longer circulation lifetimes may arise due to reduced rates of liver accumulation as such systems will penetrate less readily through the fenestrated liver vasculature.

It is important to note that these studies elucidating the delicate interplay between LNP size, activity and stability is made possible by the use of rapid mixing techniques. This has enabled the production of LNP with properties largely dictated by its lipid composition. Although this also enables the study of parameters previously unexplored, this results in an important criticism in the work presented in Chapters 3 and 4. PEG-lipid is used to produce LNP with diameters ranging from approximately 30-120 nm and because of this, the amount of PEG-lipid and particle diameter will always be confounded variables. Therefore, the contribution of each parameter to the ultimate change in LNP properties *in vivo* remain difficult to separate.

It is possible that further improvements in the potency of small (30 nm diameter) systems will only be achievable by new approaches. This is particularly true if the activity of smaller systems is fundamentally limited by the siRNA payload. It is possible to increase the amount of siRNA per particle by increasing the siRNA-to-lipid ratio to values approaching charge ratios of one, however >50 nm LNP-siRNA exhibit reduced gene silencing activity (Belliveau et al., 2012) which is consistent with our current findings for 30 nm systems (Figure 4.5A), indicating excess cationic amino-lipid is necessary for endosomal release. It is possible that gains could be made in improving the efficiency of siRNA release from endosomes following endocytosis, as it has been shown that only ~1-2% of endocytosed siRNA reaches the cytoplasm (Gilleron et al., 2013). However methods for achieving this are not obvious. Replacement of DSPC with lipids such as DOPE may facilitate endosomal fusion somewhat (Farhood et al., 1995; Hafez et al., 2001). If the

limiting factor is the amount of amino-lipid per particle, it should be noted that incorporation of more than 60 mol% amino-lipid leads to progressively lower encapsulation efficiencies (Leung et al., 2015) and larger sizes and polydispersity (data not shown). Also, raising the amino-lipid content may compromise the therapeutic index of LNP-siRNA formulations as the dose limiting toxicity is related to the nanoparticle carrier (Barros and Gollob, 2012; Chonn et al., 1991).

In summary, we have shown that although LNP-siRNA systems with diameters < 45 nm can be readily manufactured employing microfluidic mixing techniques, the gene silencing potency of these systems in hepatocytes *in vivo* is significantly reduced compared to their larger counterparts. At least part of this reduction in activity can be attributed to the reduced stability of smaller systems which leads to rapid dissociation of lipid components such as the amino-lipid. The activity of small LNP-siRNA can be improved by increasing the amino-lipid content which improves the potency by approximately a factor of three, however these LNP systems are still approximately 10 times less potent than 80 nm diameter systems. It is possible that gene silencing potency of smaller systems is fundamentally limited by the small siRNA payload and that new approaches that enhance the efficiency of endosomal escape may be required for further gains in potency.

Chapter 5: Lipophilic Dexamethasone Pro-drugs as Potent Suppressors of the Immunostimulatory Effects of Lipid Nanoparticle Formulations of Nucleic Acid Polymers

5.1 Synopsis

Lipid nanoparticle (LNP) systems are playing a leading role to enable clinical applications of gene therapies based on DNA or RNA polymers (Yin et al., 2014). A factor impeding more rapid clinical acceptance of LNP therapeutics is that LNP formulations of nucleic acid polymers can be immunostimulatory, necessitating co-administration of immunosuppressive agents such as dexamethasone. Here we develop hydrophobic pro-drug derivatives of dexamethasone that can be readily incorporated into LNP systems. We show that the presence of dexamethasone pro-drug LD003 effectively suppresses production of cytokines such as KC/GRO, TNFα, IL-1β and IL-6 following i.v. administration of LNP loaded with immune stimulatory DNA oligonucleotides containing cytosine-guanine dinucleotide (CpG) motifs. Superior immunosuppressive effects are observed at LD003 dose levels corresponding to 0.5 mg/kg dexamethasone than can be achieved from doses of 20 mg/kg of free dexamethasone. Further, the presence of LD003 in LNP containing unmodified mRNA significantly reduced pro-inflammatory cytokine levels following i.v. administration. These results suggest that incorporation of low levels of hydrophobic pro-drugs such as LD003 into LNP systems could provide a convenient method for avoiding the immunostimulatory consequences of systemic administration of LNP formulations of genetic drugs. In general, hydrophobic pro-drugs enable LNP to contain multiple therapeutic agents in addition to nucleic acids enabling it to perform multiple functions simultaneously.

5.2 Results

5.2.1 Acylated Dexamethasone Pro-drugs Can Be Incorporated into LNP with Nucleic Acid

Dexamethasone has been used prophylactically to reduce inflammatory responses to antibiotics and chemotherapeutics (Szebeni et al., 2011) as well as LNP formulations of siRNA (Abrams et al., 2010; Coelho et al., 2013). LNP systems are accumulated by cells of the immune system (macrophages and dendritic cells) following systemic administration (Basha et al., 2011; Litzinger et al., 1996), offering the possibility of delivering dexamethasone more specifically to immune cells if associated with the LNP. To achieve this association we synthesized five hydrophobic derivatives of dexamethasone (LD001-005) by attaching linoleoyl acyl chains (using a succinate linker containing biodegradable ester bonds) to the hydroxyl located on carbon 21 of dexamethasone as shown in Figure 5.1. The formulation characteristics of hydrophobic materials into LNP systems can be a sensitive function of their hydrophobicity, thus compounds were synthesized with one or two linoleoyl acyl chains and with or without ionizable amino functions. The compounds with ionizable amino functions mimic the amino-lipids that are routinely used to encapsulate nucleic acids in LNP (Jayaraman et al., 2012; Semple et al., 2010). Compounds LD001 and LD003 contain a single linoleoyl chain whereas compounds LD002 and LD004 contain two, and LD001 and LD004 also contain a single ionizable dimethylamino group. Compound LD005, which resembles LD003 as it contains a single alkyl chain and no amino function, does not have a succinate linker and is not biodegradable and thus was used as a negative control.

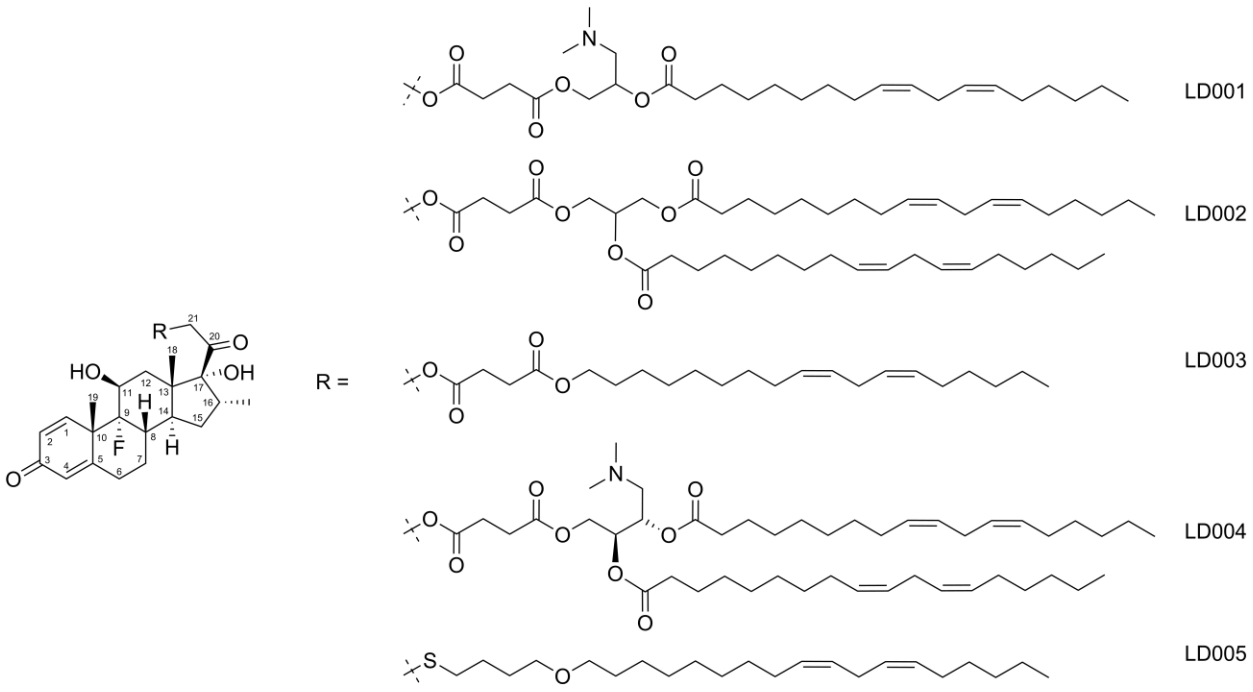

Figure 5.1 Structures of Lipophilic Dexamethasone Prodrugs.

Dexamethasone containing a single linoleyl moiety with a tertiary amine (LD001), two linoleyl moieties (LD002), single linoleyl moiety (LD003), two linoleyl moieties with a tertiary amine (LD004) and a single linoleyl moiety but no ester bonds (LD005) were synthesized to increase its relative hydrophobicity.

The physical properties and formulation characteristics of compounds LD001-005 are summarized in Table 5.1. The hydrophobicity of the compounds is reflected by their logP or logD values (for non-ionizable or ionizable compounds respectively) calculated as the predicted octanol-water partitioning coefficient. The log P (or log D) values ranged from 5 for the mono-acylated compounds to 14 for the diacylated compounds. The dexamethasone derivatives (up to 10 mol% of total lipid) were dissolved in ethanol together with DMAP-BLP (a potent ionizable cationic lipid (Chen et al., 2014; Rungta et al., 2013)), distearoylphosphatidylcholine (DSPC), cholesterol

and a polyethylene glycol-containing lipid with C_{14} acyl chains (PEG-DMG (Chen et al., 2014)) at mole ratios of 10, 40, 10, 38.5 and 1.5 respectively. LNP containing the dexamethasone derivative and an immunostimulatory CpG-containing oligonucleotide (CpG ODN) were formulated by mixing the lipid mixture in ethanol with the CpG ODN in aqueous media using rapid mixing techniques as indicated in Methods. As shown in Table 5.1 all formulations had particle diameters of approximately 50 nm with polydispersity indices (PdI) < 0.1 indicating that incorporation of the dexamethasone derivatives into the LNP did not significantly affect particle size or homogeneity. Complete entrapment of LD002, LD003 and LD005 was observed, whereas somewhat lower trapping efficiencies were observed for the dexamethasone derivatives containing amino functions (LD001 and LD004). Therefore, hydrophobicity alone cannot be used to predict the likelihood of complete entrapment of the molecule and the ionizable moiety plays a major contributing factor. This is not surprising since LNP are formed by rapid mixing of lipids dissolved in ethanol with a low pH buffer in order to entrap nucleic acid. The amino-moiety will be charged and without having anchors of sufficient hydrophobicity (such as dilinoleyl for amino-lipids), the compound may be partially soluble in the aqueous phase, reducing the incorporation into the primarily hydrophobic core of LNP.

Table 5.1 Pro-drug and Lipid Nanoparticle Parameters

Pro-drug	Structural Features	Predicted LogP (or LogD)*	Particle Diameter (nm)	PdI	Target mol%	% Pro-drug Entrapment
LD001	Monolinoleoyl, ionizable	5.07/7.57	46	0.08	10	~40
LD002	Dilinoleoyl	14.95	46	0.09	10	100
LD003	Monolinoleoyl	8.92	49	0.06	10	100
LD004	Dilinoleoyl, ionizable	11.58/14.01	48	0.04	10	~60
LD005	Monolinoleoyl, non-degradable	10.36	50	0.06	10	100

*LogD predicted at two pH values (pH 4 / pH 7.4).

5.2.2 Formulated Pro-drugs are Degradable by Esterases

Biological activity of LNP-associated dexamethasone derivatives requires the release of the active dexamethasone compound. In order to ascertain potential bioavailability, the LNP containing dexamethasone derivatives were incubated with mouse plasma and the amount of intact dexamethasone derivative was determined at various times. As shown in Figure 5.2, incubation for 1 hr resulted in degradation of approximately 90% and 70% respectively of LNP-associated LD001 and LD003. Little degradation was observed for LNP containing LD002, LD004 or LD005. Degradation can be attributed to the presence of esterases in mouse plasma (Berry et al., 2009; Rudakova et al., 2011). As LD005 did not contain any biodegradable ester linkages no degradation was expected, however the lack of degradation of LD002 and LD004 suggests that these derivatives were less accessible to plasma esterases. This could be attributed to the more hydrophobic nature of these compounds which may cause the derivative to reside deep in the

hydrophobic LNP core, where it would be less available to esterases. It is possible that the rate of dexamethasone release could be modulated by altering the hydrophobicity of the pro-drug molecule. In order to demonstrate that esterases can in fact degrade LNP-associated dexamethasone derivatives, LNP containing LD003 were incubated with purified esterases (Figure 5.3), resulting in appreciable degradation after 4 hr. This degradation was abolished by heat denaturation of the enzyme.

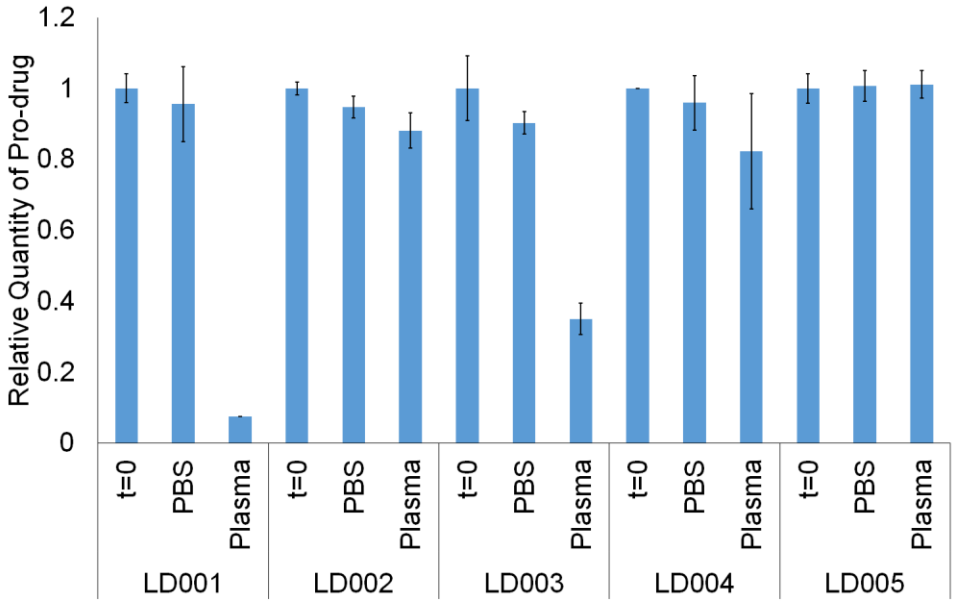

Figure 5.2 Formulated Prodrugs are Degradable by Esterase-rich Plasma.

Lipophilic dexamethasone pro-drugs were formulated into LNP containing nucleic acid and incubated in for 1 hr at 37°C in PBS or mouse plasma which is enriched in carboxylesterases. The amount of residual parent compound in the mixture was determined by UPLC analysis and the data was normalized to amounts in pre-incubation mixtures (t=0). Error bars represent ± s.d. of at least three replicates.

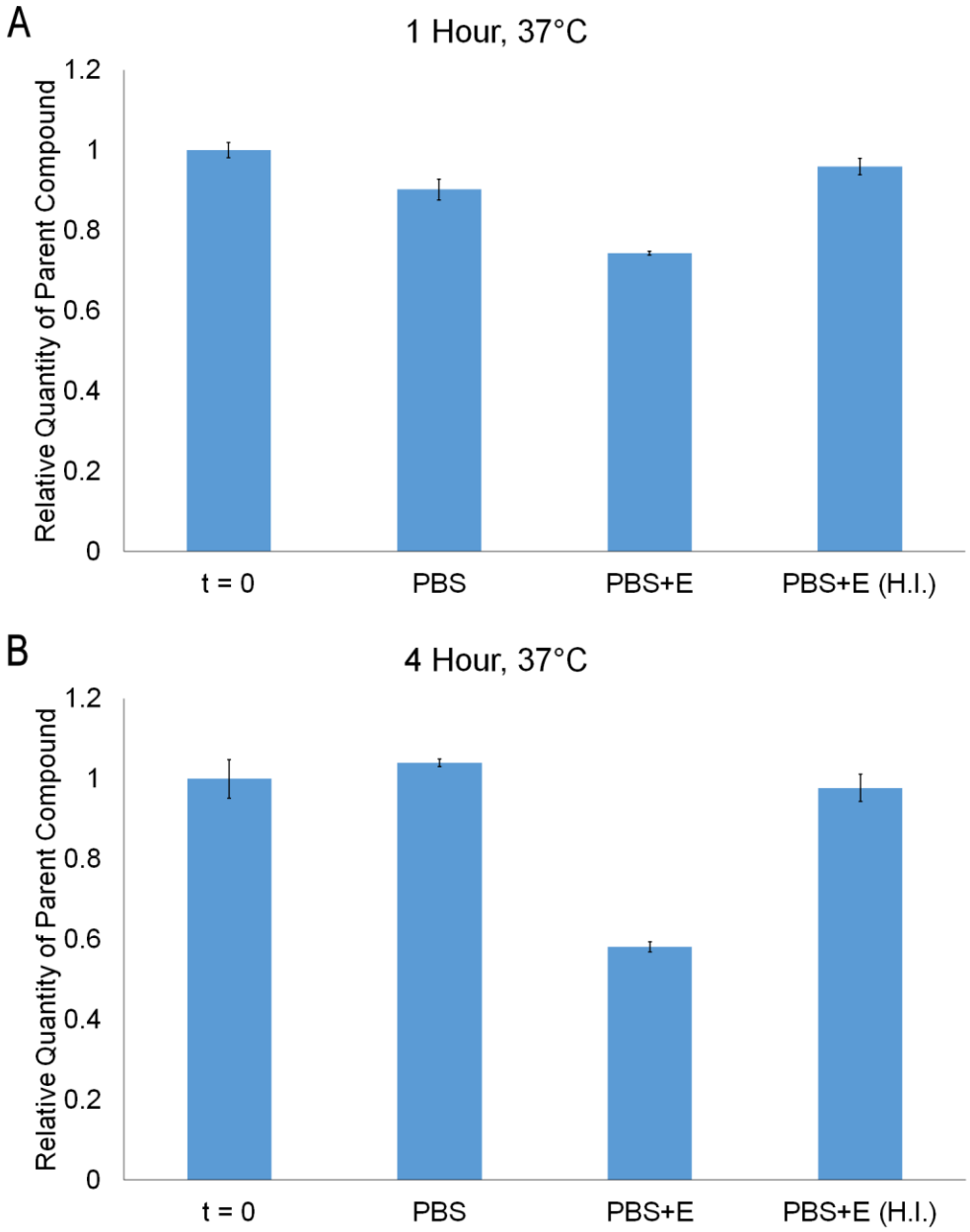

Figure 5.3 LD003 is Degraded by Esterases.

LD003 was formulated into LNP and incubated for 1 hr **(A)** or 4 hr **(B)** at 37°C with either 10U of purified porcine esterase (PBS+E) or heat inactivated esterase (H.I.) in PBS. Amount of residual parent LD003 was determined by UPLC analysis and data is normalized to pre-incubation mixtures (t=0). Error bars represent ± s.d. of at least three replicates.

5.2.3 Formulated Pro-drugs do not Impact the Tolerability of LNP

LNP has been shown to be very well tolerated in both cultured cells and *in vivo*. In order to assess whether the incorporation of pro-drugs impact LNP tolerability, the effect on HeLa cell viability and the ability of LNP to lyse red blood cells (RBC) were determined. It was found that LNP were very well tolerated over the concentration range of 0.5 ng/mL to 5 mg/mL total lipid (Figure 5.4A). When 10 mol% of LD003 was incorporated into LNP, no change in cell viability was observed indicating that LNP containing hydrophobic pro-drugs are just as well tolerated as LNP. Typically, less than 50 ug/mL of lipid is necessary for LNP-siRNA mediated gene silencing (Tam et al., 2013). Furthermore, very little hemolysis was observed for LNP with or without LD003 and up to 2 mg/mL lipid (Figure 5.4B) suggesting that pro-drug containing LNP can be used *in vivo*. It is important to note that a concentration of 2 mg/mL lipid is equivalent to a lipid dose of 160 mg/kg assuming a 25 g mouse has 80 mL/kg blood.

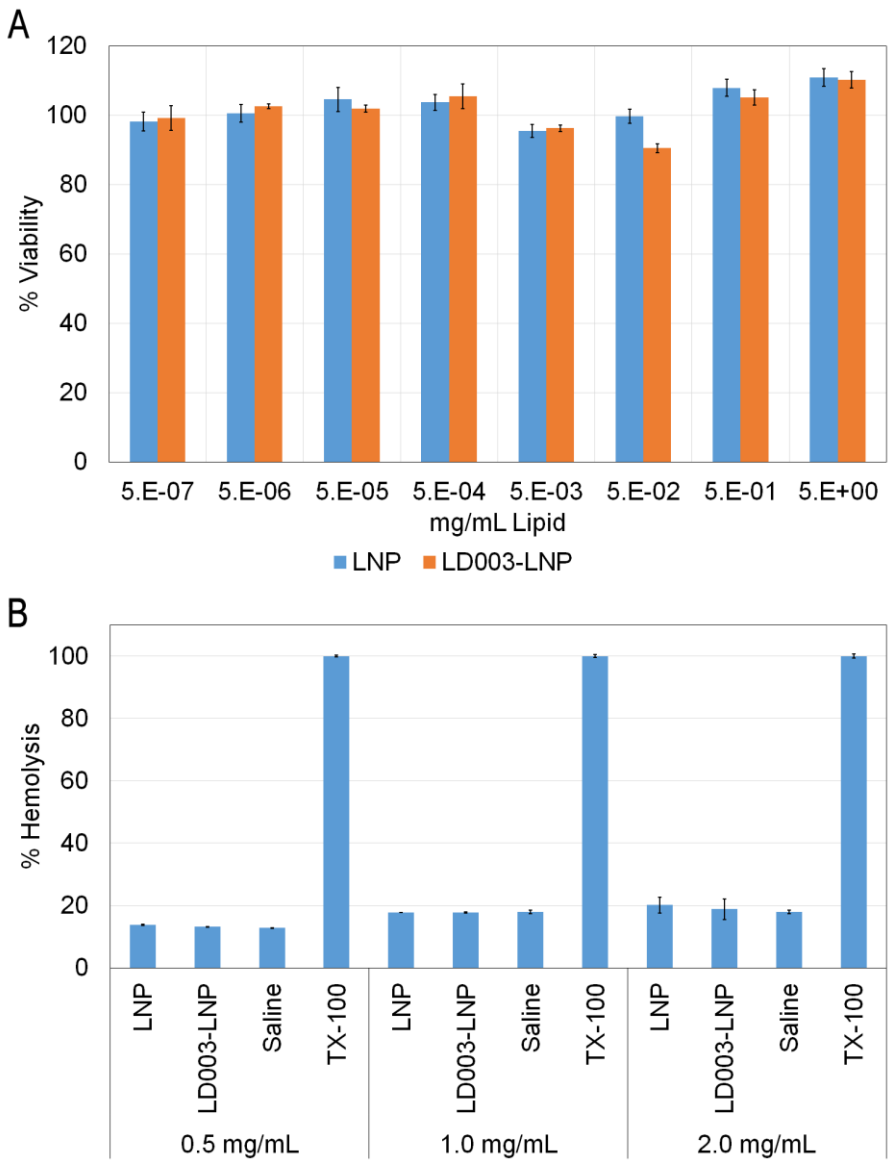

Figure 5.4 Formulated Prodrugs Do Not Impact the Tolerability of LNP.

LD003 was formulated into LNP and tolerability was assessed by measuring cell viability and hemolysis. **(A)** HeLa cells were incubated with LNP or LD003-LNP over the lipid concentration range of 5×10^{-7} to 5 mg/mL for 24 hr and cell viability was measured by MTT assay. **(B)** The ability for LD003-LNP to cause hemolysis was assessed over the concentration range of 0.5-2.0 mg/mL. Control LNP contains no LD003. Data was normalized to samples incubated with Triton X-100 (TX-100).

5.2.4 Dexamethasone Pro-drugs Ameliorate Immune Stimulation in CpG Mouse Model

LNP-mediated immune stimulation is exacerbated when the cargo is not designed to evade immune detection (Dow et al., 1999; Mui et al., 2001; Whitmore et al., 1999). It has been shown previously that co-administration of dexamethasone with LNP greatly reduces immune stimulation (Abrams et al., 2010; Coelho et al., 2013). We suspect that incorporation of dexamethasone into the LNP will greatly improve its ability to abrogate immune stimulation since it will simultaneously enter the cells and release with the immune stimulatory payload. Previous work has shown that the CpG-ODN 5'-AACGTTGAGGGGCAT-3', which is complementary to the initiation codon region of the human/mouse c-myc proto-oncogene, is highly immunostimulatory (Mui et al., 2001; Semple et al., 2005), and can serve as an effective vaccine immune adjuvant (de Jong et al., 2007). LNP formulations containing CpG-ODN (LNP-CpG) and various amounts and types of dexamethasone pro-drugs were prepared (CpG-ODN-to-total lipid ratio 0.1 wt/wt). The lipid composition was dexamethasone pro-drug, DMAP-BLP, DSPC, cholesterol and PEG-DMG at the mole ratios of X, 50-X, 10, 38.5 and 1.5 respectively. The dexamethasone pro-drugs were incorporated at X=0, 1, 4 mol% corresponding to 0, 0.5 and 2 mg/kg dexamethasone equivalents. Mice were injected with LNP-CpG or LNP-CpG with dexamethasone pro-drug at a dose level of 10 mg CpG-ODN/kg body weight and blood was collected after 2 and 4 hr. Free dexamethasone-21-phosphate (Dex-21-P) was also co-administered with LNP-CpG at doses of 5 and 20 mg/kg for comparison.

The ability of the dexamethasone derivatives and free dexamethasone to ameliorate the immunostimulatory effects of LNP-CpG are shown in Figure 5.5. Animals injected with LNP-CpG alone had elevated plasma cytokine (IL-10, KC/GRO, TNFα, IL-1β, IL-6) levels 2 hr post administration. As shown in Figure 5.5 A-D, incorporation of dexamethasone pro-drugs at 0.5

mg/kg and 2 mg/kg levels resulted in substantially reduced plasma cytokine levels, particularly for LD001 and LD003 where as little as 0.5 mg/kg dexamethasone pro-drug resulted in more than 90% inhibition of KC/GRO, TNFα, IL-1β and IL-6 production. These levels are close to background levels (Figure 5.5F). Equally impressive immunosuppressive effects were observed at 4 hr (Figure 5.6). The immunosuppressive potencies of LD001 and LD003 are particularly notable when contrasted with the effects of free dexamethasone. As shown in Figure 5.5E, a dose of Dex-21-P at 20 mg/kg resulted in markedly less cytokine inhibition as compared to 0.5 mg/kg LD001 or LD003 incorporated into the LNP. As expected, incorporation of the non-hydrolizable dexamethasone derivative LD005 into LNP-CpG formulations did not result in any immunosuppressive effects (Figure 5.7).

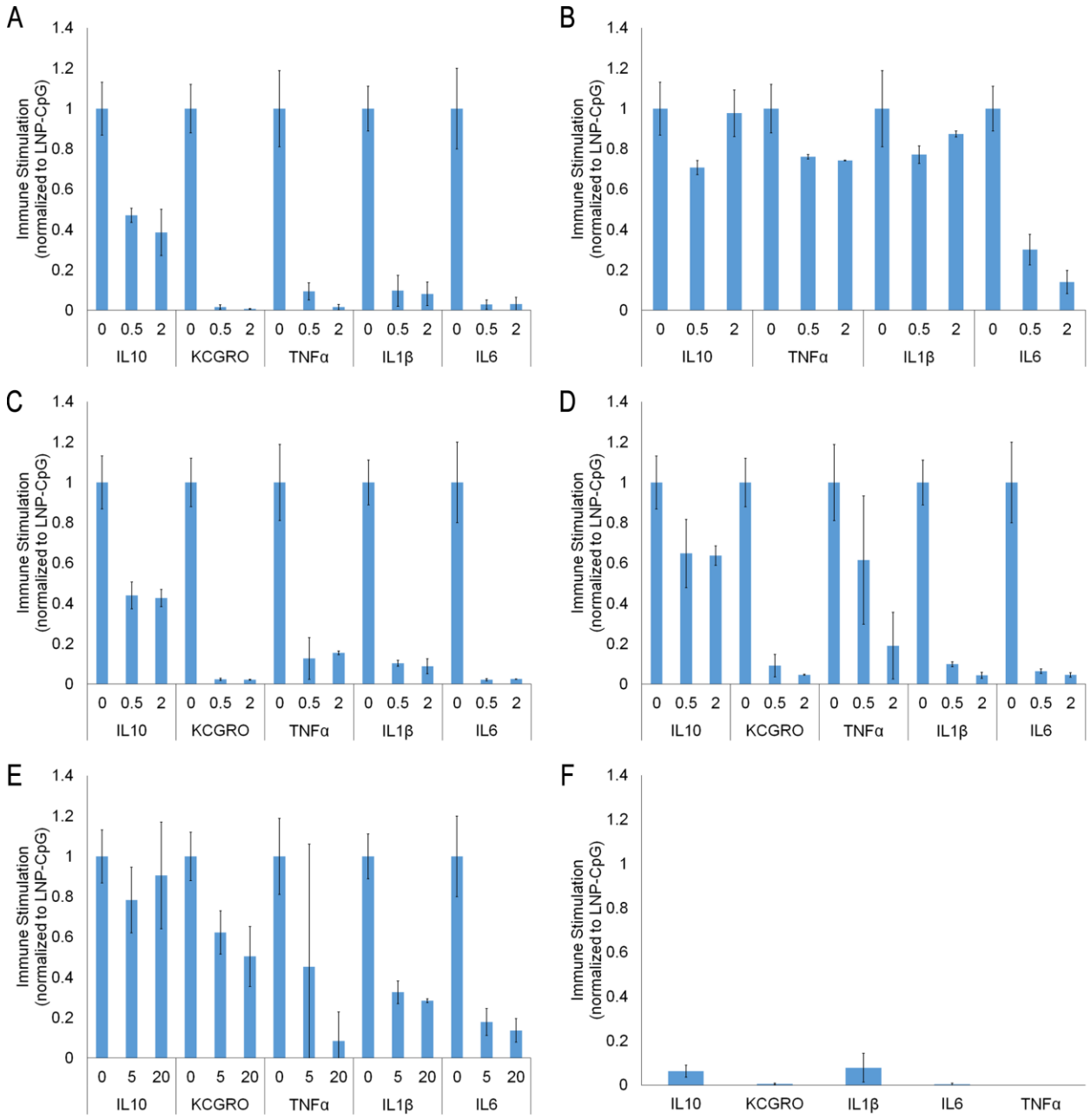

Figure 5.5 Lipophilic Pro-drug Derivatives of Dexamethasone Can Dramatically Ameliorate Immunostimulatory Effects of LNP-CpG in Mice.

Mice were injected with LNP-CpG at doses corresponding to 10 mg/kg CpG. **(A-D)** Dexamethasone pro-drugs (LD001-004) were formulated into LNP CpG-oligo at 0, 1 and 4 mol% dexamethasone derivative (corresponding to 0.5 and 2 mg/kg dexamethasone equivalents), blood

was collected after 2 hr and the levels of IL-10, KC/GRO, TNFα, IL-1β, and IL-6 were measured in the plasma. **(E)** Cytokine levels observed for mice receiving free dexamethasone (dexamethasone-21-phosphate; Dex-21-P) co-injected with LNP-CpG (10 mg/kg) at 0, 5 and 20 mg/kg Dex-21-P dose levels. **(F)** Cytokine levels observed for mice injected with PBS. Data is normalized to the cytokine levels observed for mice treated with LNP-CpG that did not contain a dexamethasone derivative. Error bars represent ± s.d. using four animals.

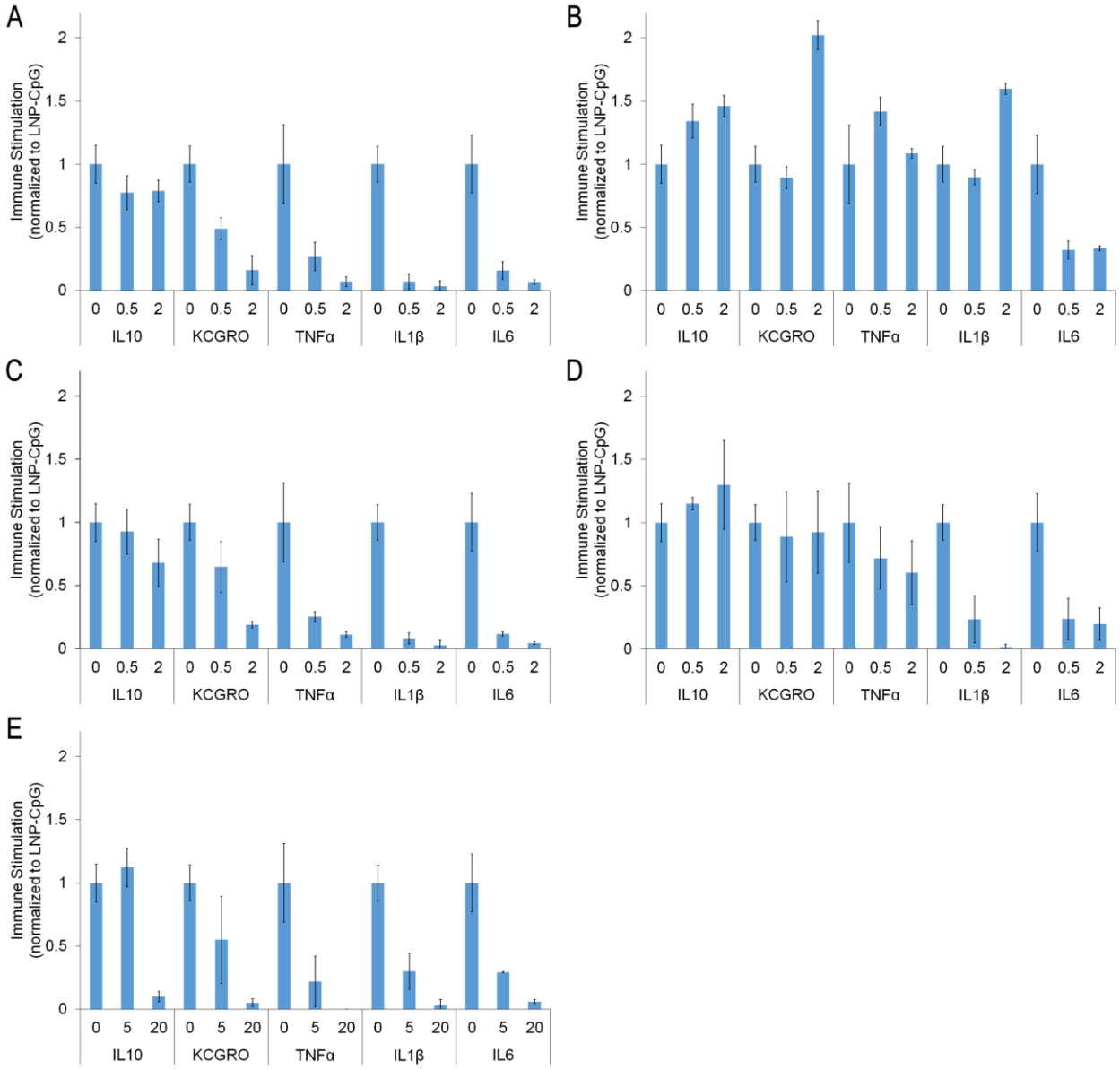

Figure 5.6 LD003 Continues to Dramatically Ameliorate Immunostimulatory Effects of LNP-CpG After 4 hr.

Mice were injected with LNP-CpG at doses corresponding to 10 mg/kg CpG. **(A-D)** Dexamethasone pro-drugs (LD001-004) were formulated into LNP-CpG at 0, 1 and 4 mol% dexamethasone derivative (corresponding to 0.5 and 2 mg/kg dexamethasone equivalents), blood was collected after 4 hr and the levels of IL-10, KC/GRO, TNFα, IL-1β, and IL-6 were measured

in the plasma. **(E)** Cytokine levels observed for mice receiving Dex-21-P co-injected with LNP-CpG (10 mg/kg) at 0, 5 and 20 mg/kg Dex-21-P dose levels. Data is normalized to the cytokine levels observed for mice treated with LNP CpG-oligo that did not contain a dexamethasone derivative. Error bars represent ± s.d. using four animals.

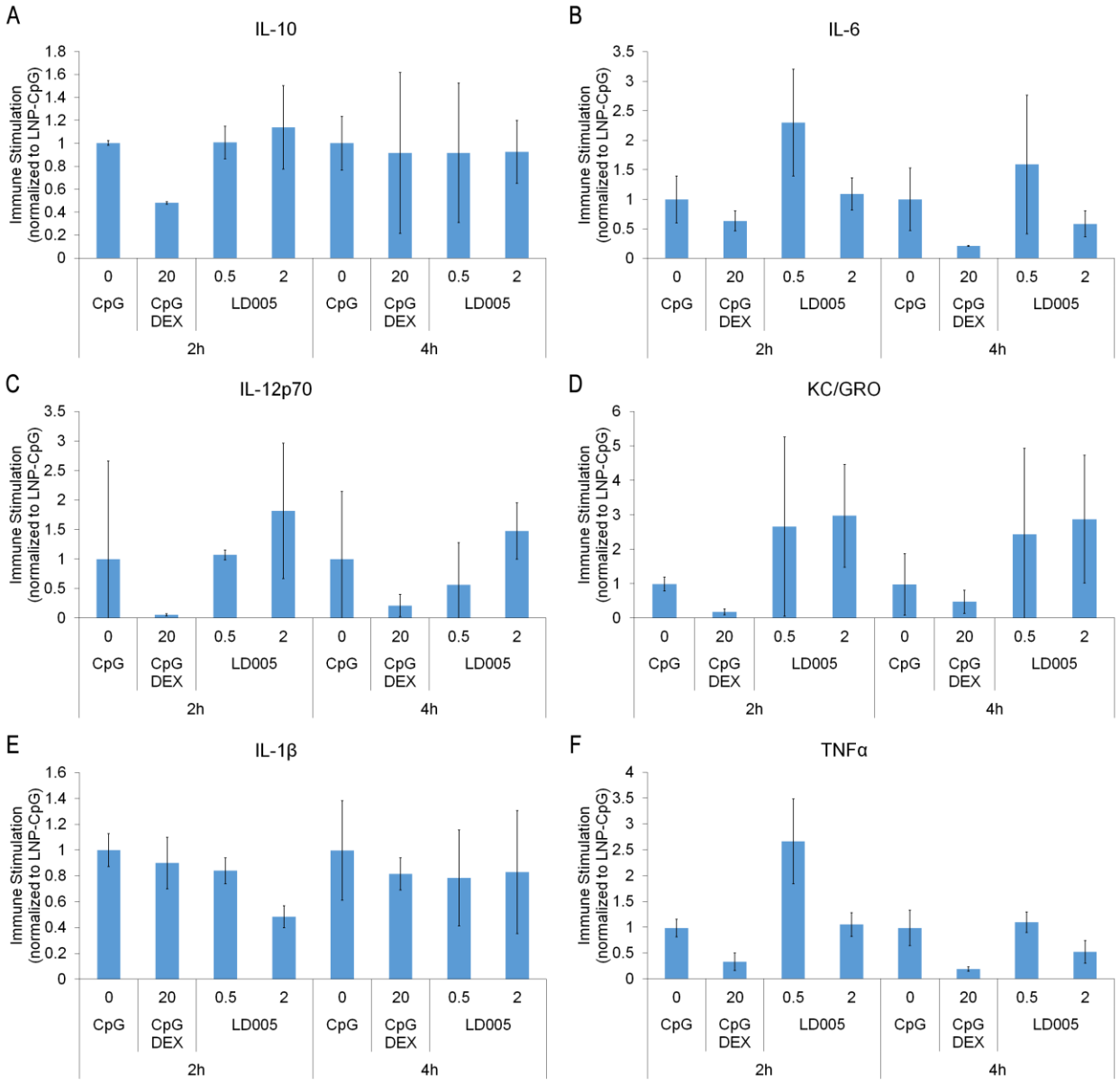

Figure 5.7 LD005 is Unable to Mitigate LNP-CpG Mediated Immune Stimulation.

Dex-21-P was co-injected at 0 and 20 mg/kg with LNP containing CpG oligonucleotide at 10 mg/kg CpG. Dexamethasone pro-drug LD005 was formulated into LNP-CpG and injected at the dexamethasone equivalence of 0.5 and 2 mg/kg. Plasma was collected after 2 and 4 hr and the amount of IL-10, IL-6, IL-12p70, KC/GRO, IL-1β and TNFα in the plasma was measured. Results shown represent the mean ± s.d. of four animals

5.2.5 LD003 Ameliorates LNP-mRNA Mediated Immune Stimulation in Mice

The immunosuppressive effects of LD001 and LD003 for LNP containing CpG-ODN suggest potential utility as a minor component in LNP formulations of antisense oligonucleotides and siRNA to avoid potential immunostimulation. However from a wider gene therapy point of view it is of interest to determine whether these immunosuppressive qualities extend to longer RNA polymers such as plasmid DNA or mRNA. LNP-mRNA formulations are showing considerable therapeutic promise (Thess et al., 2015). The potential for obviating the need to include modified nucleosides to reduce immunostimulatory potential (Anderson et al., 2011; Anderson et al., 2010; Kariko et al., 2005; Kariko et al., 2008; Kormann et al., 2011) is of particular interest as it would significantly simplify mRNA synthesis. In order to test the effectiveness of a dexamethasone derivative for preventing LNP-mRNA mediated immune activation, an unmodified 1.7 kb mRNA coding for firefly luciferase was formulated into LNP containing 0 or 10 mol% LD003 and injected into mice at a dose level of 3 mg mRNA /kg. For the LNP containing 10 mol% LD003 this corresponded to a dose of ~5 mg dexamethasone equivalents/kg body weight. Blood was collected 2 hr post-injection and IL-6, TNFα, KC/GRO, IL-12p70, IL-1β, and IL-10 levels in the plasma were determined. As shown in Figure 5.8, significantly elevated cytokine levels were observed in animals treated with LNP-mRNA as compared to the PBS control group: IL-6, TNFα and KC/GRO were highly elevated (> 10-fold compared to PBS) while IL-12p70, IL-1β, and IL-10 were mildly elevated. Animals that were treated with LNP-mRNA containing 10 mol% LD003 showed much lower cytokine levels than animals treated with LNP-mRNA without pro-drug. Production of IL-12p70, IL-1β, and IL-10 was completely prevented while IL-6 and TNFα were reduced by nearly 20-fold. KC/GRO levels were reduced four-fold.

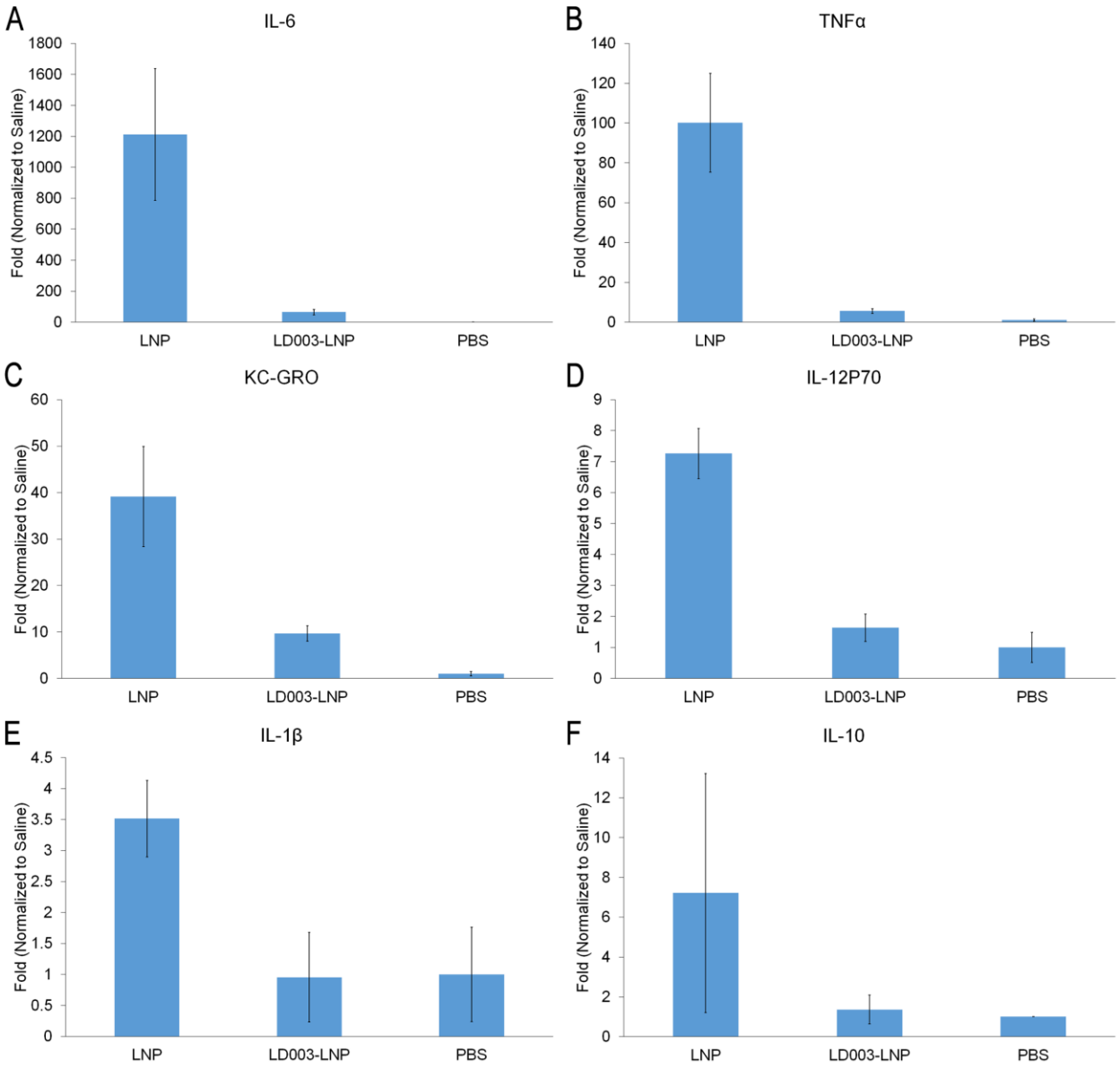

Figure 5.8 LD003 Ameliorates LNP-mRNA Mediated Immune Stimulation.

LNP-mRNA with or without 10 mol% dexamethasone pro-drug LD003 was formulated and injected at an mRNA dose of 3 mg/kg (approximately 5 mg/kg dexamethasone). Plasma was collected after 2 hr and the amount of **(A)** IL-6, **(B)** TNFα, **(C)** KC-GRO, **(D)** IL-12p70, **(E)** IL-1β and **(F)** IL-10 was measured. Data is normalized to the non-stimulated PBS control group and error bars represent the mean ± s.d. of four animals.

5.2.6 LD003 Reduces Injection Site Reactions to LNP-siRNA

It was observed previously that injection of large (80 nm) LNP-siRNA containing PEG-DMG in the interscapular subcutaneous space resulted in skin lesions at the injection site (refer to Chapter 3 (Chen et al., 2014)). This local reaction was postulated to be a local immune reaction to the LNP-siRNA deposit and these lesions are a result of irritation and discomfort. We proposed that the use of immunosuppressants could possibly ameliorate this response. Here we show that administration of soluble Dex-21-P intraperitoneally 30 minutes prior to the injection of 80 nm LNP-siRNA in the interscapular space was unable to reduce the visible irritation caused by LNP buildup the immune cell infiltration at the injection site (Figure 5.9 A and B left). In contrast, drastic improvements were observed when the 80 nm LNP-siRNA contained LD003 (Figure 5.9C left). Furthermore, the loose interscapular space for animals injected with LNP with or without Dex-21-P became very rigid while the skin remained loose for mice injected with LD003-LNP. Isolation, sectioning and staining of the injection site reveal that the cell density around the injection site was visibly higher for animals injected with LNP with or without Dex-21-P (Figure 5.9 A and B right). The cell density is visibly reduced for animals injected with LD003-LNP (Figure 5.9C right), although still greater than compared to control animals (Figure 5.9D right).

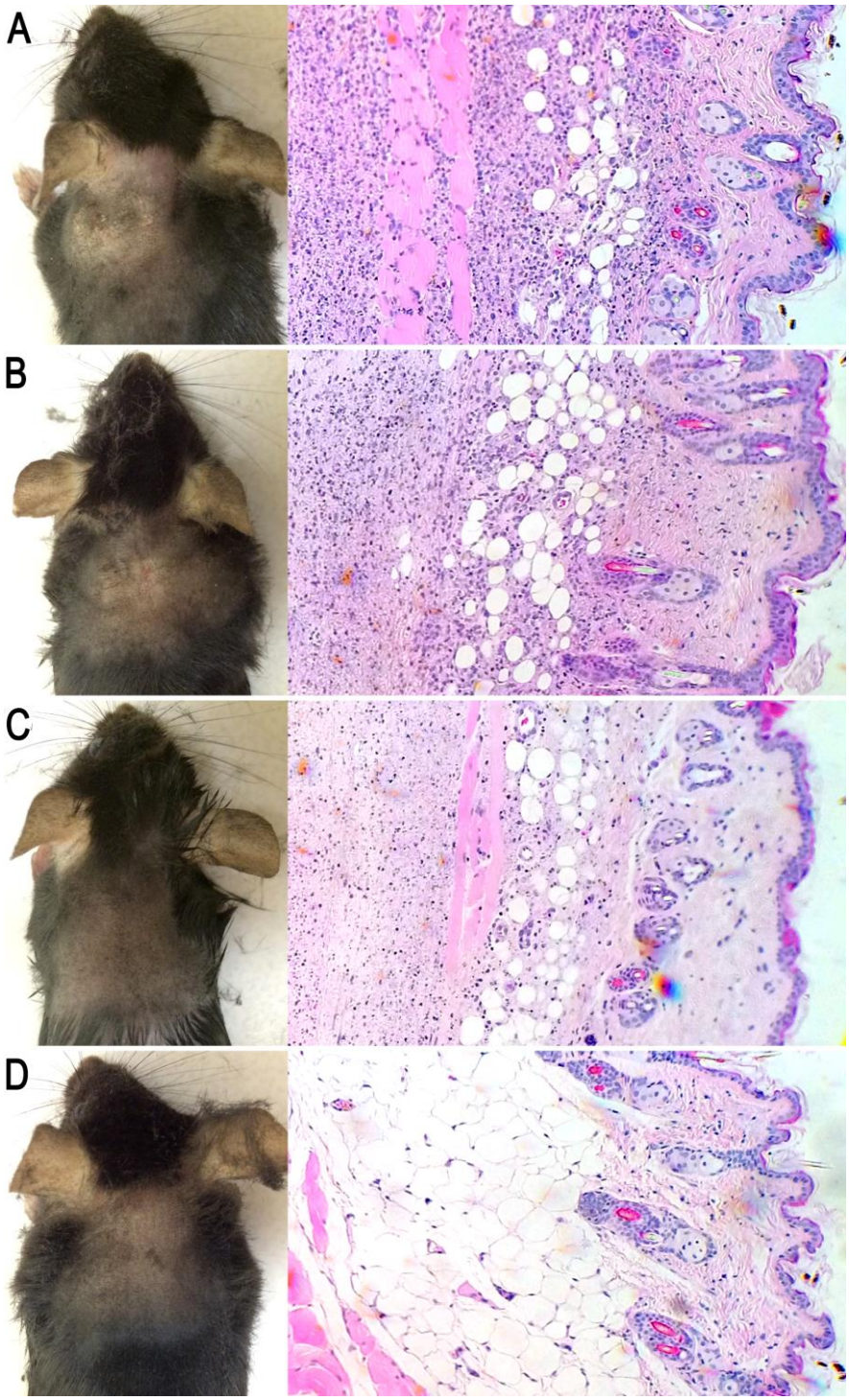

Figure 5.9 LD003 Reduces Immune Cell Infiltration of 80 nm LNP-siRNA at the Subcutaneous Injection Site

C57Bl/6 mice were injected subcutaneously with 80 nm LNP-siRNA with or without dexamethasone. (A) LNP-siRNA was injected at an siRNA dose of 5 mg/kg. (B) 30 minutes prior to the injection of LNP-siRNA, animals were injected I.P. with 5 mg/kg Dex-21-P. (C) LNP-siRNA containing 10 mol% LD003 pro-drug (approximately equivalent to 5 mg/kg Dex-21-P) was administered subcutaneously. (D) Control animals injected with PBS. LNP-siRNA and or dexamethasone was re-administered 7 days after the initial injection. Mice were euthanized 10 days after the initial injection and the interscapular space was collected, sectioned and stained. Representative images from four mice per treatment group are shown.

5.3 Discussion

There is growing interest in using nucleic acid based therapeutics for vaccines, protein expression, gene regulation and gene silencing (Sahin et al., 2014; Sehgal et al., 2013; Yin et al., 2014). Because nucleic acids are potent activators of the innate immune response (Barbalat et al., 2011), the use of chemically modified nucleoside bases is necessary to evade immune detection. Unfortunately, this has largely been limited to smaller oligonucleotides such as siRNA and ASO despite growing interest in delivering larger constructs such as plasmids or mRNA. This is further exacerbated by the need for complex delivery vehicles such as LNP, which are the most clinically advanced delivery system for therapeutic nucleic acids. In this work, we show that co-administration of dexamethasone, a potent broad spectrum corticosteroid, can ameliorate the immune stimulation induced by LNP containing nucleic acids. Specifically, co-delivering dexamethasone with the immune stimulatory payload greatly reduces the induction of immunomodulating cytokines. In order to achieve co-encapsulation, dexamethasone was acylated to increase its hydrophobicity and promote incorporation into LNP. Here, we discuss the

formulation of these pro-drugs, the ability for pro-drugs to degrade in esterase rich environments, the ability of pro-drugs to ameliorate immune stimulation by both LNP-CpG and LNP-mRNA and finally the implications and possible applications of this technology.

In order for compounds to be incorporated into LNP that contain nucleic acid, it needs to be at least weakly hydrophobic. The hydrophobic properties of these pro-drugs should allow for simple and straightforward incorporation without further modification of the formulation process. To achieve this, lipid moieties were conjugated to dexamethasone via biodegradable ester linkers (Figure 5.1). Because these compounds are expected to reside within the hydrophobic core of the LNP, bilayer promoting or cylindrical properties were avoided and therefore, linoleyl moieties were used. By changing the number of linoleyl moieties, the logD of the pro-drug can be modified (Table 5.1). For example, with a single acyl chain added, LD003 has the predicted logD of 8.92 while LD002 has a predicted logD of 14.95 compared to 1.68 for dexamethasone and -0.69 for Dex-21-P at pH 4.0 (pH of the aqueous formulation buffer). Complete incorporation of LD002 and LD003 was observed. Another parameter explored is the addition of an ionizable tertiary amine in addition to the linoleyl moiety. Interestingly, despite the overall increase in the predicted logD values for LD001 and LD004 (5.07 and 11.58 at pH 4, respectively), these pro-drugs did not fully incorporate into LNP suggesting that at pH 4.0 when the tertiary amine is protonated, these compounds remain somewhat soluble in the aqueous phase and is unable to properly incorporate into the core of the LNP. The weakly associated LD001 and LD004 is then lost during dialysis when the pH is raised to 7.4. Therefore, the overall logD of the pro-drug cannot be used as the sole predictor for LNP incorporation. Despite the inefficient entrapment, both LD001 and LD004 outperformed co-administered Dex-21-P in terms of cytokine suppression (Figure 5.5). In contrast, LD002 which exhibited complete entrapment in LNP, failed to suppress the induction of cytokines

by LNP-CpG. LD003 exhibited both excellent entrapment and immune suppression. Together, this suggests that there needs to be a degree of hydrophobicity that promotes pro-drug incorporation into LNP while compounds that are too hydrophobic may be trapped or embedded too deeply in the nanoparticle and do not efficiently breakdown to its active form. The biodegradable linker must remain accessible such that the release of the active drug would occur in the presence of esterases.

Dexamethasone pro-drugs were designed to contain several ester moieties within the linker to ensure that the active dexamethasone is released when the LNP is in an esterase rich environment. When the simplest pro-drug, LD003 was formulated into LNP and incubated with purified porcine esterase, it was confirmed that degradation occurs and this degradation is abolished when heat-inactivated enzyme was used (Figure 5.3). Because mouse plasma is known to be rich in carboxylesterases (unlike human plasma) (Berry et al., 2009; Rudakova et al., 2011), prolonged incubation should result in pro-drug degradation. LD001-005 exhibited different degrees of degradation after 1 hr incubation with mouse plasma at 37°C (Figure 5.2). In particular, LD001 and LD003 exhibited the most pronounced degradation while the majority of LD002, LD004 and LD005 parent compounds remain intact. This is in line with the ability of Dex to mitigate immune stimulation of LNP-CpG *in vivo* (Figure 5.5 and 5.6). These results also bring into question whether pro-drugs embedded in LNP would degrade in circulation prior to reaching target cells. Although this cannot be excluded and is likely occurring while LNP remain in circulation in mice, these formulations are rapidly cleared from the circulation (primarily by the liver and immune cells) (Basha et al., 2011; Chen et al., 2016). Therefore there is little time for degradation to occur in plasma. Furthermore, the ability of LD001 and LD003 to be far more effective at suppressing immune stimulation than 10-fold higher doses of Dex-21-P suggest that it is the pro-drug within the LNP that is responsible for the improved suppression.

With growing interest in the therapeutic use of nucleic acids, methods for safe and effective delivery are required. In this work, we show that incorporation of a dexamethasone pro-drug, is able to greatly reduce the immune stimulation by highly immunopotent LNP-CpG. LNP-CpG have been shown to be far more potent activators of the immune response than free CpG oligonucleotide (de Jong et al., 2007; Mui et al., 2001). However, rather than using the immunopotent properties therapeutically, in the current study we use LNP-CpG as a model for immune stimulatory LNP. With as little as 0.5 mg/kg of pro-drug incorporated into these systems, immunomodulators such as KC/GRO, TNFα, IL-1β and IL-6 could be suppressed (Figure 5.5 and 5.6). The level of suppression observed is far superior compared to co-administration of 20 mg/kg Dex-21-P. Because such small quantities of dexamethasone is required in the form of the pro-drugs, it is expected that the adverse side effects associated with high doses of corticosteroids can also be avoided. This enhanced potency is likely the result of having the immunosuppressant enter the identical cell as the immune stimulatory payload. Although LNP-CpG is only used as a model for immune stimulatory LNP, our findings translate to LNP-mRNA (Figure 5.8) suggesting broad utility for other nucleic acid based therapeutics or other immune stimulatory agents such as proteins. The lipophilic dexamethasone pro-drugs presented in this work is ideal for nanoparticles that have hydrophobic compartments and is not limited to the LNP systems described here. In fact, efficient incorporation of LD003 was observed in traditional liposomal systems composed of DSPC and cholesterol (data not shown). Using a similar strategy, a wide range of small molecules can be incorporated to achieve combination therapy, enhanced endosome destabilization or perhaps even triggered release. Ultimately, small molecules which are not amenable to traditional loading methods can be incorporated into nanoparticle delivery systems.

In summary the results presented here indicate that incorporation of a hydrophobic pro-drug of a potent immunosuppressant such as dexamethasone into LNP formulations of genetic drugs such as antisense oligonucleotides, siRNA, mRNA and plasmids could obviate the need for concomitant administration of immunosuppressive drugs such as dexamethasone. Further, the immunosuppressive properties of hydrophobic dexamethasone derivatives such as LD003 are considerably more potent than free drug, a finding that may be attributed to the rapid accumulation of LNP systems following i.v. administration. Essentially all exogenous nanoparticles such as LNP systems are eventually accumulated by macrophages and dendritic cells in the body, providing an enormous potential for "natural" targeting of immunosuppressive agents to the immune system. The dramatically improved potency that results may be expected to mitigate against toxic side effects immunosuppressive agents may have on cells and tissues other than the immune system, as effective doses can be much lower. Such dramatically improved potency may also be expected to effectively reduce or prevent potentially dangerous immune reactions to macromolecules such as RNA or DNA-based therapeutics used for gene therapies.

Chapter 6: Conclusion and Future Directions

This thesis demonstrated several novel aspects for the design of LNP formulations: First, it was shown that small LNP size and stable PEG coating was necessary for traversing tissues following subcutaneous injection (Chapter 3). Second, it was determined that the accelerated dissociation rate of ionizable amino lipids is causative for the loss of activity of small LNP and strategies were devised to improve activity of small LNP (Chapter 4). Lastly, the unwanted immune responses associated with the use of nucleic acid LNP was characterized and successfully ameliorated (Chapter 5). Here, the possible applications of these LNP systems and methods to improve LNP design are discussed.

6.1 Extra Hepatic Applications and Considerations

At the time of writing, LNP formulations that enable the therapeutic use of nucleic acids were being evaluated in a Phase III clinical trial for the treatment of transthyretin (TTR)-mediated amyloidosis. The available clinical data reveal the incredible potency and tolerability of LNP for silencing the hepatic gene TTR in humans. This success is the result of lessons learned from decades of research on LNP systems for plasmid DNA, ASO and siRNA delivery, as well as the nature of the target organ, the liver. Due to the size of the current LNP siRNA systems (< 100 nm in diameter) and their ability to bind ApoE, they can efficiently cross the liver fenestrae and enter hepatocytes via ApoE-mediated endocytosis. Although LNP delivery for liver applications is extremely promising, their potency is limited to hepatic tissues. High doses are needed to silence genes in immune cells, bone marrow cells or tumours, and such dose levels can be toxic and expensive. There is an urgent need to further improve LNP design in order to establish clinical utility for gene therapies of disorders involving extrahepatic tissues.

LNP can potentially enable the treatment of extrahepatic disorders given the proper design and administration. An example is the application of LNP in solid tumors. Traditional liposomes have been used very successfully for altering the pharmacokinetics and biodistribution of small molecule anticancer drugs. Liposomes can exploit the naturally occurring passive targeting EPR effect to prolong circulation lifetime and increase the amount of drug accumulation at the disease site. LNP containing nucleic acids have similar potential. Recently, we have shown that LNP can deliver siRNA to an orthotopic model of prostate cancer (Lee et al., 2012). In animals treated with LNP siRNA, gene silencing was observed and serum PSA levels were reduced compared to control animals. However, given these LNP were originally designed for liver applications, very high doses (6 injections of 10 mg/kg) were necessary to achieve the observed effect. LNP application can also be extended to immune disease or blood cancers. Our group and others have demonstrated that efficient delivery of LNP siRNA systems to immune cells in the peripheral blood, bone marrow and spleen. However, gene silencing in these sites require siRNA doses as high as 5 mg/kg (Basha et al., 2011; Novobrantseva et al., 2012; Ruschmann et al., 2016). Several considerations for successful extrahepatic delivery were identified in this study: particle size, administration route, and circulation lifetime. These considerations are of note due to their effects on LNP activity, stability and accumulation at disease sites. First, it was shown in this study and by others that, in general, small nanoparticles can penetrate more effectively into solid tumors and deeper into tissues (Cabral et al., 2011; Dreher et al., 2006; Huo et al., 2013; Popovic et al., 2010). Furthermore, it was shown in Chapter 3 that small LNP containing high PEG-lipid content (5 mol%) were able to traverse the loose connective tissue after an s.c. injection, reaching the local lymph nodes and beyond. S.c. administration has a clear advantage over i.v. in terms of patient self-administration, but more importantly, this route would directly access immune cells in the s.c.

space as well as local lymph nodes. However, despite the increased levels of small LNP reaching the liver after the s.c. injection, these LNP were far less active than their larger counterparts. This impairment is a potential impediment for future therapeutic applications of small LNP. Thus, the work in Chapter 4 subsequently identified that LNP containing PEG-DMG, a PEG-lipid that rapidly dissociate from LNP, also lose other lipid components including the amino-lipid. Importantly, the rates of dissociation are size dependent, with small LNP showing a dramatic reduction in amino-lipid content. Rapid lipid dissociation is also indicative of particle instability. To address this, PEG-DMG was replaced with PEG-DSG, a PEG-lipid that does not readily dissociate from LNP. Incorporation of PEG-DSG greatly reduced lipid dissociation and improved particle stability. Like the traditional liposome, LNP with persistent PEG-lipid also remained in circulation longer, which is necessary for accumulation in distal tumours via the EPR effect. It is likely that LNP for tumor applications will benefit from the improved activity, stability and circulation lifetime.

6.2 Methods for Improving LNP Design

The work presented in this dissertation proposes two distinct methods for improving LNP design. **The first method involves the optimization of existing lipid components**. Two key avenues could be explored: 1) altering the type of helper/structural lipids, and 2) altering the ionizable lipids. **The second method involves the incorporation of small molecule compounds that confer additional functions** through a lipophilic pro-drug strategy.

6.2.1 Optimizing Existing Lipid Components

Structural and helper lipids are key targets for improving existing components of LNP. In Chapter 4, it was shown that increasing the amount of amino-lipid (either by altering the composition or increasing the amine-to-phosphate ratios) results in modest improvements in small LNP activity. Increasing the amino-lipid content further would have been expected to improve the ability of LNP to destabilize membranes; however, it appears to compromise LNP integrity. This observation is in agreement with previous work from our laboratory showing that increasing amino-lipid content can result in the reduction of nucleic acid entrapment, as well as affect particle size and polydispersity concomitantly (Leung et al., 2015). Some of these issues may be overcome by incorporating helper lipids that are more conical in shape or tend to form hexagonal phases. Not only have these conical helper lipids been used to improve siRNA entrapment in similar LNP systems with high amino-lipid content (Leung et al., 2015), but lipids such as DOPE have also been shown to improve the transfection efficiency of plasmid DNA due to its membrane destabilizing property (Farhood et al., 1995; Hafez et al., 2001). Of the four primary lipid components, only amino- and PEG-lipids have been extensively studied (refer to Section 1.2.5 and 1.2.6, respectively). A future systematic or multiparametric screen of existing "structural" lipids would provide additional insights into constructing LNP with improved activity.

Another way to improve the activity of LNP is to maximize the ability to disrupt the endosome. This could be done through the modification of the ionizable amino-lipid. For example, increasing the overall charge density may enable the LNP to better interact with the negatively charged lipids found in the endosome, promoting lipid-mixing and membrane destabilization. In order to increase the charge density, the amino-lipid could be modified to contain multiple ionizable moieties. Indeed, others have shown that lipid-like materials form potent LNP systems

for the delivery of siRNA and mRNA (Akinc et al., 2009; Dong et al., 2014; Fenton et al., 2016; Love et al., 2010). These lipid-like materials are also ionizable, but many are polycationic when protonated. It would be interesting to test these lipid-like materials for extrahepatic delivery in the future. It is important to note that the current gold-standard amino-lipid, DLin-MC3-DMA, was identified from a screen of a library containing hundreds of novel ionizable amino-lipids for gene silencing in the liver (Jayaraman et al., 2012; Semple et al., 2010). Using the existing library of lipids, similar screens, but specifically focused on gene silencing in non-hepatic tissues such as the immune cells, could be carried out. These screens could identify potent lipids that are more suited for extrahepatic applications.

6.2.2 Adding Lipid Components for Synergistic Improvements

The second method to improve LNP design involves the incorporation of components that confer additional functions. In Chapter 5, a general strategy (i.e., lipophilic pro-drug) for enabling incorporation of additional compounds or drugs into LNP systems was proposed. As a first example, a commonly used corticosteroid (dexamethasone) that minimizes IRRs was directly incorporated as a lipophilic pro-drug. This greatly improved the ability of dexamethasone to ameliorate immune stimulation by LNP containing nucleic acids.

Another example is to use a lipophilic pro-drug to manipulate intracellular trafficking pathways. It was recently identified that the majority of LNP are recycled to the extracellular space (Sahay et al., 2013) and that only 1-2% of the siRNA that is endocytosed is released into the cytoplasm (Gilleron et al., 2013). These findings suggest that endosome destabilization mediated by LNP continues to be inefficient despite the incredible progress made in the rational design of amino-lipids (Jayaraman et al., 2012; Semple et al., 2010). Using the lipophilic pro-drug strategy,

small molecule compounds that disrupt endocytic or recycling processes could be incorporated into LNP to promote accumulation and release of the nucleic acid. For example, one of the regulators identified to be involved in the LNP recycling process is Niemman Pick Type C-1 protein (NPC1). Natively, NPC1 is involved with cholesterol trafficking within the cell and a loss of function results in cholesterol buildup in lysosomes. Knockdown of NPC1 results in the intracellular accumulation of LNP and concomitant improvement in gene silencing (Sahay et al., 2013). Therefore, inhibition of key regulators such as NPC1 may improve LNP activity. Small molecule inhibitors for NPC1 have been identified (Cote et al., 2011; Lee et al., 2013; Shoemaker et al., 2013) and shown to improve LNP accumulation and gene silencing in cultured cells (Wang et al., 2016). Other compounds such as UNC7938 have also been demonstrated to improve the activity of antisense, siRNA and splice-switching oligonucleotides (Yang et al., 2015). Similarly, others have screened chemical libraries for pharmacological enhancers of LNP-siRNA activity and have identified a number of compounds that improve cellular uptake or endosome disruption (Gilleron et al., 2015). When directly incorporated into the LNP using the lipophilic pro-drug approach, these compounds could be more effective than their free forms due to their co-localization within the cell and intracellular compartment. This was indeed the case for the dexamethasone pro-drugs (Chapter 5).

Reducing immune reactions or manipulating intracellular trafficking could be thought of as indirect approaches to improve LNP systems. The addition of the pro-drug either improves tolerability (eg: dexamethasone) or improves endosome disruption (eg: NPC1 inhibitors) but the pro-drugs themselves are not therapeutic agents. Another, more direct approach would be to incorporate another class of therapeutic agent, thus enabling combination treatment that comprise both nucleic acids and small molecules. Current LNP do not form strong permeability barriers and

thus cannot stably entrap small molecule compounds in the same way traditional liposomes do; on the other hand, liposomes do not efficiently entrap nucleic acid macromolecules. By adding acyl moieties via biodegradable linkers to small molecule drugs to increase their hydrophobicity, the resulting pro-drugs are fully compatible with the hydrophobic interior of LNP. Dexamethasone pro-drugs described in Chapter 5 are the first demonstration of this. Co-entrapment greatly improves the ability to suppress immune reaction to immune stimulatory nucleic acid within the LNP. Similarly, compounds that act on different pathways underlying the same disease can be used in conjunction with either induction or knockdown of gene expression. Using prostate cancer as an example, the combination of commonly used anticancer drugs (e.g., docetaxel) and siRNA against a clinically validated target (e.g., androgen receptor, clusterin) could potentially improve therapeutic outcomes by targeting two distinct mechanisms to prevent tumor progression. Similarly, molecular inhibitors of androgen production such as abiraterone can be used in conjunction with cytotoxic drugs and/or nucleic acids.

Overall, the improvements to LNP systems presented in this dissertation, ranging from control of particle size and stability to circulation lifetime and tolerability, will enable the development of next generation LNP systems for nucleic acid delivery. In particular, the ability to incorporate small molecules that can impart additional functions to the LNP can be an effective method for increasing activity and tolerability, while also enabling combination treatments.

Bibliography

Abe, M., Niibayashi, R., Koubori, S., Moriyama, I., and Miyoshi, H. (2011). Molecular mechanisms for the induction of peroxidase activity of the cytochrome c-cardiolipin complex. Biochemistry *50*, 8383-8391.

Abra, R.M., Bosworth, M.E., and Hunt, C.A. (1980). Liposome disposition in vivo: effects of pre-dosing with lipsomes. Research communications in chemical pathology and pharmacology *29*, 349-360.

Abraham, S.A., Waterhouse, D.N., Mayer, L.D., Cullis, P.R., Madden, T.D., and Bally, M.B. (2005). The liposomal formulation of doxorubicin. Methods Enzymol *391*, 71-97.

Abrams, M.T., Koser, M.L., Seitzer, J., Williams, S.C., DiPietro, M.A., Wang, W., Shaw, A.W., Mao, X., Jadhav, V., Davide, J.P., *et al.* (2010). Evaluation of efficacy, biodistribution, and inflammation for a potent siRNA nanoparticle: effect of dexamethasone co-treatment. Mol Ther *18*, 171-180.

Akinc, A., Goldberg, M., Qin, J., Dorkin, J.R., Gamba-Vitalo, C., Maier, M., Jayaprakash, K.N., Jayaraman, M., Rajeev, K.G., Manoharan, M., *et al.* (2009). Development of lipidoid-siRNA formulations for systemic delivery to the liver. Mol Ther *17*, 872-879.

Akinc, A., Querbes, W., De, S., Qin, J., Frank-Kamenetsky, M., Jayaprakash, K.N., Jayaraman, M., Rajeev, K.G., Cantley, W.L., Dorkin, J.R., *et al.* (2010). Targeted delivery of RNAi therapeutics with endogenous and exogenous ligand-based mechanisms. Mol Ther *18*, 1357-1364.

Akinc, A., Zumbuehl, A., Goldberg, M., Leshchiner, E.S., Busini, V., Hossain, N., Bacallado, S.A., Nguyen, D.N., Fuller, J., Alvarez, R., *et al.* (2008). A combinatorial library of lipid-like materials for delivery of RNAi therapeutics. Nat Biotechnol *26*, 561-569.

Allen, C., Dos Santos, N., Gallagher, R., Chiu, G.N., Shu, Y., Li, W.M., Johnstone, S.A., Janoff, A.S., Mayer, L.D., Webb, M.S., *et al.* (2002a). Controlling the physical behavior and biological performance of liposome formulations through use of surface grafted poly(ethylene glycol). Bioscience reports *22*, 225-250.

Allen, T.M. (1994). The use of glycolipids and hydrophilic polymers in avoiding rapid uptake of liposomes by the mononuclear phagocyte system. Advanced Drug Delivery Reviews *13*, 285-309.

Allen, T.M., and Chonn, A. (1987). Large unilamellar liposomes with low uptake into the reticuloendothelial system. FEBS letters *223*, 42-46.

Allen, T.M., and Cullis, P.R. (2012). Liposomal drug delivery systems: From concept to clinical applications. Adv Drug Deliv Rev.

Allen, T.M., and Hansen, C. (1991). Pharmacokinetics of stealth versus conventional liposomes: effect of dose. Biochim Biophys Acta *1068*, 133-141.

Allen, T.M., Hansen, C., Martin, F., Redemann, C., and Yau-Young, A. (1991). Liposomes containing synthetic lipid derivatives of poly(ethylene glycol) show prolonged circulation half-lives in vivo. Biochim Biophys Acta *1066*, 29-36.

Allen, T.M., Hansen, C.B., and Guo, L.S. (1993). Subcutaneous administration of liposomes: a comparison with the intravenous and intraperitoneal routes of injection. Biochim Biophys Acta *1150*, 9-16.

Allen, T.M., Sapra, P., Moase, E., Moreira, J., and Iden, D. (2002b). Adventures in targeting. Journal of liposome research *12*, 5-12.

Ambegia, E., Ansell, S., Cullis, P., Heyes, J., Palmer, L., and MacLachlan, I. (2005). Stabilized plasmid-lipid particles containing PEG-diacylglycerols exhibit extended circulation lifetimes and tumor selective gene expression. Biochim Biophys Acta *1669*, 155-163.

Anderson, B.R., Muramatsu, H., Jha, B.K., Silverman, R.H., Weissman, D., and Kariko, K. (2011). Nucleoside modifications in RNA limit activation of 2'-5'-oligoadenylate synthetase and increase resistance to cleavage by RNase L. Nucleic acids research *39*, 9329-9338.

Anderson, B.R., Muramatsu, H., Nallagatla, S.R., Bevilacqua, P.C., Sansing, L.H., Weissman, D., and Kariko, K. (2010). Incorporation of pseudouridine into mRNA enhances translation by diminishing PKR activation. Nucleic acids research *38*, 5884-5892.

Audouy, S.A., de Leij, L.F., Hoekstra, D., and Molema, G. (2002). In vivo characteristics of cationic liposomes as delivery vectors for gene therapy. Pharm Res *19*, 1599-1605.

Bailey, A.L., and Cullis, P.R. (1994). Modulation of membrane fusion by asymmetric transbilayer distributions of amino lipids. Biochemistry *33*, 12573-12580.

Bangham, A.D., and Horne, R.W. (1964). Negative Staining of Phospholipids and Their Structural Modification by Surface-Active Agents as Observed in the Electron Microscope. J Mol Biol *8*, 660-668.

Bangham, A.D., Standish, M.M., and Watkins, J.C. (1965). Diffusion of univalent ions across the lamellae of swollen phospholipids. J Mol Biol *13*, 238-252.

Barbalat, R., Ewald, S.E., Mouchess, M.L., and Barton, G.M. (2011). Nucleic acid recognition by the innate immune system. Annu Rev Immunol *29*, 185-214.

Barenholz, Y. (2012). Doxil(R)--the first FDA-approved nano-drug: lessons learned. J Control Release *160*, 117-134.

Barros, S.A., and Gollob, J.A. (2012). Safety profile of RNAi nanomedicines. Adv Drug Deliv Rev *64*, 1730-1737.

Basha, G., Novobrantseva, T.I., Rosin, N., Tam, Y.Y., Hafez, I.M., Wong, M.K., Sugo, T., Ruda, V.M., Qin, J., Klebanov, B., *et al.* (2011). Influence of Cationic Lipid Composition on Gene Silencing Properties of Lipid Nanoparticle Formulations of siRNA in Antigen-Presenting Cells. Mol Ther *19*, 2186-2200.

Belliveau, N.M., Huft, J., Lin, P.J., Chen, S., Leung, A.K., Leaver, T.J., Wild, A.W., Lee, J.B., Taylor, R.J., Tam, Y.K., *et al.* (2012). Microfluidic Synthesis of Highly Potent Limit-size Lipid Nanoparticles for In Vivo Delivery of siRNA. Molecular therapy Nucleic acids *1*, e37.

Berry, L.M., Wollenberg, L., and Zhao, Z. (2009). Esterase activities in the blood, liver and intestine of several preclinical species and humans. Drug metabolism letters *3*, 70-77.

Bisgaier, C.L., Siebenkas, M.V., and Williams, K.J. (1989). Effects of apolipoproteins A-IV and A-I on the uptake of phospholipid liposomes by hepatocytes. The Journal of biological chemistry *264*, 862-866.

Bligh, E.G., and Dyer, W.J. (1959). A rapid method of total lipid extraction and purification. Canadian journal of biochemistry and physiology *37*, 911-917.

Blume, G., and Cevc, G. (1990). Liposomes for the sustained drug release in vivo. Biochim Biophys Acta *1029*, 91-97.

Braet, F., and Wisse, E. (2002). Structural and functional aspects of liver sinusoidal endothelial cell fenestrae: a review. Comparative hepatology *1*, 1.

Brown, M.S., and Goldstein, J.L. (1986). A receptor-mediated pathway for cholesterol homeostasis. Science *232*, 34-47.

Cabral, H., Matsumoto, Y., Mizuno, K., Chen, Q., Murakami, M., Kimura, M., Terada, Y., Kano, M.R., Miyazono, K., Uesaka, M., *et al.* (2011). Accumulation of sub-100 nm polymeric micelles in poorly permeable tumours depends on size. Nat Nanotechnol *6*, 815-823.

Charrois, G.J., and Allen, T.M. (2004). Drug release rate influences the pharmacokinetics, biodistribution, therapeutic activity, and toxicity of pegylated liposomal doxorubicin formulations in murine breast cancer. Biochim Biophys Acta *1663*, 167-177.

Chen, S., Tam, Y.Y., Lin, P.J., Leung, A.K., Tam, Y.K., and Cullis, P.R. (2014). Development of lipid nanoparticle formulations of siRNA for hepatocyte gene silencing following subcutaneous administration. J Control Release *196C*, 106-112.

Chen, S., Tam, Y.Y., Lin, P.J., Sung, M.M., Tam, Y.K., and Cullis, P.R. (2016). Influence of particle size on the in vivo potency of lipid nanoparticle formulations of siRNA. J Control Release *235*, 236-244.

Chen, Y., Sen, J., Bathula, S.R., Yang, Q., Fittipaldi, R., and Huang, L. (2009). Novel cationic lipid that delivers siRNA and enhances therapeutic effect in lung cancer cells. Mol Pharm *6*, 696-705.

Chonn, A., Cullis, P.R., and Devine, D.V. (1991). The role of surface charge in the activation of the classical and alternative pathways of complement by liposomes. J Immunol *146*, 4234-4241.

Chonn, A., Semple, S.C., and Cullis, P.R. (1992). Association of blood proteins with large unilamellar liposomes in vivo. Relation to circulation lifetimes. J Biol Chem *267*, 18759-18765.

Coelho, T., Adams, D., Silva, A., Lozeron, P., Hawkins, P.N., Mant, T., Perez, J., Chiesa, J., Warrington, S., Tranter, E., *et al.* (2013). Safety and efficacy of RNAi therapy for transthyretin amyloidosis. The New England journal of medicine *369*, 819-829.

Cote, M., Misasi, J., Ren, T., Bruchez, A., Lee, K., Filone, C.M., Hensley, L., Li, Q., Ory, D., Chandran, K., *et al.* (2011). Small molecule inhibitors reveal Niemann-Pick C1 is essential for Ebola virus infection. Nature *477*, 344-348.

Crawford, R., Dogdas, B., Keough, E., Haas, R.M., Wepukhulu, W., Krotzer, S., Burke, P.A., Sepp-Lorenzino, L., Bagchi, A., and Howell, B.J. (2011). Analysis of lipid nanoparticles by Cryo-EM for characterizing siRNA delivery vehicles. International journal of pharmaceutics *403*, 237-244.

Cressman, S., Dobson, I., Lee, J.B., Tam, Y.Y., and Cullis, P.R. (2009). Synthesis of a labeled RGD-lipid, its incorporation into liposomal nanoparticles, and their trafficking in cultured endothelial cells. Bioconjug Chem *20*, 1404-1411.

Cullis, P.R., Chonn, A., and Semple, S.C. (1998). Interactions of liposomes and lipid-based carrier systems with blood proteins: Relation to clearance behaviour in vivo. Adv Drug Deliv Rev *32*, 3-17.

Cullis, P.R., and Hope, M.J. (1980). The bilayer stabilizing role of sphingomyelin in the presence of cholesterol: a 31P NMR study. Biochim Biophys Acta *597*, 533-542.

de Jong, S., Chikh, G., Sekirov, L., Raney, S., Semple, S., Klimuk, S., Yuan, N., Hope, M., Cullis, P., and Tam, Y. (2007). Encapsulation in liposomal nanoparticles enhances the immunostimulatory, adjuvant and anti-tumor activity of subcutaneously administered CpG ODN. Cancer immunology, immunotherapy : CII *56*, 1251-1264.

Di Paolo, D., Ambrogio, C., Pastorino, F., Brignole, C., Martinengo, C., Carosio, R., Loi, M., Pagnan, G., Emionite, L., Cilli, M., *et al.* (2011). Selective therapeutic targeting of the anaplastic lymphoma kinase with liposomal siRNA induces apoptosis and inhibits angiogenesis in neuroblastoma. Mol Ther *19*, 2201-2212.

Dong, Y., Love, K.T., Dorkin, J.R., Sirirungruang, S., Zhang, Y., Chen, D., Bogorad, R.L., Yin, H., Chen, Y., Vegas, A.J., *et al.* (2014). Lipopeptide nanoparticles for potent and selective siRNA delivery in rodents and nonhuman primates. Proc Natl Acad Sci U S A *111*, 3955-3960.

Dow, S.W., Fradkin, L.G., Liggitt, D.H., Willson, A.P., Heath, T.D., and Potter, T.A. (1999). Lipid-DNA complexes induce potent activation of innate immune responses and antitumor activity when administered intravenously. J Immunol *163*, 1552-1561.

Dreher, M.R., Liu, W., Michelich, C.R., Dewhirst, M.W., Yuan, F., and Chilkoti, A. (2006). Tumor vascular permeability, accumulation, and penetration of macromolecular drug carriers. Journal of the National Cancer Institute *98*, 335-344.

Eder, P.S., DeVine, R.J., Dagle, J.M., and Walder, J.A. (1991). Substrate specificity and kinetics of degradation of antisense oligonucleotides by a 3' exonuclease in plasma. Antisense Res Dev *1*, 141-151.

Fang, J., Nakamura, H., and Maeda, H. (2011). The EPR effect: Unique features of tumor blood vessels for drug delivery, factors involved, and limitations and augmentation of the effect. Advanced Drug Delivery Reviews *63*, 136-151.

Farhood, H., Serbina, N., and Huang, L. (1995). The role of dioleoyl phosphatidylethanolamine in cationic liposome mediated gene transfer. Biochim Biophys Acta *1235*, 289-295.

Felgner, J., Bennett, F., and Felgner, P.L. (1993). Cationic Lipid-Mediated Delivery of Polynucleotides. Methods *5*, 67-75.

Felgner, J.H., Kumar, R., Sridhar, C.N., Wheeler, C.J., Tsai, Y.J., Border, R., Ramsey, P., Martin, M., and Felgner, P.L. (1994). Enhanced gene delivery and mechanism studies with a novel series of cationic lipid formulations. J Biol Chem *269*, 2550-2561.

Felgner, P.L., Gadek, T.R., Holm, M., Roman, R., Chan, H.W., Wenz, M., Northrop, J.P., Ringold, G.M., and Danielsen, M. (1987). Lipofection: a highly efficient, lipid-mediated DNA-transfection procedure. Proc Natl Acad Sci U S A *84*, 7413-7417.

Fenske, D.B., MacLachlan, I., and Cullis, P.R. (2001). Long-circulating vectors for the systemic delivery of genes. Current opinion in molecular therapeutics *3*, 153-158.

Fenske, D.B., Wong, K.F., Maurer, E., Maurer, N., Leenhouts, J.M., Boman, N., Amankwa, L., and Cullis, P.R. (1998). Ionophore-mediated uptake of ciprofloxacin and vincristine into large unilamellar vesicles exhibiting transmembrane ion gradients. Biochim Biophys Acta *1414*, 188-204.

Fenton, O.S., Kauffman, K.J., McClellan, R.L., Appel, E.A., Dorkin, J.R., Tibbitt, M.W., Heartlein, M.W., DeRosa, F., Langer, R., and Anderson, D.G. (2016). Bioinspired Alkenyl Amino Alcohol Ionizable Lipid Materials for Highly Potent In Vivo mRNA Delivery. Advanced materials.

Fielding, C.J., and Fielding, P.E. (2008). Dynamics of Lipoprotein Transport in the Circulatory System. In Biochemistry of Lipids, Lipoproteins and Membranes, D.E. Vance, and J.E. Vance, eds. (Elsevier B.V.), pp. 533-553.

Fitzgerald, K., Frank-Kamenetsky, M., Shulga-Morskaya, S., Liebow, A., Bettencourt, B.R., Sutherland, J.E., Hutabarat, R.M., Clausen, V.A., Karsten, V., Cehelsky, J., *et al.* (2014). Effect of an RNA interference drug on the synthesis of proprotein convertase subtilisin/kexin type 9

(PCSK9) and the concentration of serum LDL cholesterol in healthy volunteers: a randomised, single-blind, placebo-controlled, phase 1 trial. Lancet *383*, 60-68.

Gabizon, A., Catane, R., Uziely, B., Kaufman, B., Safra, T., Cohen, R., Martin, F., Huang, A., and Barenholz, Y. (1994). Prolonged circulation time and enhanced accumulation in malignant exudates of doxorubicin encapsulated in polyethylene-glycol coated liposomes. Cancer Res *54*, 987-992.

Gabizon, A., and Papahadjopoulos, D. (1988). Liposome formulations with prolonged circulation time in blood and enhanced uptake by tumors. Proc Natl Acad Sci U S A *85*, 6949-6953.

Gabizon, A.A., Barenholz, Y., and Bialer, M. (1993). Prolongation of the circulation time of doxorubicin encapsulated in liposomes containing a polyethylene glycol-derivatized phospholipid: pharmacokinetic studies in rodents and dogs. Pharm Res *10*, 703-708.

Geary, R.S., Watanabe, T.A., Truong, L., Freier, S., Lesnik, E.A., Sioufi, N.B., Sasmor, H., Manoharan, M., and Levin, A.A. (2001). Pharmacokinetic properties of 2'-O-(2-methoxyethyl)-modified oligonucleotide analogs in rats. J Pharmacol Exp Ther *296*, 890-897.

Gilleron, J., Paramasivam, P., Zeigerer, A., Querbes, W., Marsico, G., Andree, C., Seifert, S., Amaya, P., Stoter, M., Koteliansky, V., *et al.* (2015). Identification of siRNA delivery enhancers by a chemical library screen. Nucleic acids research *43*, 7984-8001.

Gilleron, J., Querbes, W., Zeigerer, A., Borodovsky, A., Marsico, G., Schubert, U., Manygoats, K., Seifert, S., Andree, C., Stoter, M., *et al.* (2013). Image-based analysis of lipid nanoparticle-mediated siRNA delivery, intracellular trafficking and endosomal escape. Nat Biotechnol *31*, 638-646.

Hafez, I.M., Maurer, N., and Cullis, P.R. (2001). On the mechanism whereby cationic lipids promote intracellular delivery of polynucleic acids. Gene Ther *8*, 1188-1196.

Haran, G., Cohen, R., Bar, L.K., and Barenholz, Y. (1993). Transmembrane ammonium sulfate gradients in liposomes produce efficient and stable entrapment of amphipathic weak bases. Biochim Biophys Acta *1151*, 201-215.

Heyes, J., Hall, K., Tailor, V., Lenz, R., and MacLachlan, I. (2006). Synthesis and characterization of novel poly(ethylene glycol)-lipid conjugates suitable for use in drug delivery. J Control Release *112*, 280-290.

Heyes, J., Palmer, L., Bremner, K., and MacLachlan, I. (2005). Cationic lipid saturation influences intracellular delivery of encapsulated nucleic acids. J Control Release *107*, 276-287.

Hill, J.A., Ichim, T.E., Kusznieruk, K.P., Li, M., Huang, X., Yan, X., Zhong, R., Cairns, E., Bell, D.A., and Min, W.P. (2003). Immune modulation by silencing IL-12 production in dendritic cells using small interfering RNA. J Immunol *171*, 691-696.

Hoekstra, D., and Scherphof, G. (1979). Effect of fetal calf serum and serum protein fractions on the uptake of liposomal phosphatidylcholine by rat hepatocytes in primary monolayer culture. Biochim Biophys Acta *551*, 109-121.

Hope, M.J., Bally, M.B., Mayer, L.D., Janoff, A.S., and Cullis, P.R. (1986). Generation of multilamellar and unilamellar phospholipid vesicles. Chemistry and Physics of Lipids *40*, 89-107.

Huo, S., Ma, H., Huang, K., Liu, J., Wei, T., Jin, S., Zhang, J., He, S., and Liang, X.J. (2013). Superior Penetration and Retention Behavior of 50 nm Gold Nanoparticles in Tumors. Cancer Res *73*, 319-330.

Ichim, T.E., Zhong, R., and Min, W.P. (2003). Prevention of allograft rejection by in vitro generated tolerogenic dendritic cells. Transplant immunology *11*, 295-306.

Ishida, T., Harashima, H., and Kiwada, H. (2002). Liposome clearance. Bioscience reports *22*, 197-224.

Jain, R.K., and Stylianopoulos, T. (2010). Delivering nanomedicine to solid tumors. Nature reviews Clinical oncology *7*, 653-664.

Jayaraman, M., Ansell, S.M., Mui, B.L., Tam, Y.K., Chen, J., Du, X., Butler, D., Eltepu, L., Matsuda, S., Narayanannair, J.K., *et al.* (2012). Maximizing the potency of siRNA lipid nanoparticles for hepatic gene silencing in vivo. Angew Chem Int Ed Engl *51*, 8529-8533.

Jeffs, L.B., Palmer, L.R., Ambegia, E.G., Giesbrecht, C., Ewanick, S., and MacLachlan, I. (2005). A scalable, extrusion-free method for efficient liposomal encapsulation of plasmid DNA. Pharm Res *22*, 362-372.

Johnson, S.M., Miller, K.W., and Bangham, A.D. (1973). The opposing effects of pressure and general anaesthetics on the cation permeability of liposomes of varying lipid composition. Biochim Biophys Acta *307*, 42-57.

Jonas, A., and Phillips, M.C. (2008). Lipoprotein Structure. In Biochemistry of Lipids, Lipoproteins and Membranes, D.E. Vance, and J.E. Vance, eds. (Elsevier B.V.), pp. 485-506.

Judge, A., McClintock, K., Phelps, J.R., and Maclachlan, I. (2006). Hypersensitivity and loss of disease site targeting caused by antibody responses to PEGylated liposomes. Mol Ther *13*, 328-337.

Judge, A.D., Sood, V., Shaw, J.R., Fang, D., McClintock, K., and MacLachlan, I. (2005). Sequence-dependent stimulation of the mammalian innate immune response by synthetic siRNA. Nat Biotechnol *23*, 457-462.

Jung, H., Park, J.S., Yeom, J., Selvapalam, N., Park, K.M., Oh, K., Yang, J.A., Park, K.H., Hahn, S.K., and Kim, K. (2014). 3D tissue engineered supramolecular hydrogels for controlled chondrogenesis of human mesenchymal stem cells. Biomacromolecules *15*, 707-714.

Kao, Y.J., and Juliano, R.L. (1981). Interactions of liposomes with the reticuloendothelial system. Effects of reticuloendothelial blockade on the clearance of large unilamellar vesicles. Biochim Biophys Acta *677*, 453-461.

Kariko, K., Buckstein, M., Ni, H., and Weissman, D. (2005). Suppression of RNA recognition by Toll-like receptors: the impact of nucleoside modification and the evolutionary origin of RNA. Immunity *23*, 165-175.

Kariko, K., Muramatsu, H., Welsh, F.A., Ludwig, J., Kato, H., Akira, S., and Weissman, D. (2008). Incorporation of pseudouridine into mRNA yields superior nonimmunogenic vector with increased translational capacity and biological stability. Mol Ther *16*, 1833-1840.

Kawabata, K., Takakura, Y., and Hashida, M. (1995). The fate of plasmid DNA after intravenous injection in mice: involvement of scavenger receptors in its hepatic uptake. Pharm Res *12*, 825-830.

Klibanov, A.L., Maruyama, K., Torchilin, V.P., and Huang, L. (1990). Amphipathic polyethyleneglycols effectively prolong the circulation time of liposomes. FEBS letters *268*, 235-237.

Kormann, M.S., Hasenpusch, G., Aneja, M.K., Nica, G., Flemmer, A.W., Herber-Jonat, S., Huppmann, M., Mays, L.E., Illenyi, M., Schams, A., *et al.* (2011). Expression of therapeutic proteins after delivery of chemically modified mRNA in mice. Nat Biotechnol *29*, 154-157.

Lachmann, H.J., Gallimore, R., Gillmore, J.D., Carr-Smith, H.D., Bradwell, A.R., Pepys, M.B., and Hawkins, P.N. (2003). Outcome in systemic AL amyloidosis in relation to changes in concentration of circulating free immunoglobulin light chains following chemotherapy. British journal of haematology *122*, 78-84.

Lee, J.B., Zhang, K., Tam, Y.Y., Tam, Y.K., Belliveau, N.M., Sung, V.Y., Lin, P.J., LeBlanc, E., Ciufolini, M.A., Rennie, P.S., *et al.* (2012). Lipid nanoparticle siRNA systems for silencing the androgen receptor in human prostate cancer in vivo. Int J Cancer *131*, E781-790.

Lee, K., Ren, T., Cote, M., Gholamreza, B., Misasi, J., Bruchez, A., and Cunningham, J. (2013). Inhibition of Ebola Virus Infection: Identification of Niemann-Pick C1 as the Target by Optimization of a Chemical Probe. ACS medicinal chemistry letters *4*, 239-243.

Leung, A.K., Hafez, I.M., Baoukina, S., Belliveau, N.M., Zhigaltsev, I.V., Afshinmanesh, E., Tieleman, D.P., Hansen, C.L., Hope, M.J., and Cullis, P.R. (2012). Lipid Nanoparticles Containing siRNA Synthesized by Microfluidic Mixing Exhibit an Electron-Dense Nanostructured Core. The journal of physical chemistry C, Nanomaterials and interfaces *116*, 18440-18450.

Leung, A.K., Tam, Y.Y., Chen, S., Hafez, I.M., and Cullis, P.R. (2015). Microfluidic Mixing: A General Method for Encapsulating Macromolecules in Lipid Nanoparticle Systems. The journal of physical chemistry B *119*, 8698-8706.

Li, S.D., Chono, S., and Huang, L. (2008). Efficient oncogene silencing and metastasis inhibition via systemic delivery of siRNA. Mol Ther *16*, 942-946.

Li, S.D., and Huang, L. (2006). Surface-modified LPD nanoparticles for tumor targeting. Ann N Y Acad Sci *1082*, 1-8.

Litzinger, D.C., Brown, J.M., Wala, I., Kaufman, S.A., Van, G.Y., Farrell, C.L., and Collins, D. (1996). Fate of cationic liposomes and their complex with oligonucleotide in vivo. Biochim Biophys Acta *1281*, 139-149.

Lopez, S., and Simons, S.S., Jr. (1991). Dexamethasone 21-(beta-isothiocyanatoethyl) thioether: a new affinity label for glucocorticoid receptors. J Med Chem *34*, 1762-1767.

Love, K.T., Mahon, K.P., Levins, C.G., Whitehead, K.A., Querbes, W., Dorkin, J.R., Qin, J., Cantley, W., Qin, L.L., Racie, T., *et al.* (2010). Lipid-like materials for low-dose, in vivo gene silencing. Proc Natl Acad Sci U S A *107*, 1864-1869.

Madden, T.D., Harrigan, P.R., Tai, L.C., Bally, M.B., Mayer, L.D., Redelmeier, T.E., Loughrey, H.C., Tilcock, C.P., Reinish, L.W., and Cullis, P.R. (1990). The accumulation of drugs within large unilamellar vesicles exhibiting a proton gradient: a survey. Chem Phys Lipids *53*, 37-46.

Maeda, H., Wu, J., Sawa, T., Matsumura, Y., and Hori, K. (2000). Tumor vascular permeability and the EPR effect in macromolecular therapeutics: a review. Journal of Controlled Release *65*, 271-284.

Mahley, R.W., Innerarity, T.L., Rall, S.C., Jr., and Weisgraber, K.H. (1984). Plasma lipoproteins: apolipoprotein structure and function. Journal of lipid research *25*, 1277-1294.

Maier, M.A., Jayaraman, M., Matsuda, S., Liu, J., Barros, S., Querbes, W., Tam, Y.K., Ansell, S.M., Kumar, V., Qin, J., *et al.* (2013). Biodegradable Lipids Enabling Rapidly Eliminated Lipid Nanoparticles for Systemic Delivery of RNAi Therapeutics. Mol Ther *21*, 1570-1578.

Mao, L., Wang, H., Tan, M., Ou, L., Kong, D., and Yang, Z. (2012). Conjugation of two complementary anti-cancer drugs confers molecular hydrogels as a co-delivery system. Chemical communications *48*, 395-397.

Matsumura, Y., and Maeda, H. (1986). A new concept for macromolecular therapeutics in cancer chemotherapy: mechanism of tumoritropic accumulation of proteins and the antitumor agent smancs. Cancer Res *46*, 6387-6392.

Maurer, N., Wong, K.F., Hope, M.J., and Cullis, P.R. (1998). Anomalous solubility behavior of the antibiotic ciprofloxacin encapsulated in liposomes: a 1H-NMR study. Biochim Biophys Acta *1374*, 9-20.

Maurer, N., Wong, K.F., Stark, H., Louie, L., McIntosh, D., Wong, T., Scherrer, P., Semple, S.C., and Cullis, P.R. (2001). Spontaneous entrapment of polynucleotides upon electrostatic interaction with ethanol-destabilized cationic liposomes. Biophys J *80*, 2310-2326.

Mayer, L.D., Bally, M.B., and Cullis, P.R. (1986). Uptake of adriamycin into large unilamellar vesicles in response to a pH gradient. Biochim Biophys Acta *857*, 123-126.

Mendez, A.J., He, J.L., Huang, H.S., Wen, S.R., and Hsia, S.L. (1988). Interaction of rabbit lipoproteins and red blood cells with liposomes of egg yolk phospholipids. Lipids *23*, 961-967.

Miller, N.E. (1990). HDL metabolism and its role in lipid transport. European heart journal *11 Suppl H*, 1-3.

Mok, K.W., Lam, A.M., and Cullis, P.R. (1999). Stabilized plasmid-lipid particles: factors influencing plasmid entrapment and transfection properties. Biochim Biophys Acta *1419*, 137-150.

Monck, M.A., Mori, A., Lee, D., Tam, P., Wheeler, J.J., Cullis, P.R., and Scherrer, P. (2000). Stabilized plasmid-lipid particles: pharmacokinetics and plasmid delivery to distal tumors following intravenous injection. Journal of drug targeting *7*, 439-452.

Morrissey, D.V., Lockridge, J.A., Shaw, L., Blanchard, K., Jensen, K., Breen, W., Hartsough, K., Machemer, L., Radka, S., Jadhav, V., *et al.* (2005). Potent and persistent in vivo anti-HBV activity of chemically modified siRNAs. Nat Biotechnol *23*, 1002-1007.

Mui, B., Raney, S.G., Semple, S.C., and Hope, M.J. (2001). Immune stimulation by a CpG-containing oligodeoxynucleotide is enhanced when encapsulated and delivered in lipid particles. J Pharmacol Exp Ther *298*, 1185-1192.

Mui, B.L., Tam, Y.K., Jayaraman, M., Ansell, S.M., Du, X., Tam, Y.Y., Lin, P.J., Chen, S., Narayanannair, J.K., Rajeev, K.G., *et al.* (2013). Influence of Polyethylene Glycol Lipid Desorption Rates on Pharmacokinetics and Pharmacodynamics of siRNA Lipid Nanoparticles. Molecular therapy Nucleic acids *2*, e139.

Nair, J.K., Willoughby, J.L.S., Chan, A., Charisse, K., Alam, M.R., Wang, Q., Hoekstra, M., Kandasamy, P., Kel'in, A.V., Milstein, S., *et al.* (2014). Multivalent N-Acetylgalactosamine-Conjugated siRNA Localizes in Hepatocytes and Elicits Robust RNAi-Mediated Gene Silencing. Journal of the American Chemical Society *136*, 16958-16961.

Nichols, J.W., and Deamer, D.W. (1976). Catecholamine uptake and concentration by liposomes maintaining pH gradients. Biochimica et Biophysica Acta (BBA) - Biomembranes *455*, 269-271.

Novobrantseva, T.I., Borodovsky, A., Wong, J., Klebanov, B., Zafari, M., Yucius, K., Querbes, W., Ge, P., Ruda, V.M., Milstein, S., *et al.* (2012). Systemic RNAi-mediated Gene Silencing in Nonhuman Primate and Rodent Myeloid Cells. Molecular therapy Nucleic acids *1*, e4.

Ohwada, J., Inouye, Y., Kimura, M., and Kakisawa, H. (1990). Acyliminium Cyclization of Several Chiral <I>N</I>-Alkenylsuccinimide Derivatives. Bulletin of the Chemical Society of Japan *63*, 287-289.

Oussoren, C., and Storm, G. (2001). Liposomes to target the lymphatics by subcutaneous administration. Adv Drug Deliv Rev *50*, 143-156.

Oussoren, C., Zuidema, J., Crommelin, D.J., and Storm, G. (1997). Lymphatic uptake and biodistribution of liposomes after subcutaneous injection. II. Influence of liposomal size, lipid compostion and lipid dose. Biochim Biophys Acta *1328*, 261-272.

Papahadjopoulos, D., Allen, T.M., Gabizon, A., Mayhew, E., Matthay, K., Huang, S.K., Lee, K.D., Woodle, M.C., Lasic, D.D., Redemann, C., *et al.* (1991). Sterically stabilized liposomes: improvements in pharmacokinetics and antitumor therapeutic efficacy. Proc Natl Acad Sci U S A *88*, 11460-11464.

Papahadjopoulos, D., Jacobson, K., Nir, S., and Isac, T. (1973). Phase transitions in phospholipid vesicles. Fluorescence polarization and permeability measurements concerning the effect of temperature and cholesterol. Biochim Biophys Acta *311*, 330-348.

Papahadjopoulos, D., Nir, S., and Oki, S. (1972). Permeability properties of phospholipid membranes: effect of cholesterol and temperature. Biochim Biophys Acta *266*, 561-583.

Phillips, W.T., Klipper, R., and Goins, B. (2000). Novel method of greatly enhanced delivery of liposomes to lymph nodes. J Pharmacol Exp Ther *295*, 309-313.

Popovic, Z., Liu, W., Chauhan, V.P., Lee, J., Wong, C., Greytak, A.B., Insin, N., Nocera, D.G., Fukumura, D., Jain, R.K., *et al.* (2010). A nanoparticle size series for in vivo fluorescence imaging. Angew Chem Int Ed Engl *49*, 8649-8652.

Rensen, P.C., Schiffelers, R.M., Versluis, A.J., Bijsterbosch, M.K., Van Kuijk-Meuwissen, M.E., and Van Berkel, T.J. (1997). Human recombinant apolipoprotein E-enriched liposomes can mimic low-density lipoproteins as carriers for the site-specific delivery of antitumor agents. Molecular pharmacology *52*, 445-455.

Roth, C.M., and Sundaram, S. (2004). Engineering synthetic vectors for improved DNA delivery: insights from intracellular pathways. Annual review of biomedical engineering *6*, 397-426.

Rudakova, E.V., Boltneva, N.P., and Makhaeva, G.F. (2011). Comparative analysis of esterase activities of human, mouse, and rat blood. Bulletin of experimental biology and medicine *152*, 73-75.

Rungta, R.L., Choi, H.B., Lin, P.J., Ko, R.W., Ashby, D., Nair, J., Manoharan, M., Cullis, P.R., and Macvicar, B.A. (2013). Lipid Nanoparticle Delivery of siRNA to Silence Neuronal Gene Expression in the Brain. Molecular therapy Nucleic acids *2*, e136.

Ruschmann, J., Lin, P.J.C., Wan, C., Chen, S., Tam, Y.Y.C., Humphries, R.K., Cullis, P.R., and Tam, Y.K. (2016). siRNA Lipid Nanoparticles as an Effective In Vivo Functional Genomics Tool for the Study of In Situ Hematopoiesis. Manuscript submitted.

Sahay, G., Querbes, W., Alabi, C., Eltoukhy, A., Sarkar, S., Zurenko, C., Karagiannis, E., Love, K., Chen, D., Zoncu, R., *et al.* (2013). Efficiency of siRNA delivery by lipid nanoparticles is limited by endocytic recycling. Nat Biotechnol *31*, 653-658.

Sahin, U., Kariko, K., and Tureci, O. (2014). mRNA-based therapeutics--developing a new class of drugs. Nat Rev Drug Discov *13*, 759-780.

Sands, H., Gorey-Feret, L.J., Cocuzza, A.J., Hobbs, F.W., Chidester, D., and Trainor, G.L. (1994). Biodistribution and metabolism of internally 3H-labeled oligonucleotides. I. Comparison of a phosphodiester and a phosphorothioate. Mol Pharmacol *45*, 932-943.

Sapra, P., and Allen, T.M. (2003). Ligand-targeted liposomal anticancer drugs. Prog Lipid Res *42*, 439-462.

Scherphof, G., Damen, J., Dijkstra, J., Roerdink, F., and Spanjer, H. (1984). Interactions of Liposomes with Lipoproteins and Liver Cells In Vivo and In Vitro Studies. In Receptor-Mediated Targeting of Drugs, G. Gregoriadis, G. Poste, J. Senior, and A. Trouet, eds. (Springer US), pp. 267-295.

Sehgal, A., Barros, S., Ivanciu, L., Cooley, B., Qin, J., Racie, T., Hettinger, J., Carioto, M., Jiang, Y., Brodsky, J., *et al.* (2015). An RNAi therapeutic targeting antithrombin to rebalance the coagulation system and promote hemostasis in hemophilia. Nat Med *21*, 492-497.

Sehgal, A., Vaishnaw, A., and Fitzgerald, K. (2013). Liver as a target for oligonucleotide therapeutics. Journal of hepatology *59*, 1354-1359.

Sekijima, Y., Kelly, J.W., and Ikeda, S. (2008). Pathogenesis of and therapeutic strategies to ameliorate the transthyretin amyloidoses. Current pharmaceutical design *14*, 3219-3230.

Semple, S.C., Akinc, A., Chen, J., Sandhu, A.P., Mui, B.L., Cho, C.K., Sah, D.W., Stebbing, D., Crosley, E.J., Yaworski, E., *et al.* (2010). Rational design of cationic lipids for siRNA delivery. Nat Biotechnol *28*, 172-176.

Semple, S.C., Harasym, T.O., Clow, K.A., Ansell, S.M., Klimuk, S.K., and Hope, M.J. (2005). Immunogenicity and rapid blood clearance of liposomes containing polyethylene glycol-lipid conjugates and nucleic Acid. J Pharmacol Exp Ther *312*, 1020-1026.

Semple, S.C., Klimuk, S.K., Harasym, T.O., Dos Santos, N., Ansell, S.M., Wong, K.F., Maurer, N., Stark, H., Cullis, P.R., Hope, M.J., *et al.* (2001). Efficient encapsulation of antisense oligonucleotides in lipid vesicles using ionizable aminolipids: formation of novel small multilamellar vesicle structures. Biochim Biophys Acta *1510*, 152-166.

Senior, J., Delgado, C., Fisher, D., Tilcock, C., and Gregoriadis, G. (1991). Influence of surface hydrophilicity of liposomes on their interaction with plasma protein and clearance from the circulation: studies with poly(ethylene glycol)-coated vesicles. Biochim Biophys Acta *1062*, 77-82.

Sharma, A., Mayhew, E., Bolcsak, L., Cavanaugh, C., Harmon, P., Janoff, A., and Bernacki, R.J. (1997). Activity of paclitaxel liposome formulations against human ovarian tumor xenografts. Int J Cancer *71*, 103-107.

Shoemaker, C.J., Schornberg, K.L., Delos, S.E., Scully, C., Pajouhesh, H., Olinger, G.G., Johansen, L.M., and White, J.M. (2013). Multiple cationic amphiphiles induce a Niemann-Pick C phenotype and inhibit Ebola virus entry and infection. PLoS One *8*, e56265.

Simons, S.S., Pons, M., and Johnson, D.F. (1980). .alpha.-Keto mesylate: a reactive, thiol-specific functional group. The Journal of Organic Chemistry *45*, 3084-3088.

Smith, P.A.S. (1969). Reagents for organic synthesis. L. F. Fieser and M. Fieser. Wiley, New York, 1967. ix + 1457 pp. $27.50. Journal of Polymer Science Part A-1: Polymer Chemistry *7*, 795-796.

Snoeys, J., Lievens, J., Wisse, E., Jacobs, F., Duimel, H., Collen, D., Frederik, P., and De Geest, B. (2007). Species differences in transgene DNA uptake in hepatocytes after adenoviral transfer correlate with the size of endothelial fenestrae. Gene Ther *14*, 604-612.

Soepenberg, O., Sparreboom, A., de Jonge, M.J., Planting, A.S., de Heus, G., Loos, W.J., Hartman, C.M., Bowden, C., and Verweij, J. (2004). Real-time pharmacokinetics guiding clinical decisions; phase I study of a weekly schedule of liposome encapsulated paclitaxel in patients with solid tumours. European journal of cancer *40*, 681-688.

Song, L.Y., Ahkong, Q.F., Rong, Q., Wang, Z., Ansell, S., Hope, M.J., and Mui, B. (2002). Characterization of the inhibitory effect of PEG-lipid conjugates on the intracellular delivery of plasmid and antisense DNA mediated by cationic lipid liposomes. Biochim Biophys Acta *1558*, 1-13.

Stein, Y., Halperin, G., and Stein, O. (1980). Biological stability of [3H]cholesteryl oleyl ether in cultured fibroblasts and intact rat. FEBS letters *111*, 104-106.

Suhr, O.B., Coelho, T., Buades, J., Pouget, J., Conceicao, I., Berk, J., Schmidt, H., Waddington-Cruz, M., Campistol, J.M., Bettencourt, B.R., *et al.* (2015). Efficacy and safety of patisiran for familial amyloidotic polyneuropathy: a phase II multi-dose study. Orphanet journal of rare diseases *10*, 109.

Szebeni, J., Muggia, F., Gabizon, A., and Barenholz, Y. (2011). Activation of complement by therapeutic liposomes and other lipid excipient-based therapeutic products: prediction and prevention. Adv Drug Deliv Rev *63*, 1020-1030.

Tabernero, J., Shapiro, G.I., LoRusso, P.M., Cervantes, A., Schwartz, G.K., Weiss, G.J., Paz-Ares, L., Cho, D.C., Infante, J.R., Alsina, M., *et al.* (2013). First-in-humans trial of an RNA interference therapeutic targeting VEGF and KSP in cancer patients with liver involvement. Cancer discovery *3*, 406-417.

Tam, P., Monck, M., Lee, D., Ludkovski, O., Leng, E.C., Clow, K., Stark, H., Scherrer, P., Graham, R.W., and Cullis, P.R. (2000). Stabilized plasmid-lipid particles for systemic gene therapy. Gene Ther *7*, 1867-1874.

Tam, Y.Y., Chen, S., Zaifman, J., Tam, Y.K., Lin, P.J., Ansell, S., Roberge, M., Ciufolini, M.A., and Cullis, P.R. (2013). Small molecule ligands for enhanced intracellular delivery of lipid nanoparticle formulations of siRNA. Nanomedicine : nanotechnology, biology, and medicine *9*, 665-674.

Thess, A., Grund, S., Mui, B.L., Hope, M.J., Baumhof, P., Fotin-Mleczek, M., and Schlake, T. (2015). Sequence-engineered mRNA Without Chemical Nucleoside Modifications Enables an Effective Protein Therapy in Large Animals. Mol Ther *23*, 1456-1464.

Tilney, N.L. (1971). Patterns of lymphatic drainage in the adult laboratory rat. Journal of anatomy *109*, 369-383.

Tsui, N.B., Ng, E.K., and Lo, Y.M. (2002). Stability of endogenous and added RNA in blood specimens, serum, and plasma. Clinical chemistry *48*, 1647-1653.

Ueda, M., and Ando, Y. (2014). Recent advances in transthyretin amyloidosis therapy. Translational neurodegeneration *3*, 19.

van de Water, F.M., Boerman, O.C., Wouterse, A.C., Peters, J.G., Russel, F.G., and Masereeuw, R. (2006). Intravenously administered short interfering RNA accumulates in the kidney and selectively suppresses gene function in renal proximal tubules. Drug metabolism and disposition: the biological fate of chemicals *34*, 1393-1397.

Vance, J.E., and Adeli, K. (2008). Assembly and Secretion of Triacylglycerol-rich Lipoproteins. In Biochemistry of Lipids, Lipoproteins and Membranes, D.E. Vance, and J.E. Vance, eds. (Elsevier B.V.), pp. 507-531.

Viswanadhan, V.N., Ghose, A.K., Revankar, G.R., and Robins, R.K. (1989). Atomic physicochemical parameters for three dimensional structure directed quantitative structure-activity relationships. 4. Additional parameters for hydrophobic and dispersive interactions and their application for an automated superposition of certain naturally occurring nucleoside antibiotics. Journal of Chemical Information and Computer Sciences *29*, 163-172.

Volante, R.P. (1981). A new, highly efficient method for the conversion of alcohols to thiolesters and thiols. Tetrahedron Letters *22*, 3119-3122.

Walsh, C., Ou, K., Belliveau, N.M., Leaver, T.J., Wild, A.W., Huft, J., Lin, P.J., Chen, S., Leung, A.K., Lee, J.B., *et al.* (2014). Microfluidic-based manufacture of siRNA-lipid nanoparticles for therapeutic applications. Methods in molecular biology *1141*, 109-120.

Wang, H., Tam, Y.Y.C., Chen, S., Zaifman, J., van der Meel, R., and Cullis, P.R. (2016). The Niemann-Pick C1 Inhibitor NP3.47 Enhances The Gene Silencing Potency of Lipid Nanoparticles Containing siRNA. Manuscript submitted.

Wang, Q.S., Au, H.H., and Jan, E. (2013). Methods for studying IRES-mediated translation of positive-strand RNA viruses. Methods *59*, 167-179.

Webb, M.S., Harasym, T.O., Masin, D., Bally, M.B., and Mayer, L.D. (1995). Sphingomyelin-cholesterol liposomes significantly enhance the pharmacokinetic and therapeutic properties of vincristine in murine and human tumour models. British journal of cancer *72*, 896-904.

Webb, M.S., Saxon, D., Wong, F.M., Lim, H.J., Wang, Z., Bally, M.B., Choi, L.S., Cullis, P.R., and Mayer, L.D. (1998). Comparison of different hydrophobic anchors conjugated to poly(ethylene glycol): effects on the pharmacokinetics of liposomal vincristine. Biochim Biophys Acta *1372*, 272-282.

Wheeler, J.J., Palmer, L., Ossanlou, M., MacLachlan, I., Graham, R.W., Zhang, Y.P., Hope, M.J., Scherrer, P., and Cullis, P.R. (1999). Stabilized plasmid-lipid particles: construction and characterization. Gene Ther *6*, 271-281.

Whitehead, K.A., Langer, R., and Anderson, D.G. (2009). Knocking down barriers: advances in siRNA delivery. Nat Rev Drug Discov *8*, 129-138.

Whitmore, M., Li, S., and Huang, L. (1999). LPD lipopolyplex initiates a potent cytokine response and inhibits tumor growth. Gene Ther *6*, 1867-1875.

Wilson, K.D., Raney, S.G., Sekirov, L., Chikh, G., deJong, S.D., Cullis, P.R., and Tam, Y.K. (2007). Effects of intravenous and subcutaneous administration on the pharmacokinetics, biodistribution, cellular uptake and immunostimulatory activity of CpG ODN encapsulated in liposomal nanoparticles. International immunopharmacology *7*, 1064-1075.

Woodle, M.C., and Lasic, D.D. (1992). Sterically stabilized liposomes. Biochim Biophys Acta *1113*, 171-199.

Xu, Y., and Szoka, F.C., Jr. (1996). Mechanism of DNA release from cationic liposome/DNA complexes used in cell transfection. Biochemistry *35*, 5616-5623.

Yan, X., Kuipers, F., Havekes, L.M., Havinga, R., Dontje, B., Poelstra, K., Scherphof, G.L., and Kamps, J.A. (2005). The role of apolipoprotein E in the elimination of liposomes from blood by hepatocytes in the mouse. Biochem Biophys Res Commun *328*, 57-62.

Yang, B., Ming, X., Cao, C., Laing, B., Yuan, A., Porter, M.A., Hull-Ryde, E.A., Maddry, J., Suto, M., Janzen, W.P., *et al.* (2015). High-throughput screening identifies small molecules that enhance the pharmacological effects of oligonucleotides. Nucleic acids research *43*, 1987-1996.

Yin, H., Kanasty, R.L., Eltoukhy, A.A., Vegas, A.J., Dorkin, J.R., and Anderson, D.G. (2014). Non-viral vectors for gene-based therapy. Nat Rev Genet *15*, 541-555.

Zhang, J.S., Liu, F., and Huang, L. (2005). Implications of pharmacokinetic behavior of lipoplex for its inflammatory toxicity. Adv Drug Deliv Rev *57*, 689-698.

Zhang, Y.P., Sekirov, L., Saravolac, E.G., Wheeler, J.J., Tardi, P., Clow, K., Leng, E., Sun, R., Cullis, P.R., and Scherrer, P. (1999). Stabilized plasmid-lipid particles for regional gene therapy: formulation and transfection properties. Gene Ther *6*, 1438-1447.

Zheng, X., Vladau, C., Zhang, X., Suzuki, M., Ichim, T.E., Zhang, Z.X., Li, M., Carrier, E., Garcia, B., Jevnikar, A.M., *et al.* (2009). A novel in vivo siRNA delivery system specifically targeting dendritic cells and silencing CD40 genes for immunomodulation. Blood *113*, 2646-2654.

Zhigaltsev, I.V., Belliveau, N., Hafez, I., Leung, A.K., Huft, J., Hansen, C., and Cullis, P.R. (2012). Bottom-up design and synthesis of limit size lipid nanoparticle systems with aqueous and triglyceride cores using millisecond microfluidic mixing. Langmuir *28*, 3633-3640.

Zhigaltsev, I.V., Maurer, N., Edwards, K., Karlsson, G., and Cullis, P.R. (2006). Formation of drug-arylsulfonate complexes inside liposomes: a novel approach to improve drug retention. J Control Release *110*, 378-386.

Zimmermann, T.S., Lee, A.C., Akinc, A., Bramlage, B., Bumcrot, D., Fedoruk, M.N., Harborth, J., Heyes, J.A., Jeffs, L.B., John, M., *et al.* (2006). RNAi-mediated gene silencing in non-human primates. Nature *441*, 111-114.

Appendices

Appendix A Detailed Synthesis of Lipophilic Dexamethasone Prodrugs (Chapter 5)

A.1 General Procedures

Unless otherwise stated, ^{1}H and ^{13}C NMR spectra were recorded at room temperature on a Bruker Avance 300. Chemical shifts are reported in parts per million (ppm) on the δ scale and coupling constants, *J*, are in hertz (Hz). Multiplicities are reported as "s" (singlet), "d" (doublet), "dd" (doublet of doublets), "dt" (doublet of triplets), "ddd" (doublet of doublets of doublets), "t" (triplet), "td" (triplet of doublets), "q" (quartet), "quin" (quintuplet), "sex" (sextet), "m" (multiplet), and further qualified as "app" (apparent) and "br" (broad). Low-resolution mass spectra (m/z) were obtained in the electrospray ionization (ESI) mode. Dexamethasone (Dex) was purchased from MP Biomedicals (CA, USA) and used without further purification. All reagents and solvents were purchased from commercial suppliers and used without further purification, except THF, (freshly distilled from Na/benzophenone under Ar), and Et_3N and CH_2Cl_2 (freshly distilled from CaH_2 under Ar). Flash chromatography was performed on Silicycle 230-400 mesh silica gel. Analytic TLC was carried out with Merck silica gel 60 plates with fluorescent indicator. Spots were visualized with UV light, or stained with iodine or aqueous $KMnO_4$.

A.2 Synthesis of LD001

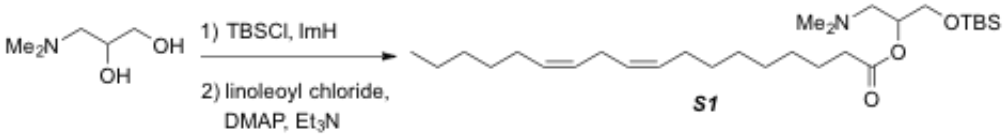

Scheme A.2.1: (±)-1-(*tert*-butyldimethylsilyloxy)-3-(dimethylamino)propan-2-yl-(9*Z*,12*Z*)-octadeca-9,12-dienoate (**S1**).

Solid TBSCl (1.36 g, 9.00 mmol, 1.00 equiv.) was added to a stirring, ice-cold CH_2Cl_2 (11 mL) solution of 3-dimethylaminopropane-1,2-diol (1.07 g, 9.00 mmol) and imidazole (613 mg, 9.00 mmol, 1.00 equiv.) in a round bottom flask under argon. After 2.5 h, the reaction mixture was diluted with CH_2Cl_2 and washed with distilled water (1 x 25 mL). The aqueous layer was extracted with CH_2Cl_2 (1 x 15 mL) and the combined organic layers washed with brine (1 x 15 mL), dried over Na_2SO_4 and concentrated to afford a clear, colourless oil as the intermediate primary silyl ether (1.83 g, 87% yield), which was used in the subsequent acylation without further purification.

Linoleoyl chloride was prepared by adding oxalyl chloride (0.30 mL, 3.60 mmol, 1.80 equiv.) to a stirring, room temperature benzene (5 mL) solution of linoleic acid (673 mg, 2.40 mmol, 1.20 equiv. relative to alcohol) and DMF (18 µL, 0.24 mmol, 0.12 equiv.) in a round bottom flask under argon. After 3 h, the volatiles were removed on a rotary evaporator and the residue azeotroped with benzene (2 x 5 mL), then dried under high vacuum for 3 h and used immediately without further purification.

A CH_2Cl_2 (4 mL) solution of the above intermediate silyl ether (467 mg, 2.00 mmol, 1.00 equiv.) and Et_3N (0.69 mL, 5.00 mmol, 2.50 equiv.) was added to a stirring, ice-cold CH_2Cl_2 (4 mL) solution of the linoleoyl chloride in a round bottom flask under argon, followed by solid DMAP (293 mg, 2.40 mmol, 1.20 equiv.). The reaction mixture was allowed to warm up over 14 h, then then diluted with CH_2Cl_2, washed with aq. 5% $NaHCO_3$ (2 x 10 mL), dried over Na_2SO_4 and concentrated on a rotary evaporator to afford the crude as a brown semi-solid. The crude was purified by flash column chromatography (130 mL SiO_2, 79:20:1 $\rightarrow$ 69:30:1 hexanes/EtOAc/Et_3N) to afford a clear, yellow oil as desired ester **S1** (828 mg, 84% yield).

^{1}H NMR ($CDCl_3$, 300 MHz): 5.47-5.24 (m, 4H), 5.01 (app q, J = 5.3, 1H), 3.79-3.62 (m, 2H), 2.77 (t, J = 5.9, 2H), 2.49 (d, J = 6.0, 2H), 2.36-2.23 (m, 2H), 2.27 (s, 6H), 2.11-1.98 (m, 4H), 1.69-1.5

(m, 2H), 1.45-1.21 (m, 16H), 0.88 (m, 12H), 0.05 (6H). ^{13}C NMR ($CDCl_3$, 300 MHz): 173.4, 130.2, 130.0, 128.0, 127.9, 63.0, 59.3, 46.0, 34.5, 31.5, 29.6, 29.3, 29.2, 29.1, 27.2, 25.8, 25.6, 24.9, 22.6, 18.2, 14.1, –5.4, –5.2.

LRMS: 496.8 [M+H$^+$].

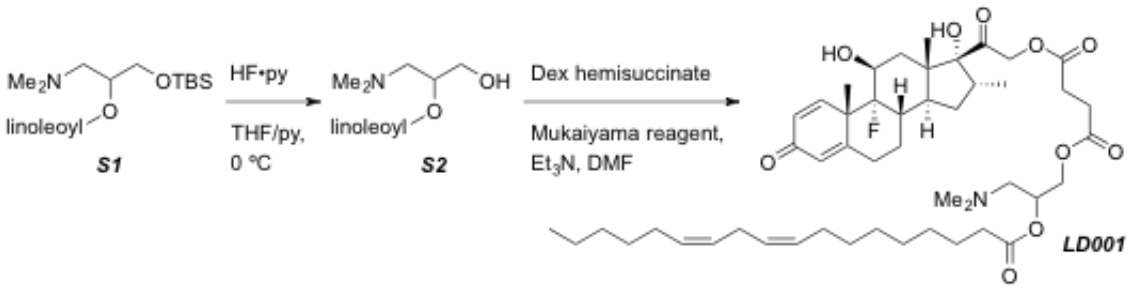

Scheme A.2.2: 3-(dimethylamino)-2-(((9*Z*,12*Z*)-octadeca-9,12-dienoyl)oxy)propyl (2-((8*S*,9*R*,10*S*,11*S*,13*S*,14*S*,16*R*,17*R*)-9-fluoro-11,17-dihydroxy-10,13,16-trimethyl-3-oxo-6,7,8,9,10,11,12,13,14,15,16,17-dodecahydro-3H-cyclopenta[a]phenanthren-17-yl)-2-oxoethyl) succinate (**LD001**).

Neat HF•pyridine solution (68 µL of 70% HF in pyridine, 0.54 mmol, 3.00 equiv.) was added to a stirring, ice-cold THF (1.2 mL) solution containing pyridine (44 µL, 0.54 mmol, 3.00 equiv.) and silyl ether **S1** (90 mg, 0.18 mmol) in a round bottom flask under argon. After 2 h, the reaction mixture was quenched with aq. 5% $NaHCO_3$. The mixture was extracted with EtOAc (3 x 5 mL), then the combined organic extracts were washed with brine, dried over Na_2SO_4 and concentrated on a rotary evaporator to afford intermediate primary alcohol **S2** (68 mg, theoretical yield of 69 mg) as a clear, colourless oil that was used immediately and without further purification. It should be noted that intermediate **S2** is unstable and complete transesterification to the primary alcohol was observed (^{1}H NMR, TLC) in <24 h, when stored neat at –20 °C.

Solid dexamethasone-21-hemisuccinate (Jung et al., 2014; Mao et al., 2012) (45 mg, 0.18 mmol, 0.50 equiv.) was added to a room temperature DMF (1 mL) solution of alcohol **S2** (68 mg, 0.18 mmol, 2.00 equiv.) and Et_3N (38 µL, 0.27 mmol, 1.50 equiv.) in a round bottom flask under argon, followed by 2-chloro-1-methylpyridinium iodide (28 mg, 0.11 mmol, 0.60 equiv.). After 14 h, the mixture was quenched with aq. 5% $NaHCO_3$. The mixture was extracted with EtOAc (2 x 3 mL), then the combined organic extracts were washed with aq. 5% $NaHCO_3$ (1 x 3 mL), brine, dried over Na_2SO_4 and concentrated on a rotary evaporator to afford the crude as a yellow oil. The crude was purified by flash column chromatography (20 mL SiO_2, 97:3 $CHCl_3$/MeOH) to afford a clear, colourless oil as desired conjugate **LD001** (72 mg, 94% yield).

^1H NMR ($CDCl_3$, 300 MHz): 7.20 (d, *J* = 10.2, 1H), 6.31 (d, *J* = 10.2, 1H), 6.09 (s, 1H), 5.48-5.25 (m, 4H), 5.24-5.12 (m, 1H), 4.96 (dd, *J* = 12.0, 6.6, 1H), 4.83 (dd, *J* = 12.0, 6.6, 1H), 4.48-4.24 (m, 2H), 4.22-3.97 (m, 1H), 3.08 (m, 2H), 2.85-2.70 (m, 4H), 2.75-2.40 (m, 6H), 2.44-2.18 (m, 12H), 2.20-1.93 (m, 6H), 1.90-1.45 (m, 7H), 1.53 (s, 3H), 1.43-1.24 (m, 18H), 1.02 (s, 3H), 0.93-0.80 (m, 6H). ^{13}C NMR ($CDCl_3$, 300 MHz): 173.4, 130.2, 130.0, 128.0, 127.9, 63.0, 59.3, 46.0, 34.5, 31.5, 29.6, 29.3, 29.2, 29.1, 27.2, 25.8, 25.6, 24.9, 22.6, 18.2, 14.1, –5.4, –5.2.

LRMS: 857.2 [$M+H^+$].

A.3 Synthesis of LD002

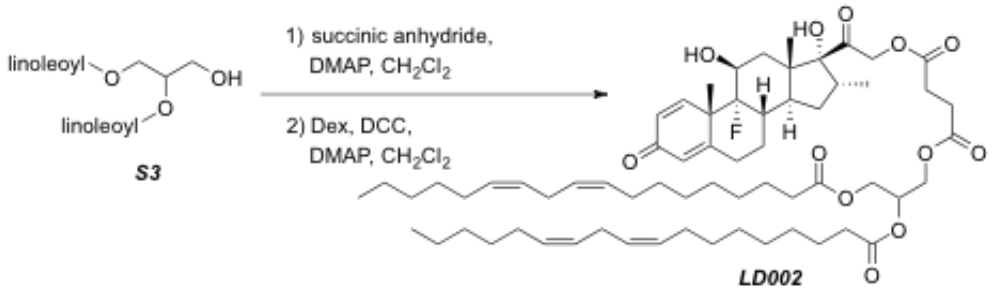

Scheme A.3.1: 2,3-bis(((9*Z*,12*Z*)-octadeca-9,12-dienoyl)oxy)propyl (2-((8*S*,9*R*,10*S*,11*S*,13*S*,14*S*,16*R*,17*R*)-9-fluoro-11,17-dihydroxy-10,13,16-trimethyl-3-oxo-6,7,8,9,10,11,12,13,14,15,16,17-dodecahydro-3H-cyclopenta[a]phenanthren-17-yl)-2-oxoethyl) succinate (**LD002**).

Solid succinic anhydride (67 mg, 0.66 mmol, 2.0 equiv.) and DMAP (102 mg, 0.83 mmol, 2.5 equiv.) were added to a stirring room temperature CH_2Cl_2 (3.5 mL) solution of 1,2-dilinoleoyl glycerol **S3 (Abe et al., 2011)** (205 mg, 0.33 mmol, 1.0 equiv.) in a round bottom flask under argon. After 12 hours, the reaction was quenched with aq. 1 M HCl, extracted with CH_2Cl_2 (2 x 15 mL), the combined organic extracts were then washed with aq. 1 M HCl (1 x 15 mL), dried over Na_2SO_4 and concentrated on a rotary evaporator to afford the intermediate hemisuccinate (245 mg, 238 mg theoretical yield) as a pale yellow oil that was used without further purification. A portion of the hemisuccinate was used in the subsequent esterification.

Solid DCC (28 mg, 0.13 mmol, 1.10 equiv.) was added to a stirring, room temperature CH_2Cl_2 (1.5 mL) solution of the above hemisuccinate (105 mg, 0.15 mmol, 1.10 equiv.) in a round bottom flask under argon. After stirring for 5 min, solid dexamethasone (52 mg, 0.13 mmol) and DMAP (24 mg, 0.20 mmol, 1.50 equiv.) were added. The reaction mixture was allowed to stir for 14 h, diluted with CH_2Cl_2, filtered through Celite and the filtrate was concentrated to afford the crude as a pale yellow oil. The crude was purified by flash column chromatography (25 mL SiO_2, 80:20 $\rightarrow$ 70:30 $\rightarrow$ 50:50 hexanes/EtOAc) to afford a clear, colourless oil as desired conjugate **LD002** (67 mg, 46% yield)

^{1}H NMR ($CDCl_3$, 300 MHz): 7.22 (dd, J = 10.2, 3.9, 1H), 6.32 (dd, J = 10.2, 1.7, 1H), 6.1 (s, 1H), 5.44-5.17 (m, 9H), 5.00-4.81 (m, 2H), 4.43-4.22 (m, 4H), 4.21-4.06 (m, 2H), 3.16-3.01

(m, 1H), 2.84-2.51 (m, 11H), 2.50-2.23 (m, 9H), 2.21-1.48 (m, 25H), 1.45-1.15 (m, 34H), 1.14-1.00 (m, 1H), 1.03 (s, 3H), 0.95-0.81 (m, 10H).

^{13}C NMR ($CDCl_3$, 300 MHz): 204.5, 186.6, 173.7, 173.6, 173.3, 173.1, 171.9, 171.8, 171.6, 166.8, 152.3, 152.2, 130.2, 129.9, 129.7, 128.0, 127.8, 125.0, 101.4, 99.1, 91.1, 72.2, 71.7, 69.0, 68.9, 68.7, 62.2, 53.4, 48.4, 44.0, 36.2, 35.83, 35.75, 34.3, 34.2, 34.0, 33.8, 32.2, 31.5, 31.0, 29.6, 29.3, 29.2, 29.1, 29.04, 29.0, 28.9, 28.7, 27.23, 27.2, 25.6, 24.9, 23.0, 22.9, 22.5, 16.4, 14.6, 14.0. LRMS: 1114.5 [$M+Na^+$].

A.4 Synthesis of LD003

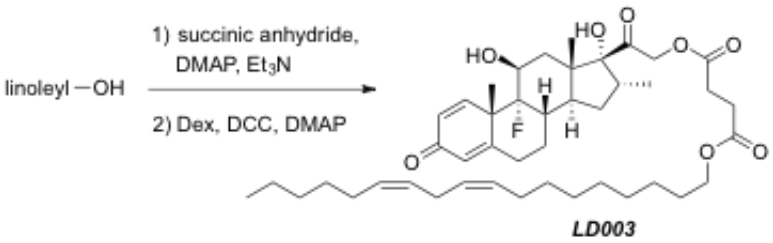

Scheme A.4.1: 2-((8*S*,9*R*,10*S*,11*S*,13*S*,14*S*,16*R*,17*R*)-9-fluoro-11,17-dihydroxy-10,13,16-trimethyl-3-oxo-6,7,8,9,10,11,12,13,14,15,16,17-dodecahydro-3H-cyclopenta[a]phenanthren-17-yl)-2-oxoethyl ((9*Z*,12*Z*)-octadeca-9,12-dien-1-yl) succinate (**LD003**).

Solid succinic anhydride (500 mg, 5.00 mmol, 2.00 equiv.) and DMAP (764 mg, 6.25 mmol, 2.50 equiv.) were added to a stirring, room temperature CH_2Cl_2 (10 mL) solution of linoleyl alcohol (666 mg, 2.50 mmol) in a round bottom flask under argon. After 14 h, the reaction mixture was diluted with CH_2Cl_2, washed with aq. 1 M HCl (2 x 10 mL), dried over Na_2SO_4 and concentrated on a rotary evaporator to afford a white semisolid as the desired hemisuccinate (915 mg, quantitative yield), which was used without further purification.

Solid DCC (37 mg, 0.18 mmol, 1.10 equiv.) was added to a stirring, room temperature CH_2Cl_2 (1.6 mL) solution of the above hemisuccinate (65 mg, 0.18 mmol, 1.10 equiv.) in a round bottom flask under argon. After stirring for 5 min, solid dexamethasone (63 mg, 0.16 mmol) and DMAP (30 mg, 0.24 mmol, 1.5 equiv.) were added. The reaction mixture was allowed to stir for 14 h, diluted with CH_2Cl_2, filtered through Celite and the filtrate was concentrated to afford the crude as a clear, colourless oil. The crude was purified by flash column chromatography (25 mL SiO_2, 70:30 → 60:40 hexanes/EtOAc) to afford a clear, colourless oil as desired conjugate **LD003** (76 mg, 64% yield). ^{1}H NMR ($CDCl_3$, 300 MHz): 7.25 (d, *J* = 10.2, 1H), 6.33 (d, *J* = 10.1, 1H), 6.1 (s, 1H), 5.45-5.25 (m, 4H), 4.93 (s, 2H), 4.45-4.27 (m, 1H), 4.08 (t, *J* = 6.7, 2H), 3.17-3.01 (m, 1H), 2.92 (s, 1H), 2.77 (t, *J* = 6.5, 4H), 2.72-2.52 (m, 4H), 2.50-2.24 (m, 4H), 2.23-2.07 (m, 1H), 2.05 (q, *J* = 6.6, 4H), 1.97-1.45 (m, 10H), 1.44-1.01 (m, 20H), 1.02 (s, 3H), 0.97-0.80 (m, 6H). ^{13}C NMR ($CDCl_3$, 300 MHz): 204.7, 186.8, 172.3, 172.2, 166.7, 152.7, 130.1, 130.0, 129.5, 128.0, 127.8, 124.9, 101.4, 99.1, 91.1, 72.2, 71.6, 68.6, 65.0, 48.5, 48.4, 48.2, 43.9, 36.3, 35.9, 34.3, 34.0, 33.8, 32.2, 31.4, 31.0, 29.6, 29.4, 29.2, 29.1, 28.8, 28.5, 27.3, 27.1, 25.8, 25.6, 24.9, 22.9, 22.8, 22.5, 16.4, 14.6, 14.0. LRMS: 765.0 [M+Na$^+$].

A.5 Synthesis of LD004

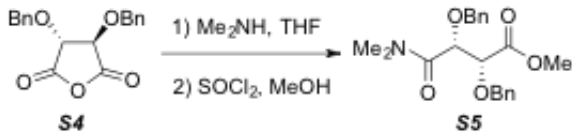

S4 *S5*

Scheme A.5.1: Methyl (2*R*,3*R*)-2,3-bis(benzyloxy)-4-(dimethylamino)-4-oxobutanoate (**S5**).

A Me_2NH/THF solution (22.5 mL of 2.0 M in THF, 45.0 mmol, 3.00 equiv.) was added over 5 min to a stirring, ice-cold THF (30 mL) solution of (3*R*,4*R*)-bis(benzyloxy)succinc

anhydride **S4** (Ohwada et al., 1990) (4.68 g, 15.0 mmol) in a round bottom flask under argon. After 16 h, the reaction mixture was diluted with Et_2O and quenched with saturated aq. NH_4Cl. The aqueous layer was extracted with Et_2O (1 x 25 mL), the combined organic extracts were washed with brine, dried over Na_2SO_4 and concentrated on a rotary evaporator to afford the intermediate amidoacid as a viscous, yellow oil (5.36 g theoretical yield).

Thionyl chloride (1.14 mL, 15.7 mmol, 1.05 equiv.) was added to a stirring, ice-cold MeOH (25 mL) solution of the amidoacid in a round bottom flask under argon and the mixture was allowed to warm up. After 14 h, the volatiles were removed on a rotary evaporator and saturated aq. $NaHCO_3$ was added. The mixture was extracted with Et_2O (2 x 75 mL), the combined organic extracts were washed with saturated aq. $NaHCO_3$ (1 x 100 mL), dried over Na_2SO_4 and concentrated on a rotary evaporator to afford the crude as a yellow oil. The crude was purified by flash column chromatography (220 mL SiO_2, 60:40 EtOAc/hexanes) to afford a pale, yellow oil as amidoester **S5** (4.44 g, 80% yield).

^{1}H NMR ($CDCl_3$, 300 MHz): 7.43-7.19 (m, 10H), 4.84 (d, *J* = 11.6, 1H), ZZZ, 3.68 (s, 3H), 3.02 (s, 3H, rotamers), 2.91 (s, 3H, rotamers). ^{13}C NMR ($CDCl_3$, 300 MHz): 170.1, 168.5, 137.1, 136.7, 128.3, 128.2, 128.1, 127.9, 80.1, 78.9, 73.5, 72.4, 52.1, 36.9, 36.4. LRMS: 394.3 [M+Na^+].

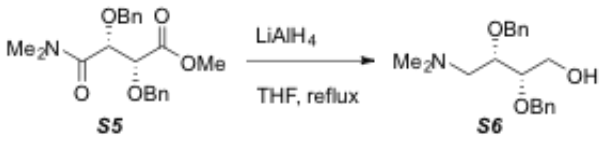

S5 *S6*

Scheme A.5.2: (2*S*,3*S*)-2,3-bis(benzyloxy)-4-(dimethylamino)butan-1-ol (**S6**).

A THF (15 mL) solution of amidoester **S5** (2.26 g, 6.08 mmol) was added over 1 h from an addition funnel to a refluxing THF (20 mL) suspension of $LiAlH_4$ (1.15 g, 30.4 mmol, 5.00 equiv.) in a two-necked round bottom flask fitted with a condenser and under argon. After an additional 5 min, the reaction mixture was cooled in an ice bath, diluted with Et_2O, quenched by the Fieser method (Smith, 1969) (1.2 mL water, 1.2 mL aq. 1 M NaOH, 3.6 ml water), then removed from the ice bath and stirred at room temperature until the precipitates turned white (~1 h). The mixture was filtered through Celite and the filtrate concentrated on a rotary evaporator to afford a clear, colourless oil as desired aminoalcohol **S6** (1.99 g, 99% yield), which was used without further purification. ^{1}H NMR ($CDCl_3$, 300 MHz): 7.41-7.24 (m, 10H), 6.04 (br s, 1H), 4.73 (d, *J* = 11.7, 1H), 4.64 (d, *J* = 11.7, 1H), 4.64 (s, 2H), 3.74 (br d, *J* = 3.6, 2H), 3.70 (dt, *J* = 6.9, 3.3, 1H), 3.62-3.55 (m, 1H), 2.61 (dd, *J* = 13.2, 6.9, 1H), 2.51 (dd, *J* = 13.3, 3.3, 1H), 2.30 (s, 6H). ^{13}C NMR ($CDCl_3$, 300 MHz): 138.5, 138.2, 128.33, 128.29, 127.81, 127.76, 127.6, 127.5, 81.7, 79.2, 72.6, 72.2, 60.1, 59.0, 46.0. LRMS: 330.4 [M+H$^+$].

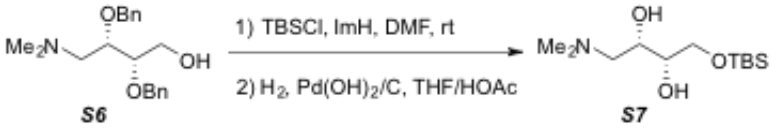

Scheme A.5.3: (2*S*,3*S*)-2,3-dihydroxy-4-((tert-butyldimethylsilyl)oxy)-*N*,*N*-dimethylaminobutane (**S7**).

Solid TBSCl (497 mg, 3.30 mmol, 1.10 equiv.) was added to a stirring, room temperature DMF (6 mL) solution of primary alcohol **S6** (1.00 g, 3.00 mmol) and imidazole (449 mg, 6.60 mmol, 2.20 equiv.) in a round bottom flask under argon. After 14 h, the reaction mixture was quenched with aq. 5% $NaHCO_3$ (25 mL) and extracted with Et_2O (3 x 20 mL). The combined

organic extracts were washed with water (3 x 20 mL), brine, dried over Na_2SO_4 and concentrated on a rotary evaporator to afford the crude as a clear, colourless oil. The crude was purified by flash column chromatography (100 mL SiO_2, 70:30:0 → 55:40:5 hexanes/EtOAc/MeOH) to afford a clear, colourless oil as the intermediate silyl ether (1.17 g, 87% yield).

Solid $Pd(OH)_2/C$ (177 mg of 10 wt% stock, 0.12 mmol, 0.10 equiv.) was added to a stirring, room temperature 7:3 THF/HOAc (8.5 mL) solution of bisbenzylated **S10** (558 mg, 1.26 mmol) in a round bottom flask under argon. The argon balloon was replaced with a hydrogen balloon and hydrogen gas was bubbled through the mixture for 5 min, before allowing it to stir under balloon pressure hydrogen for 18 h. The mixture was diluted with EtOAc and filtered through Celite. The pH of the filtrate was raised to pH 8-10 by the addition of saturated aq. Na_2CO_3, extracted with EtOAc (2 x 10 mL), then the combined organic extracts were washed with brine, dried over Na_2SO_4 and concentrated to obtain a clear, colourless oil as desired diol **S7** (230 mg, 331 mg theoretical yield). ^{1}H NMR ($CDCl_3$, 300 MHz): δ 3.85-3.76 (m, 1H), 3.72 (dd, *J* = 5.9, 2.7, 2H), 3.55 (dt, *J* = 5.7, 2.5, 1H), 3.31 (br s, 2H), 2.60 (dd, *J* = 12.4, 8.8, 1H), 2.37-2.28 (m,1H), 2.29 (s, 6H), 0.89 (s, 9H), 0.08 (s,6H). ^{13}C NMR ($CDCl_3$, 300 MHz): δ 72.3, 67.4, 64.9, 62.0, 45.8, 25.8, 18.2, –5.46. LRMS: 264.4 [$M+H^+$].

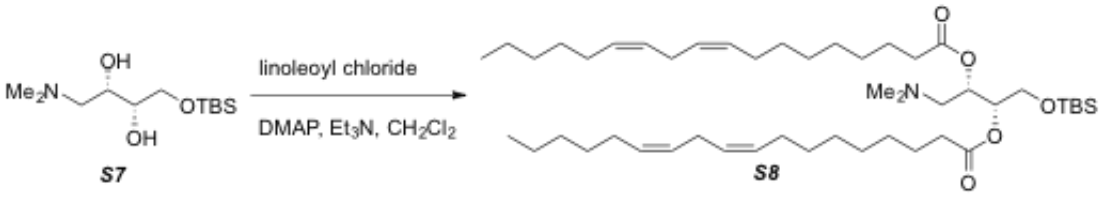

Scheme A.5.4: (2*S*,3*S*)-1-((tert-butyldimethylsilyl)oxy)-4-(dimethylamino)butane-2,3-diyl (9*Z*,9'*Z*,12*Z*,12'*Z*)-bis(octadeca-9,12-dienoate) (**S8**).

A portion of diol **S7** was used in the subsequent acylation. Linoleyl chloride was prepared by adding oxalyl chloride (0.19 mL, 2.25 mmol) to a stirring, room temperature benzene (5 mL) solution of linoleic acid (422 mg, 1.50 mmol, 2.20 equiv. relative to diol) and DMF (12 µL, 0.15 mmol) in a round bottom flask under argon. After 4 h, the volatiles were removed on a rotary evaporator and the residue azeotroped with benzene (2 x 5 mL), then dried under high vacuum for 3 h and used immediately without further purification. A CH_2Cl_2 (1.5 mL) solution of the above diol (180 mg, 0.68 mmol, 1.00 equiv.) and Et_3N (0.47 mL, 3.42 mmol, 5.00 equiv.) was added to a stirring, ice-cold CH_2Cl_2 (2 mL) solution of the linoleyl chloride in a round bottom flask under argon, followed by solid DMAP (184 mg, 1.50 mmol, 2.20 equiv.). The reaction mixture was allowed to warm up over 14 h, was then diluted with CH_2Cl_2, washed with aq. 5% $NaHCO_3$ (2 x 10 mL), dried over Na_2SO_4 and concentrated on a rotary evaporator to afford the crude as a yellow semi-solid. The crude was purified by flash column chromatography (50 mL SiO_2, 90:10 hexanes/EtOAc) to afford a clear, colourless oil as desired diester **S8** (319 mg, 59% yield). ^{1}H NMR ($CDCl_3$, 300 MHz): 5.46-5.22 (m, 9H), 5.18-5.09 (m, 1H), 3.66 (dd, *J* = 5.6, 1.3, 2H), 2.77 (t, *J* = 5.8, 4H), 2.49-2.26 (m, 6H), 2.22 (s, 6H), 2.05 (app q, *J* = 13.0, 6.6, 8H), 1.70-1.47 (m, 6H), 1.44-1.19 (m, 27H), 0.94-0.84 (m, 6H), 0.87 (s, 9H), 0.03 (s, 6H). ^{13}C NMR ($CDCl_3$, 300 MHz): 173.0, 172.9, 130.2, 130.0, 128.0, 127.8, 72.9, 69.0, 61.3, 59.3, 45.9, 34.33, 34.28, 31.5, 29.6, 29.3, 29.21, 29.19, 29.12, 29.07, 27.2, 25.7, 25.6, 25.0, 22.5, 18.1, 14.0, –5.6. LRMS: 789.4 [M+H$^+$].

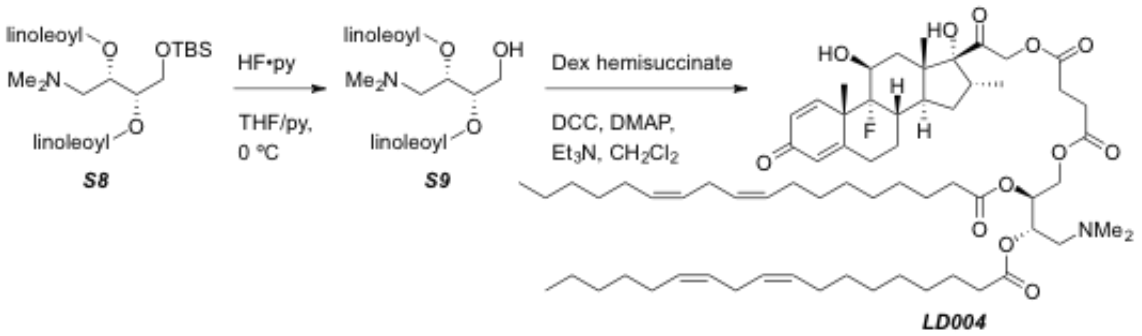

Scheme A.5.6: (2S,3S)-4-(dimethylamino)-2,3-bis(((9*Z*,12*Z*)-octadeca-9,12-dienoyl)oxy)butyl (2-((8*S*,9*R*,10*S*,11*S*,13*S*,14*S*,16*R*,17*R*)-9-fluoro-11,17-dihydroxy-10,13,16-trimethyl-3-oxo-6,7,8,9,10,11,12,13,14,15,16,17-dodecahydro-3H-cyclopenta[a]phenanthren-17-yl)-2-oxoethyl) succinate (**LD004**).

Neat HF•pyridine solution (87 µL of 70% HF in pyridine, 0.70 mmol, 3.00 equiv.) was added to a stirring, –10 °C THF (1.2 mL) solution containing pyridine (57 µL, 0.70 mmol, 3.00 equiv.) and silyl ether **S8** (185 mg, 0.23 mmol) in a round bottom flask under argon. After 20 min, the reaction mixture was transferred to an ice bath, stirred for a further 2 h, then quenched with aq. 5% $NaHCO_3$. The mixture was extracted with EtOAc (3 x 5 mL), then the combined organic extracts were washed with brine, dried over Na_2SO_4 and concentrated on a rotary evaporator to afford desired primary alcohol **S9** (162 mg, theoretical yield of 158 mg) as a pale yellow oil that was used immediately and without further purification. It should be noted that complete transesterification to the primary alcohol was observed (^{1}H NMR, TLC) in <24 h when stored neat at –20 °C.

Solid dexamethasone-21-hemisuccinate**Error! Bookmark not defined.** (88 mg, 0.18 mol, 1.10 equiv.) was added to a room temperature THF (0.8 mL) solution of DCC (37 mg, 0.18 mmol, 1.10 equiv.) in a round bottom flask under argon. After 10 min, the mixture was cooled in

an ice bath, a THF (0.8 mL) solution of alcohol **S13** (109 mg, 0.16 mmol), DMAP (22 mg, 0.18 mmol, 1.10 equiv.) and Et_3N (25 uL, 0.18 mmol, 1.10 equiv.) was added and the mixture was allowed to warm up overnight. After 20 h, the reaction mixture was diluted with THF, filtered through Celite and concentrated on a rotary evaporator to afford the crude as a pale yellow semisolid. The crude was purified by flash column chromatography (50 mL SiO_2, 36:60:4 Et_2O/hexanes/MeOH) to afford a clear, colourless oil as desired conjugate **LD004** (103 mg, 55% yield). ^1H NMR ($CDCl_3$, 300 MHz): 7.24 (d, *J* = 10.1, 1H), 6.34 (d, *J* = 10.1, 1H), 6.12 (s, 1H), 5.47-5.26 (m, 10H), 5.26-5.15 (m, 1H), 5.01 (d, *J* = 17.5, 1H), 4.86 (d, *J* = 17.5, 1H), 4.43-4.27 (m, 2H), 4.20-4.08 (m, 1H), 3.20-3.02 (m, 1H), 2.78 (app t, *J* = 5.6, 7H), 2.70-2.60 (m, 2H), 2.60-2.5 (m, 18H), 2.24 (s, 6H), 2.18-2.03 (m, 3H), 2.06 (app q, *J* = 13.1, 6.7, 8H), 1.90-1.49 (m, 13H), 1.47-1.16 (m, 39H), 1.05 (s, 3H), 0.90 (app t, *J* = 6.7, 11H). ^{13}C NMR ($CDCl_3$, 300 MHz): 204.5, 186.6, 173.2, 173.0, 172.1, 171.7, 166.2, 152.3, 130.2, 130.0, 129.9, 129.7, 128.08, 128.06, 127.8, 125.0, 101.4, 99.1, 91.1, 72.2, 71.7, 70.2, 69.2, 68.8, 62.5, 59.0, 48.4, 48.1, 45.9, 44.0, 36.2, 35.8, 34.3, 34.2, 34.1, 32.2, 31.5, 31.0, 29.6, 29.3, 29.2, 29.12, 29.09, 29.06, 28.9, 28.7, 27.2, 25.6, 24.9, 22.5, 16.4, 14.6, 14.0. LRMS: 1149.5 [$M+H^+$].

A.6 Synthesis of LD005

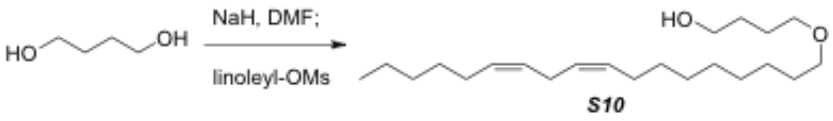

Scheme A.6.1: 4-(((9*Z*,12*Z*)-octadeca-9,12-dien-1-yl)oxy)butan-1-ol (**S10**).

A DMF (1 mL) solution of 1,4-butanediol (135 mg, 1.50 mmol, 1.20 equiv.) was added to a stirring, ice-cold DMF (3 mL) suspension of NaH (80 mg, 2.50 mmol, 1.50 equiv.; previously

washed with hexanes, 2 x 3 mL) in a round bottom flask under argon. The cold bath was then removed and the mixture stirred for 30 min. It was then cooled again in an ice bath and a DMF (1 mL) solution of linoleyl methanesulfonate (345 mg, 1.00 mmol) was added, allowing the mixture to warm up over 15 h. The reaction mixture was quenched by addition of water (10 mL), extracted with Et_2O (3 x 5 mL), then the combined extracts were washed with water (3 x 5 mL), dried over Na_2SO_4 and concentrated on a rotary evaporator to afford the crude as a pale yellow oil. It was evident by ^1H NMR that some (~25%) olefin isomerization had occurred during the reaction and attempts to mitigate or eliminate this were unsuccessful. The crude was purified by flash column chromatography (50 mL SiO_2, 80:20 hexanes/EtOAc) to afford a clear, colourless oil as desired ether **S10** (276 mg, 82% yield, ~3:1 mixture of desired/isomerized). ^1H NMR ($CDCl_3$, 300 MHz): 5.49-5.22 (m, 4H), 3.65 (t, *J* = 5.7, 2H), 3.5-3.38 (m, 4H), 2.79 (t, *J* = 5.9, 2H), 2.06 (q, *J* = 6.4, 4H), 1.76-1.62 (m, 4H), 1.65-1.51 (m, 2H), 1.46-1.18 (m, 17H), 0.90 (t, *J* = 6.5, 3H). ^{13}C NMR ($CDCl_3$, 300 MHz): 130.15, 130.10, 127.93, 127.90, 71.2, 70.8, 62.7, 31.5, 30.4, 29.62, 29.59, 29.43, 29.41, 29.3, 29.23, 29.18, 27.19, 27.16, 27.0, 26.1, 25.6, 22.5, 14.0. LRMS: 361.6 [$M+Na^+$].

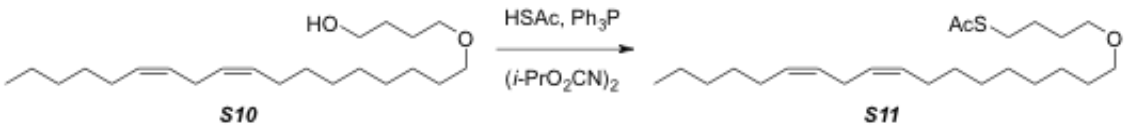

Scheme A.6.2: S-(4-(((9*Z*,12*Z*)-octadeca-9,12-dien-1-yl)oxy)butyl) ethanethioate (**S11**).

In analogy to Volante(Volante, 1981), neat diisopropyl azodicarboxylate (0.59 mL, 3.00 mmol, 2.00 equiv.) was added to a stirring, ice-cold THF (6 mL) solution of Ph_3P (787 mg, 3.00 mmol, 2.00 equiv.) in a round bottom flask under argon, which resulted in the formation of an off-

white precipitate, and the resultant was stirred for 1 h. A THF (2 mL) solution of thioacetic acid (0.21 mL, 3.00 mmol, 2.00 equiv.) and alcohol **S10** (508 mg, 1.50 mmol) was then added to the above ice-cold mixture, which was allowed to warm to room temperature. After 16 h, the volatiles were removed on a rotary evaporator. The residue was resuspended in 80:20 hexanes/EtOAc, stirred for 15 min, at which point the white solids were removed by filtration through Celite and the filtrate concentrated on a rotary evaporator to afford the crude as a yellow oil. The crude was purified by flash column chromatography (80 mL SiO_2, 99:1 $\rightarrow$ 95:5 hexanes/EtOAc) to afford a clear, colourless oil as desired thioacetate **S11** (549 mg, 92% yield). ^{1}H NMR ($CDCl_3$, 300 MHz): 5.47-5.24 (m, 4H), 3.49-3.12 (m, 4H), 2.98-2.86 (m, 2H), 2.78 (t, *J* = 6.1, 2H), 2.33 (s, 3H), 2.06 (q, *J* = 6.3, 4H), 1.75-1.61 (m, 4H), 1.63-1.48 (m, 2H), 1.46-1.18 (m, 17H), 0.90 (t, *J* = 6.5, 3H). ^{13}C NMR ($CDCl_3$, 300 MHz): 195.9, 130.15, 130.11, 127.93, 127.90, 71.0, 70.1, 31.5, 30.6, 29.7, 29.6, 29.5, 29.4, 29.3, 29.2, 28.9, 28.8, 27.20, 27.17, 26.3, 26.1, 25.6, 22.5, 14.0. LRMS: 419.8 [M+Na$^+$].

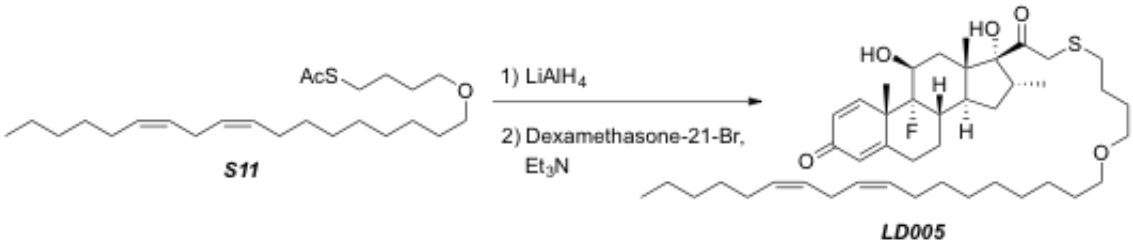

Scheme A.6.3: (8*S*,9*R*,10*S*,11*S*,13*S*,14*S*,16*R*,17*R*)-9-fluoro-11,17-dihydroxy-10,13,16-trimethyl-17-(2-((4-(((9*Z*,12*Z*)-octadeca-9,12-dien-1-yl)oxy)butyl)thio)acetyl)-6,7,8,9,10,11,12,13,14,15,16,17-dodecahydro-3H-cyclopenta[a]phenanthren-3-one (**S17**).

A THF (1 mL) solution of thioacetate **S11** (119 mg, 0.30 mmol) was added dropwise to a stirring, ice-cold THF (2 mL) suspension of $LiAlH_4$ (46 mg, 1.20 mmol, 4.00 equiv.) in a round bottom flask under argon, which was allowed to warm up over time. After 4.5 h, the reaction was cooled in an ice bath, diluted with Et_2O and quenched with aq. 1 M HCl (3 mL). The aqueous layer was extracted with Et_2O (2 x 5 mL), then the combined extracts were washed with brine (1 x 5 mL), dried over Na_2SO_4 and concentrated on a rotary evaporator to afford the desired thiol (101 mg, 95% yield) as a clear, colourless oil that was used immediately and without further purification.

A THF (0.6 mL) solution of the intermediate thiol (66 mg, 0.19 mmol, 1.90 equiv.) was added to a stirring, ice-cold THF (0.4 mL) solution of dexamethasone-21-bromide (Lopez and Simons, 1991; Simons et al., 1980) (48 mg, 0.10 mmol) in a round bottom flask under argon. After 8 h, the reaction mixture was diluted with THF, filtered through Celite and concentrated on a rotary evaporator to afford the crude as a yellow oil. The crude was purified by flash column chromatography (25 mL SiO_2, 80:20 $\rightarrow$ 65:35 hexanes/EtOAc) to afford a clear, colourless oil as desired sulfide **LD005** (48 mg, 62% yield). ^{1}H NMR ($CDCl_3$, 300 MHz): 7.18 (d, *J* = 10.2, 1H), 6.32 (dd, *J* = 10.1, 1.7, 1H), 6.11 (s, 1H), 5.47-5.23 (m, 4H), 4.34 (br d, *J* = 10.0, 1H), 3.52 (d, *J* = 13.4, 1H), 3.48-3.29 (m, 5H), 3.18 (d, *J* = 13.2, 1H), 3.14-2.99 (m, 1H), 2.77 (t, *J* = 6.0, 2H), 2.65 (s, 1H), 2.69-2.19 (m, 8H), 2.04 (q, *J* = 6.5, 4H), 1.90-1.46 (m, 17H), 1.46-1.15 (m, 23H), 1.05 (s, 3H), 0.95-0.82 (m, 7H). ^{13}C NMR ($CDCl_3$, 300 MHz): 05.9, 186.5, 166.0, 151.9, 130.2, 130.1, 129.8, 128.0, 127.9, 125.1, 101.3, 91.4, 72.4, 71.9, 71.0, 70.1, 48.6, 48.4, 48.1, 43.9, 37.2, 37.1, 36.0, 34.4, 34.2, 32.4, 31.5, 31.4, 31.0, 29.6, 29.48, 29.46, 29.3, 29.2, 28.8, 27.3, 27.20, 27.18, 26.1, 25.65, 25.61, 23.0, 22.9, 22.6, 17.3, 14.6, 14.1. LRMS: 752.1 [$M+Na^+$].